

<http://researchcommons.waikato.ac.nz/>

## **Research Commons at the University of Waikato**

### **Copyright Statement:**

The digital copy of this thesis is protected by the Copyright Act 1994 (New Zealand).

The thesis may be consulted by you, provided you comply with the provisions of the Act and the following conditions of use:

- Any use you make of these documents or images must be for research or private study purposes only, and you may not make them available to any other person.
- Authors control the copyright of their thesis. You will recognise the author's right to be identified as the author of the thesis, and due acknowledgement will be made to the author where appropriate.
- You will obtain the author's permission before publishing any material from the thesis.

# **Supercapacitor assisted power converter for DC microgrid applications with self-contained DC-UPS capability**

A thesis submitted in partial fulfilment  
of the requirements for the degree

of

**Master of Engineering**

at

**The University of Waikato**

by

**Yang Hu**

---

The University of Waikato

2017



THE UNIVERSITY OF  
**WAIKATO**  
*Te Whare Wānanga o Waikato*



# Abstract

Nowadays, due to the advantages inherent in using renewable energy, renewable power generation is becoming established worldwide. Direct current (DC) microgrid systems, which have been proposed as alternatives for traditional alternating current (AC) networks, enable the introduction of a large amount of solar energy by using distributed photovoltaic generation units. Meanwhile, small-scale DC microgrid systems designed at the household level are also viable options used to harness renewable energy (like solar energy) and have broad development prospects.

One of the 'hot topics' in the field of renewable energies is how to make efficient use of this type of energy. In this thesis, a high-efficiency DC microgrid system with supercapacitor (SC)-assisted power converter is introduced as a way to harness solar energy to run a 12 V, 50 W household lighting system.

Supercapacitor-assisted low dropout regulator (SCALDO) techniques were used to build an SC-assisted converter for a DC microgrid system. Supercapacitors in the DC microgrid acted as voltage droppers to convert 24 V solar panel's output to 11 V – 13 V. Supercapacitors were also used as energy storage devices, and performed as a power source to run the household lighting system for a period of time after a sudden mains power outage.

Real weather condition data, including local Hamilton illuminance values, were required to design this system. These data were measured at the University of Waikato. They were converted into irradiance data and were used to create similar patterns for simulation. Prototype circuit of the complete DC microgrid system, with an SC-assisted converter was also developed and shown at the end of the thesis.



# Acknowledgements

First of all, I would like to thank my supervisor, Assoc. Prof. Nihal Kularatna, for this research opportunity, and I am really grateful for his guidance and encouragement throughout the whole process. I am especially thankful for his patience with my poor English. I certainly could not have learned so much nor finished this project without his assistance.

Next, I would like to express my sincere thanks to Ph.D. students Nicoloy Gurusinghe and Jayathu Fernando. They helped me a lot by giving me much advice to solve technical problems. Without them, it would have taken me much longer to finish testing and building drivers for the MOSFET switch circuit.

Also, I am grateful to laboratory technicians, Mr. Viking Zhou and Mr. Benson Chang, for their continued support during the project. They both helped me find components I needed to achieve the final project outcome, and they both gave me good ideas about how to use the Altium Designer software to finish building a PCB prototype circuit.

Finally, a special thanks to my parents. They give me financial support and kept encouraging me when I struggled with difficulties and felt depressed. Your prayers for me were what sustained me thus far.

Again, thank you to everyone who gave me so much generous support.



# Table of Contents

<b>Abstract.....</b>	<b>i</b>
<b>Acknowledgements.....</b>	<b>iii</b>
<b>Table of Contents.....</b>	<b>v</b>
<b>List of Tables.....</b>	<b>ix</b>
<b>List of Figures.....</b>	<b>xi</b>
<b>Chapter 1.....</b>	<b>1</b>
<b>Introduction .....</b>	<b>1</b>
1.1 Introduction.....	3
1.2 Objectives .....	4
1.3 Dissertation Outline.....	5
<b>Chapter 2.....</b>	<b>7</b>
<b>Background .....</b>	<b>7</b>
2.1 The DC microgrid .....	9
2.2 DC Generators .....	9
2.2.1 Fuel Cells.....	9
2.2.2 Wind Turbines .....	11
2.2.3 Solar Panels .....	12
2.2.3.1 Maximum Power Point (MPP) Tracking .....	13
2.3 DC Power Distribution .....	16
2.3.1 Different Types of DC–DC Converters and Techniques .....	16
2.3.1.1 Linear Regulators and Switch-mode Regulators Techniques .....	17
2.3.1.2 Supercapacitor-assisted Low Dropout (SCALDO) Regulators Techniques.....	18
2.4 Energy Storage Devices .....	25
2.4.1 Batteries .....	26
2.4.2 Superconducting Magnetic Energy Storage .....	29
2.4.3 Supercapacitors (SCs) .....	29



2.5 DC Loads .....	30
2.5.1 Light-emitting Diode (LED) Loads .....	31
2.5.2 White-ware Loads.....	32
<b>Chapter 3.....</b>	<b>33</b>
<b>Hamilton Illuminance Field Measurements and the Use of a PV simulator and associated software .....</b>	<b>33</b>
3.1 Introduction.....	35
3.2 Waikato Climate and Weather .....	35
3.2.1 Wind .....	36
3.2.2 Rainfall Distribution .....	36
3.2.3 Air Temperature .....	36
3.2.4 Sunshine and Solar Radiation .....	36
3.2.4.1 Sunny Day Illuminance .....	38
3.2.3.2 Cloudy Day Illuminance .....	39
3.2.3.3 Rainy Day Illuminance .....	40
3.3 Illuminance-to-Irradiance Conversion.....	42
3.4 The Photovoltaic (PV) Simulator and Associated Software.....	45
3.4.1 Model, Manufacturer and Main Specifications.....	45
3.4.2 Photovoltaic (PV) Simulator Operation .....	45
3.4.2.1 Demonstration Mode .....	46
3.4.2.2 Power supply (P/S) mode .....	47
3.4.2.3 Simulation Mode .....	48
3.4.3 Creating Irradiance Profiles by Coding .....	49
3.4.3.1 A Simulated Sunny Day in Hamilton.....	50
3.4.3.2 A Simulated Cloudy Day in Hamilton.....	53
3.4.3.3 A Simulated Rainy Day in Hamilton .....	54
3.4.4 Photovoltaic (PV) Curve Creation .....	54
<b>Chapter 4.....</b>	<b>57</b>

<b>Components Testing .....</b>	<b>57</b>
4.1 Supercapacitor (SC) Characteristics.....	59
4.1.1 SC Charging Characteristics .....	59
4.1.1.2 Charging Efficiency Improvement .....	63
4.1.2 SC Discharging Characteristics.....	65
4.1.3 Equivalent Series Resistance Measurements.....	68
4.2 Light-emitting Diode (LED) Lamp Testing .....	71
<b>Chapter 5.....</b>	<b>75</b>
<b>Circuit Design and System Implementation.....</b>	<b>75</b>
5.1 Introduction.....	77
5.2 Control Circuit Design and Implementation.....	79
5.2.1 Sampling circuit .....	79
5.2.2 The MOSFET Driver Circuit .....	83
5.2.2.1 MOSFET .....	84
5.2.2.2 Gate Drivers.....	86
5.3 Switch Circuit Design and Implementation .....	90
5.3 Selection of SC Bank Size .....	96
<b>Chapter 6.....</b>	<b>97</b>
<b>Results, Conclusions and Future Developments .....</b>	<b>97</b>
6.1 Results .....	99
6.1.1 Efficiency of the DC microgrid system.....	99
6.1.2 Light Emission Times After a mains Power Outage .....	104
6.2 Discussion and Conclusions.....	104
6.3 Recommended Future Developments .....	105
<b>References.....</b>	<b>107</b>
<b>Appendix A: Prototype Circuit (SC Assisted Power Converter) .....</b>	<b>111</b>
<b>Appendix B: Prototype PCB (SC Assisted Power Converter) .....</b>	<b>112</b>
<b>Appendix C: Prototype Circuit (LED loads).....</b>	<b>113</b>

<b>Appendix D: Prototype PCB (LED loads) .....</b>	<b>114</b>
<b>Appendix E: Microcontroller Code for Switch Circuit .....</b>	<b>115</b>
<b>Appendix F: PV Simulator Codes for Creating Irradiance Profiles of a Cloudy Day and a Rainy Day .....</b>	<b>125</b>

# List of Tables

Table 2.1: Differences between linear regulators and switch-mode regulators. ....	18
Table 2.2: Rechargeable battery chemistry characteristics. ....	28
Table 3.1: The Hamilton sunny day irradiance profile codes. ....	51
Table 5.3 Switch operation.....	78
Table 5.1: Resistance selection for sampling source and terminal voltages.....	82
Table 5.2: the values of $I_G$ and $R_g$ for P-Channel and N-Channel MOSFET drivers.....	88
Table 5.5: Capacitance selection for LEDs. ....	96
Table 6.1: System running time during simulated mains power outage. ....	104
Table 7.1: Hamilton Cloudy Day Irradiance Profile Codes.....	125
Table 7.2: Hamilton Rainy Day Irradiance Profile Codes.....	127



# List of Figures

Figure 2.1: Topology of a DC microgrid. ....	9
Figure 2.2: How a hydrogen fuel cell works. ....	10
Figure 2.3: A solid oxide fuel cell (SOFC). ....	11
Figure 2.4: Wind turbines. ....	12
Figure 2.5: Photo of a solar panel array [9]. ....	13
Figure 2.6: MPP when PV modules are exposed to irradiance of 1,050 W/m <sup>2</sup> ....	14
Figure 2.7: The process of determining a MPP for a 5 Ω resistor, as per the AMETEK brand programmable PV simulator ETS600X. ....	14
Figure 2.8: Irradiance vs. time and solar panel surface temperature vs. time on a typical sunny day. ....	15
Figure 2.9: Charging an SC directly with a power supply. ....	19
Figure 2.10: The basic concept of SC (supercapacitor) energy storage and recovery. ....	20
Figure 2.11: The concept of SC energy storage and recovery. ....	21
Figure 2.12: Oscilloscope waveforms of 12-to-5 V SCALDO regulator. ....	22
Figure 2.13: The concept of SCALDO for $V_P > 2V_{in}^{min}$ ....	22
Figure 2.14: The concept of the supercapacitor-assisted low dropout (SCALDO) regulator defined by $V_P < 2V_{in}^{min}$ ....	24
Figure 2.15: The Ragone plot. ....	25
Figure 2.16: Different kinds of batteries ....	26
Figure 2.17: The typical superconducting magnetic energy storage (SMES). ....	29
Figure 2.18: Supercapacitors (SCs). ....	30
Figure 2.19: TCP brand light-emitting diode (LED) lamps used as DC loads in the current research project. ....	31
Figure 3.1: A block diagram of equipment and data processing. ....	35
Figure 3.2: Hamilton cumulative solar energy. ....	37
Figure 3.3: Sunny day illuminance at the University of Waikato (UoW) in Hamilton. ....	38

Figure 3.4: Cloudy day illuminance at the University of Waikato (UoW) in Hamilton. ....	39
Figure 3.5: Rainy day illuminance (light rain) at the University of Waikato (UoW) in Hamilton. .....	40
Figure 3.6: Rainy day illuminance (heavy rain) at the University of Waikato in Hamilton. ....	41
Figure 3.7: The calculated average sunny day irradiance curve for Hamilton. ....	44
Figure 3.8: The average calculated cloudy day irradiance curve for Hamilton. ....	44
Figure 3.9: The average calculated rainy day irradiance curve for Hamilton. ....	45
Figure 3.10: A screenshot of TerraSAS™ in demonstration mode. ....	46
Figure 3.11: Switching modes on the PV simulator.....	47
Figure 3.12: The open-circuit voltage reference and short-circuit reference settings. ....	48
Figure 3.13: A screenshot of a sunny day simulation.....	48
Figure 3.14: A screenshot of irradiance profile sample codes for irradiance profile testing..	49
Figure 3.15: A sample of irradiance profile testing. ....	50
Figure 3.16: A simulated sunny day irradiance profile I created for Hamilton. ....	51
Figure 3.17: A simulated cloudy day irradiance profile I created for Hamilton. ....	53
Figure 3.18: A simulated rainy day irradiance profile I created for Hamilton.....	54
Figure 3.19: A screenshot of the window for setting the specifications of a virtual solar panel. .....	55
Figure 3.20: A PV curve with an open-circuit voltage of 24 V and a short-circuit current of 8.3 .....	55
Figure 4.1: Charging a SC from a voltage source.....	59
Figure 4.2: Charging curve of a 2.5 F SC. ....	62
Figure 4.3: The energy distribution over time in a SC charging process. ....	63
Figure 4.4: Charging a supercapacitor (SC) by using a constant voltage source and with a resistive load (LED) connected. ....	63
Figure 4.5: Time vs. terminal voltage of the SC when it is charging and discharging, with a LED load connected. ....	64
Figure 4.6: Energy distribution over time as charging progresses. ....	65
Figure 4.7: Discharging a SC. ....	65

Figure 4.8: The energy distribution over time during a SC discharging process. ....	67
Figure 4.9: A circuit diagram of a typical discharging RC circuit.....	67
Figure 4.10: The discharge curve of a 2.5 F SC. ....	68
Figure 4.11: The equivalent circuit of a SC. ....	68
Figure 4.12: A circuit diagram of ESR measurement.....	69
Figure 4.13: A voltage drop occurs after removing the current source suddenly. ....	70
Figure 4.14: A line graph showing the performance of a single TCP brand LED .....	71
Figure 4.15: A circuit diagram of a LED performance test. ....	72
Figure 4.16: A diagram showing the moment when turned on a TCP brand LED ( $V_s = 12\text{ V}$ ). 72	
Figure 4.17: A diagram showing the moment when turned on a TCP brand LED ( $V_s = 18\text{ V}$ ). 72	
Figure 5.1: Circuit diagram of the complete DC microgrid system. ....	77
Figure 5.2: A block diagram of a DC microgrid system.....	78
Figure 5.3: Photo of the complete DC microgrid System with 12V LED loads. ....	79
Figure 5.4: The diagram for the sampling circuit. ....	80
Figure 5.5: Equivalent circuit for the case of removing OP-AMP.....	80
Figure 5.6: Equivalent circuit after adding an OP-AMP.....	82
Figure 5.7: Response of the sampling circuit. ....	83
Figure 5.8: A schematic drawing of a switch circuit with a load and a SC.....	84
Figure 5.9: A MOSFET equivalent circuit. ....	84
Figure 5.10: Resulting gate and drain waveforms during a gate-charge test. ....	86
Figure 5.11: A schematic drawing of a P-channel power MOSFET switch 1 ( $S_1$ ) gate driver. .	87
Figure 5.12: A schematic drawing of an N-channel power MOSFET switch 2 ( $S_2$ ) gate driver.	87
Figure 5.13: The MOSFET response to a 10 V PWM input signal via the MOSFET driver. ....	88
Figure 5.14: The delay (59 ns) in turning on the MOSFET SPP80P06P H without the small resistor ( $I_D = 1.5\text{ A}$ ; $V_{GS} = 10\text{ V}$ ; $R_g = 1.5\ \Omega$ ). ....	89
Figure 5.15: The delay (881 ns) in turning on the MOSFET SPP80P06P H with the small resistor ( $I_D = 1.5\text{ A}$ ; $V_{GS} = 10\text{ V}$ ; $R_g = 10\ \Omega$ ). ....	89
Figure 5.1: Circuit diagram of the complete DC microgrid system. ....	90



Figure 5.16: The ideal running situation for the DC microgrid.....	91
Figure 5.17: ‘Real life’ oscilloscope reading obtained when running the DC microgrid switch circuit. ....	93
Figure 5.18: A flow chart showing how the microcontroller ‘makes decisions’ in directing DC microgrid operations. ....	95
Figure 6.1: The terminal voltage of one of the SC banks, when the system was running at a steady state. ....	100
Figure 6.2: Stage 1, $t_1$ – $t_2$ , as the SC bank 2 charged. ....	100
Figure 6.3: Stage 2, $t_2$ – $t_3$ , when the right-hand SC bank 2 was disconnected from its power source and released its stored energy to power the LED array 2. ....	101
Figure 6.4: Irradiance vsDC microgrid system efficiency on a sunny day. ....	102
Figure 6.5: Irradiance vs. DC microgrid system efficiency on a cloudy day. ....	102
Figure 6.6: Irradiance vs. DC microgrid system efficiency on a rainy day. ....	103
Figure 6.7: Efficiency vs. line voltage at various capacitances. ....	103
Figure 7.1: Prototype Circuit of the SC Assisted Power Converter .....	111
Figure 7.2: Prototype PCB of the SC Assisted Power Converter .....	112
Figure 7.3: Prototype Circuit of the LED loads .....	113
Figure 7.4: Prototype PCB of the LED loads .....	114

# **Chapter 1**

## **Introduction**



# 1.1 Introduction

Today, mains electrical systems provide alternating current (AC) power to our electrical devices. However, with the increasing popularity of renewable technologies, such as wind power, fuel cells and solar photovoltaics (PVs), direct current (DC) microgrids at a household level could be a more efficient alternative. The surplus energy generated by these DC generators could also be fed back to AC mains, which could help to reduce electricity costs as well.

One of the 'hot topics' currently being discussed about DC microgrids is how to make good use of this unregulated power, which is generated by DC generators. Two types of DC-to-DC converter are suitable for a DC microgrid: DC-to-DC converters with isolation or without isolation. The non-isolated converter does not use a transformer. Without the transformer, the overall size of the converter can be reduced by removing this bulky component. Also, a significant amount of energy wastage from having a transformer can also be minimised.

In modern electronics, the following three basic approaches are available for DC-to-DC conversion [1]:

- linear regulators,
- switched-mode converters, and
- charge pumps.

In linear regulators, a power semiconductor device is used as a voltage dropper in the series path between the unregulated DC input and the regulated output [1]. It has very low noise output, with fast transient response to sudden changes in load current. However, the voltage drop on the voltage dropper can be very high, and this leads to a very low efficiency (30%–60%) [1]. Switched-mode converters use inductors and capacitors as energy storage devices to convert one DC voltage to another, with a theoretical 100% efficiency. The switches of this converter operate at a high frequency, which causes electrical noise problems if not carefully suppressed. Charge pumps have their own problems: they have a low current capability, typically limited to few hundred mA only [1].

Because of the disadvantages inherent in these three commercially available DC-to-DC converters, there are still opportunities to develop novel DC-to-DC converters. Therefore, my aim in the current dissertation was to design a converter that was not only highly efficient but that also had a high current capability and low electrical noise.

## 1.2 Objectives

In this dissertation project, a low electrical noise, high current capability and high efficiency DC-to-DC converter was designed and implemented using supercapacitors (SCs) and metal-oxide semiconductor field effect transistors (MOSFETs). The SC-assisted low dropout regulator (SCALDO) was one of the main technologies used to design this converter. This design required an SC or an SC array as a voltage dropper. A low dropout regulator (LDO) was followed and placed in series with the SC. Since the capacitance is large (of the order of farads [F]), the SC can pass current for a period of time when it is being charged. Therefore, a switching circuit with MOSFET switches was used to discharge the SC to deliver energy to loads via LDO after the SC was charged to a certain level.

As mentioned in detail in Chapter 4, Section 4.1.1, there is a non-negligible amount of energy wasted in the loop resistance when charging a capacitor in a simple resistor–capacitor (RC) circuit. The efficiency of this RC circuit is just 50 % in case that the capacitor is fully discharged before charging, which means half of the total energy delivered from a power supply is wasted in the loop. However, if a resistive load is connected in series into the loop, this large amount of wasted energy is mostly used by the resistive load. By applying this simple principle, it is possible to improve system efficiency.

In a DC microgrid system, solar panels are commonly used as a DC power supply. In the present research, the main purpose was to design a converter and a related circuit for a DC microgrid that used a solar panel as a power supply and that could be used to power a 12 V household light-emitting diode (LED) system (10 LED lamps, 5 W each). Therefore, how to extract the maximum power from a solar panel was another problem that required solving in the current dissertation project, because output current increases while output voltage drops.

Therefore, the overall objectives of the design were as follows.

- Understand a technology to ascertain the maximum power that a solar panel can provide.
- Collect Hamilton region illuminance and irradiance data to create similar patterns for a photovoltaic (PV) simulator (with prior knowledge of regional illuminance and irradiance patterns, experiments can be performed at any time and at any place, and the experiments will not be influenced by outdoor weather conditions).
- Develop a converter with a switching circuit to run a 12 V household lighting system powered by 20 V (or higher) solar panels.
- Estimate the efficiency of this DC microgrid system.

## 1.3 Dissertation Outline

This dissertation is divided into six chapters.

**Chapter 1** provides a summary of the entire dissertation, including the reasons why I chose to undertake this project, the overall objectives of the design and a brief description of each of the following five chapters.

**Chapter 2** is a general overview of the components, applications and technologies that are a part of a DC microgrid. In this chapter, I aim to provide a general understanding of today's status quo for DC microgrids, DC generators and DC appliances. Since AC electrical systems already exist, I also explore the reasons why further development of the DC microgrid is important. In this chapter, three types of DC-to-DC converters were compared in terms of the technologies used and their advantages and disadvantages. Two types are commonly used today, while the third one (an SC-assisted converter) is not commonly used but has broad development prospects. Finally, the last section provides a brief analysis of LED lamps. Knowing LED lamp characteristics helps the inventor build a better DC microgrid system with LED loads.

**Chapter 3** is broadly divided into three parts. In the first sections, I explore Waikato region weather and explain field measurements of illuminance. The field measurements were done at the C block of the University of Waikato (UoW). The UoW is located in Hamilton, a city in the middle of the North island of New Zealand. Hamilton's weather changes frequently. By collecting and analysing Hamilton weather data over time, users were able to create similar patterns of illuminance for testing. These patterns were therefore representative, which helped users to avoid bias when testing outdoors and when using solar panels to power the DC microgrid system in differing weather conditions. In Chapter 3, there is an explanation on how to convert illuminance to irradiance, because irradiance data are useful for a solar panel or a PV simulator, while the light meter available in the laboratory is only able to measure illuminance, rather than irradiance. Finally, I showcase the laboratory equipment (a PV simulator and its associated software) I used for generating simulated outputs similar to the real-time outputs of a solar panel. These sections begin with a brief introduction of the programmable photovoltaic simulator ETS600X, its main specifications and operating modes. In the following sections, I show how to create the irradiance profiles and photovoltaic curves (necessary for subsequent DC microgrid development) by coding.

**Chapter 4** contains a description of the testing of the main components (SCs and TCP brand LED lamps) used in the current research. I did the SC experiments to measure the equivalent series resistance of an SC and to ascertain its charging / discharging

characteristics. In Chapter 4, I also describe a test to evaluate TCP brand LED lamp performance and how I made the lamps work normally.

**Chapter 5** deals with the design and the implementation of the DC-to-DC converter, which was based on two SC banks. This chapter is broadly divided into three sections. In the first section, the design and operation of a control circuit were described. This circuit was further divided into a sample circuit and a driver circuit for MOSFET switches. In the second part of the chapter, I explain the design and implementation of a switch circuit. This part also shows switching routines and how decisions are made by a microcontroller under particular situations. The last section of Chapter 5 shows my calculations of the needed capacitance for each SC bank. Capacitance selection influences how long the system can remain working after a sudden power outage.

**Chapter 6** focuses on research results, main findings and a discussion of the findings in relation to my research objectives. Some recommendations are given for improving system performance and provide a conclusion about how fit-for-purpose the DC microgrid actually is. There is also a discussion about the possible future developments of this type of DC-to-DC converter in order to adjust the converter to power large appliances (loads), such as whiteware.

# **Chapter 2**

# **Background**





## 2.1 The DC microgrid

A DC microgrid (Figure 2.1) is a localised power system. It consists of distributed DC generation assets (e.g., wind turbines, solar panels or fuel cells), energy storage devices (e.g., batteries, SCs or superconducting magnetic energy storage), loads (e.g., appliances, computers or lighting) and smart distribution technologies that interoperate through controls and software-based intelligence systems [2].

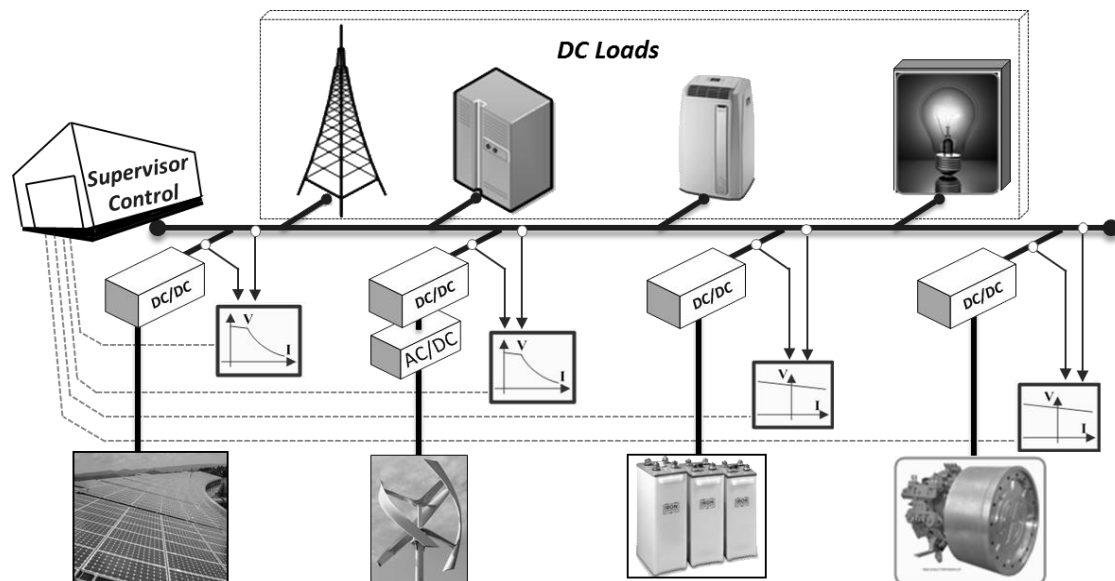


Figure 2.1: Topology of a DC microgrid [3].

## 2.2 DC Generators

The DC generator is a machine that converts mechanical, solar, wind or other forms of energy into electrical energy. This type of generator provides DC power to the loads. The most popular DC generators available now are fuel cells, wind turbines and solar panels.

### 2.2.1 Fuel Cells

Like a battery, a fuel cell generates electricity from an electrochemical reaction. Both of them convert chemical energy into electrical energy. This process also generates heat as a by-product. However, a battery holds a closed store of energy within it. Once the energy is depleted, the battery must be discarded or recharged by using an

external power supply to drive the electrochemical reaction in the reverse direction. On the other hand, a fuel cell uses an external supply of chemical energy and can run as long as it is supplied with enough fuel.

There are many types of fuel cell, but they are all based on a similar design. A fuel cell is made up of many cell units. Each unit consists of a stack, which is composed of a number of individual cells. Each cell has two electrodes: the cathode and the anode. One is positive and the other is negative. The chemical reactions producing electricity take place at the electrodes. Figure 2.2 below illustrates how a typical fuel cell (a hydrogen fuel cell) works. Every fuel cell has either a liquid or a solid electrolyte as well as a catalyst. The catalyst accelerates the reactions at the electrodes, while the electrolyte carries ions from one electrode to the other. The electrolyte used must permit only the appropriate ions to pass between the electrodes. If free electrons or other substances pass through the electrolyte, they may cause negative impacts on chemical reactions and may lower the efficiency of the cell.

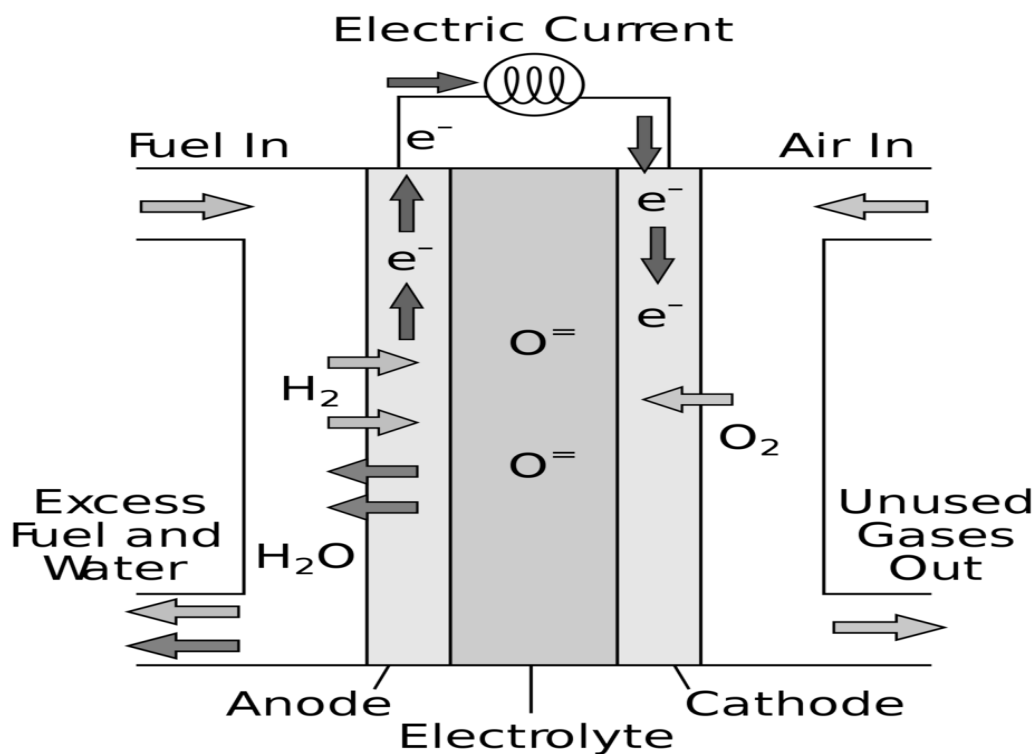


Figure 2.2: How a hydrogen fuel cell works [4].

Fuel cells are generally classified according to the type of the electrolyte used. Each type of fuel cell requires a particular fuel and materials. Each kind of fuel cell also has its own characteristics, offering advantages in particular applications. Figure 2.3 shows one of the typical fuel cells available today (a solid oxide fuel cell [SOFC]).



Figure 2.3: A solid oxide fuel cell (SOFC) [5].

However, fuel cells that use non-renewable fuel (e.g., natural gas) are not clean. To make fuel cells cleaner, natural gas can be replaced by biofuels. Unfortunately, biofuels are still not a viable technology — they are expensive to produce and store. In order to be fully deployable, biofuel sources have to be near customer-rich cities, which limits biofuels to places in some countries that have very high population density, such as cities in China, Japan and India. In addition, the hydrogen necessary for running hydrogen fuel cells is difficult to generate, handle and store; it requires heavy and bulky tanks like those used for compressed natural gas.

## 2.2.2 Wind Turbines

Wind energy is a source of renewable energy that comes from air currents flowing across the Earth's surface. Wind turbines (Figure 2.4) harvest this kinetic energy and convert it into usable energy, which can provide electricity.



Figure 2.4: Wind turbines [6].

Wind power is one of the fastest growing sources of energy in the world today. In New Zealand, wind power generates a small but rapidly growing proportion of the country's electricity. As of 2016, wind power accounted for 690 MW of installed capacity and nearly 5 % of electricity generated in the country [7].

The electricity produced from wind power is clean because this process does not produce any pollution or greenhouse gases. However, wind energy is unpredictable and is not constantly available because wind is not always there. Turbine noise can also be a problem for those people who live near the wind turbines. Therefore, building wind turbines in urban areas should be considered carefully in relation to other available options.

### 2.2.3 Solar Panels

Solar panels (Figure 2.5) harness the sun's energy in the form of light and convert the energy into electricity. The smallest unit of a solar panel is a solar cell, also called a PV or photovoltaic cell; it is the individual PV cell that turns sunlight into electricity. Individual cells arranged in a group are called a "module" or panel [8]. Each panel can gather between 10 W and 300 W.



Figure 2.5: Photo of a solar panel array [9].

The advantages of using solar power are worth noting. Obviously, solar panels give off no contamination. Therefore, just like wind energy, solar energy is also a clean energy source. In other words, once the panels are installed, they are doing almost nothing negative to the atmosphere. In addition, solar energy is one of the renewable energies. This means we can use it as long as we want while the sun is there, unlike fossil energies, which will expire in another few hundred years.

### 2.2.3.1 Maximum Power Point (MPP) Tracking

Maximum power point tracking (MPPT) is an algorithm and a method used for extracting maximum available power from PV modules. This algorithm is fulfilled by a charge controller. This controller, a high-power sampling resistor and a current limiter, is integrated into a maximum power point (MPP) tracker. By sampling the resistor, it is viable for the controller to ascertain the real-time output power. How long it takes to determine the MPP is dependent on how good the proportional–integral–derivative (PID) algorithm is. The MPP tracker integrated into the AMETEK brand programmable PV simulator ETS600X requires 1.08 s to determine the MPP for a resistor. It may be longer if the load is a non-linear element. In Figure 2.6, the yellow dash shows the MPP under specific conditions. The procedure for tracking MPP begins from the time when maximum current limit is applied to the loop. Thereafter, this limit diminishes gradually. The process of tracking MPP is illustrated in Figure 2.7.

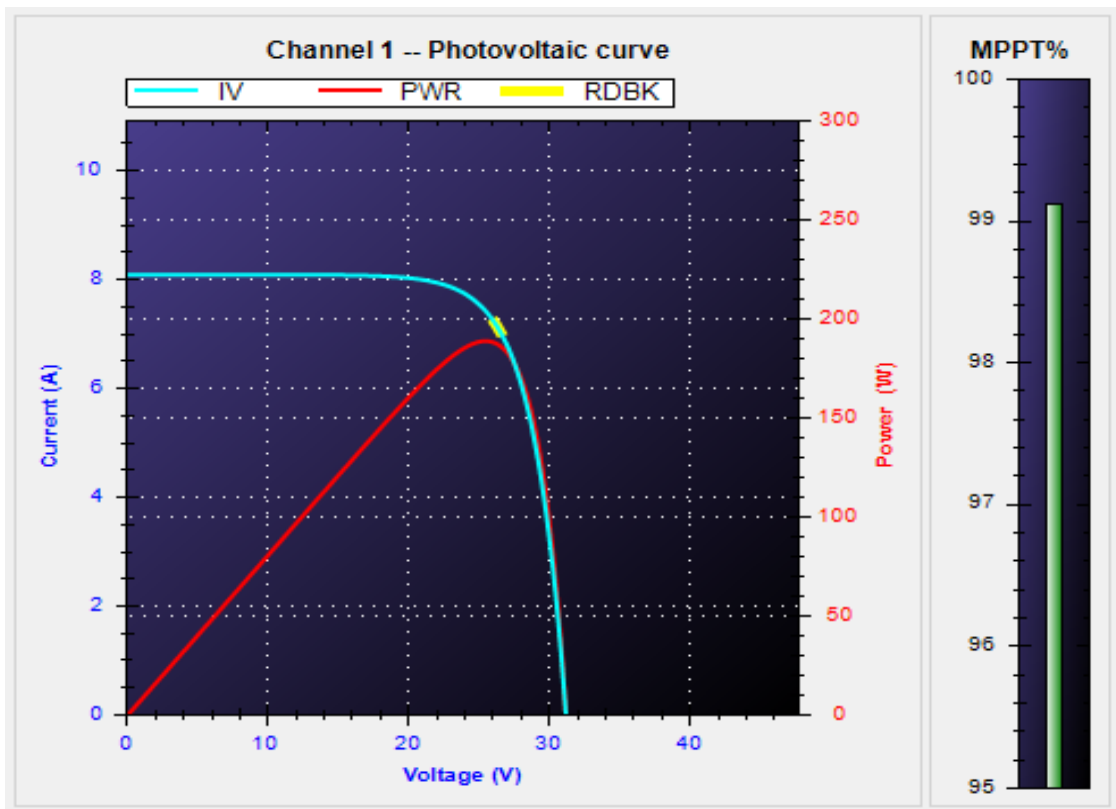


Figure 2.6: The maximum power point (MPP) when photovoltaic (PV) modules are exposed to irradiance of 1,050 W/m<sup>2</sup>.

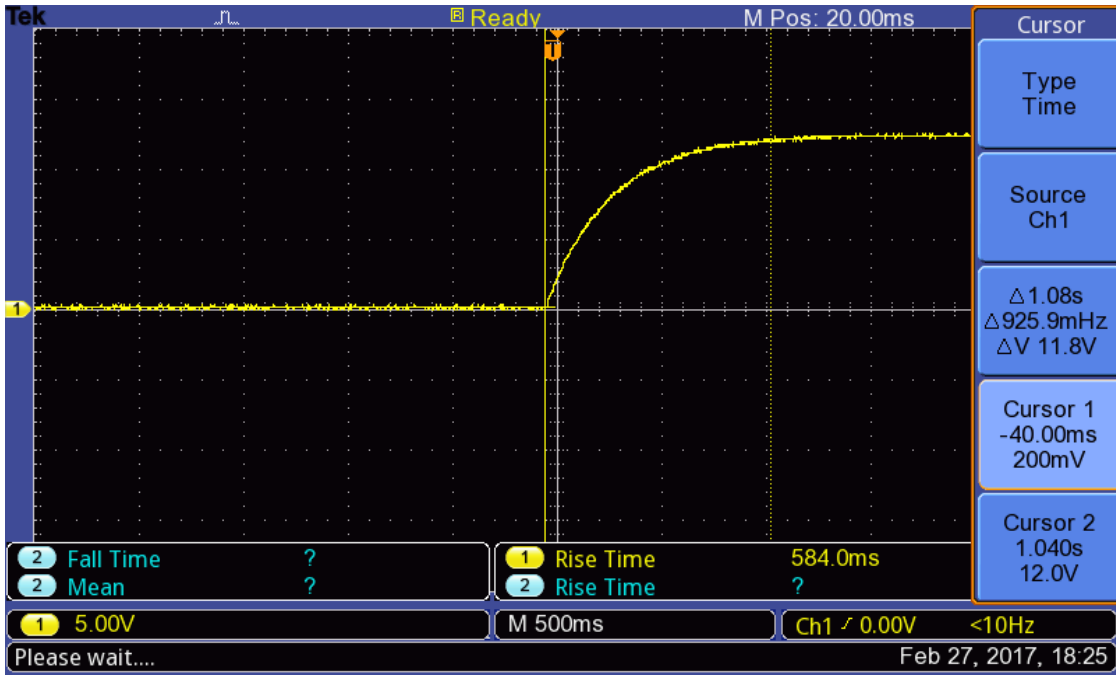


Figure 2.7: The process of determining a maximum power point (MPP) for a 5  $\Omega$  resistor, as per the AMETEK brand programmable photovoltaic (PV) simulator ETS600X.

Maximum power varies with solar radiation and solar cell temperature. The AMETEK brand PV module in the UoW laboratory produces power with maximum voltage of around 30 V (different types of PV module have different output voltage), when it is measured at a cell temperature of 25 °C. The output voltage increases while solar radiation increases. The voltage may drop to 27 V on a very hot day and may rise to around 32 V on a very cold day. Figure 2.8 illustrates irradiance and temperature curves on a typical sunny day.

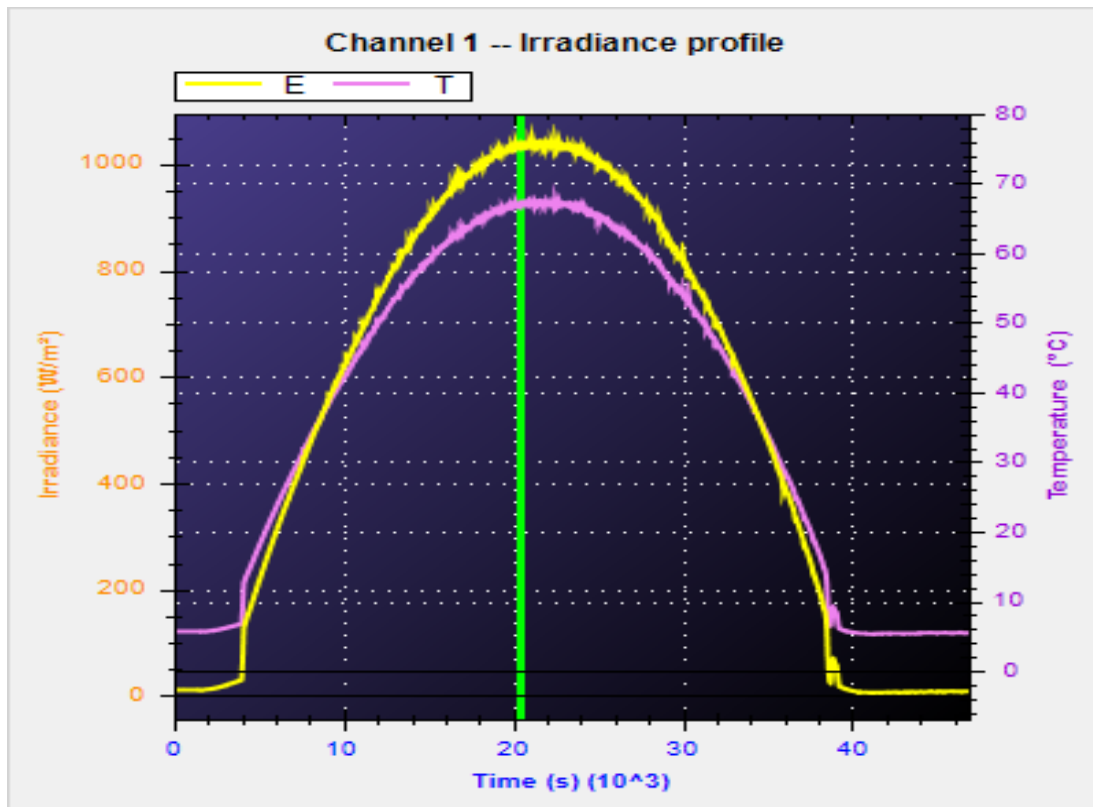


Figure 2.8: Irradiance versus (vs.) time and solar panel surface temperature vs. time on a typical sunny day.

Figures 2.6–2.8 are screenshot images generated in a laboratory setting by the AMETEK brand programmable PV simulator ETS600 internal software [10]. An MMP tracker is an integral part of the AMETEK PV simulator. However, not all solar panels have MPP trackers. Where solar panels do not have their own MPP trackers, an external tracker between the solar panels and the microgrid is required.



## 2.3 DC Power Distribution

DC power is typically distributed at extra-low voltage power systems of 12 V or 24 V, or at the telecommunications standard voltage of 48 V. This type of power distribution provides immunity to sensitive electronic equipment from harmonic distortions. In addition, replacing AC-to-DC converters attached to individual loads with more efficient, centralised inverters can decrease power consumption by 15 %, compared with conventional AC configurations [11].

DC power distributions in commercial facilities are also evolving as cost-competitive options due to the availability of inexpensive, highly efficient LED lamps. In addition, DC-powered air-conditioning or washing machine units yield greater efficiency compared to their AC counterparts. Modern AC-powered, efficient air-conditioning or washing machine units with brushless DC permanent magnet motors are driven by variable frequency drives. This type of drive initially converts the AC input into DC power, and then applies pulse-width modulation (PWM) to create the desired output frequency. Hence, DC-powered variable frequency drives can bypass the losses associated with power rectification. Similarly, variable-speed compressors with brushless DC motors in air conditioners offer utmost energy savings for refrigerating equipment. Thus, DC-powered refrigerating equipment has inherent efficiency advantages in the marketplace.

In fact, the authors of a recent study [12] calculated that there was a 33 % energy saving for a typical residential building when conventional AC appliances were replaced by more efficient, DC power-driven appliances. DC power distribution is especially economical when a facility incorporates distributed renewable energy resources, such as solar PV panels, because they can supply power to the DC loads directly, without the double conversions involved in AC distribution systems (e.g., DC–AC–DC conversions) [11].

### 2.3.1 Different Types of DC–DC Converters and Techniques

Another important item available in the DC power distribution systems is the DC–DC converter. These converters can be found in any DC appliance. They convert DC power from a given voltage to a needed level. Voltage regulator LM7805, available from many suppliers, is one of the most popular linear regulator integrated circuits (ICs) used to convert high input voltage (abbreviated as  $V_{in}$ , which usually should be within the range of 7 V to 25 V) to a 5 V output. The universal serial bus (USB) car

charger is another common DC-to-DC converter used to convert a 12 V output from an automobile storage battery into 5 V power.

One or more DC–DC converter techniques are applied to all converters. The most commonly used techniques are the linear regulator technique and the switch-mode regulator technique. They are discussed in detail in Chapter 3. However, in the present research, the SC-assisted low drop-out regulator (SCALDO) technique, a new technique developed at the University of Waikato (UoW), was applied to build an SC-assisted converter for a DC microgrid system.

### 2.3.1.1 Linear Regulators and Switch-mode Regulator Techniques

Linear regulators are a great choice for powering very low-powered devices or applications where the difference between the input and output is small. Unfortunately, even though they are easy to use, simple to make and are cheap to buy, linear regulators are normally inefficient [13].

The equation for dissipated power,  $P$ , in a linear regulator is:

$$P = (V_{in} - V_{out}) \times I_{load} \quad (2.1),$$

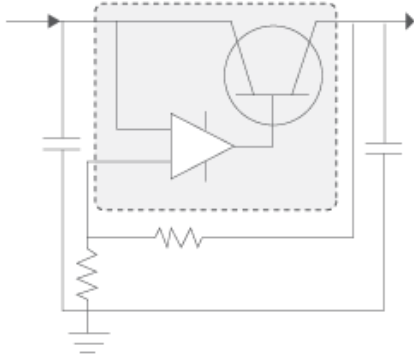
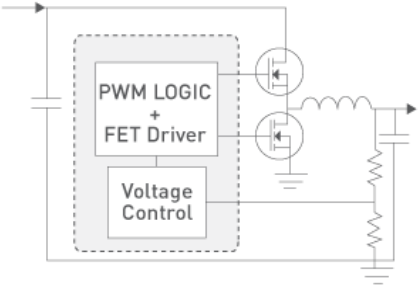
Where  $V_{in}$  is the input voltage,  $V_{out}$  is the output voltage and  $I_{load}$  is the current flowing through the load.

If a linear regulator is used to power devices in which there is a big difference between the input and output, the energy dissipating on the voltage dropper (e.g., MOSFET, insulated-gate bipolar transistor [IGBT] or a bipolar power transistor) will generate a large amount of heat. This leads to a very low efficiency and causes components to burn out.

Compared to linear regulators, switch-mode regulators are highly efficient and have a theoretical efficiency of 100 %. Switch-mode regulators are available as modular chips, which are compact and reliable. Their disadvantage is that switch-mode power supplies are more complicated and can cause electrical noise problems if not carefully suppressed.

The main differences between linear regulators and switch-mode regulators are depicted in Table 2.1.

Table 2.1: Differences between linear regulators and switch-mode regulators.

	Linear regulator	Switch-mode regulator
<b>Control</b>		
<b>Design flexibility</b>	Buck	Buck, boost, buck-boost
<b>Efficiency</b>	Normally low to medium-high for low differences between $V_{in}$ and $V_{out}$	High
<b>Complexity</b>	Low	Medium to high
<b>Size</b>	Small to medium, larger at higher power	Smaller at similar higher power (depending on the switching frequency)
<b>Total cost</b>	Low	Medium to high — external components
<b>Ripple/noise/EMI</b>	Low	Medium to high
<b><math>V_{in}</math> range</b>	Narrow (depending on power dissipation)	Wide

### 2.3.1.2 Supercapacitor-assisted Low Dropout (SCALDO) Regulator

#### Techniques

Supercapacitor-assisted low drop-out regulator designs are not common. This is a new research area currently under development at UOW. Therefore, before discussing the concepts of SCALDO, some of the following fundamentals are reviewed to aid understanding.

If a capacitor is charged directly by a power supply, as show in Figure 2.9, the terminal voltage of that SC is (assuming that at the outset, there is no energy stored in the SC) defined by the following equation:

$$U_c = U_s \cdot \left(1 - e^{-\frac{t}{rC}}\right) \quad (2.2),$$

where  $C$  is the capacitance of the SC, and  $U_c$  and  $U_s$  are the terminal voltage of the SC and the power source, respectively.

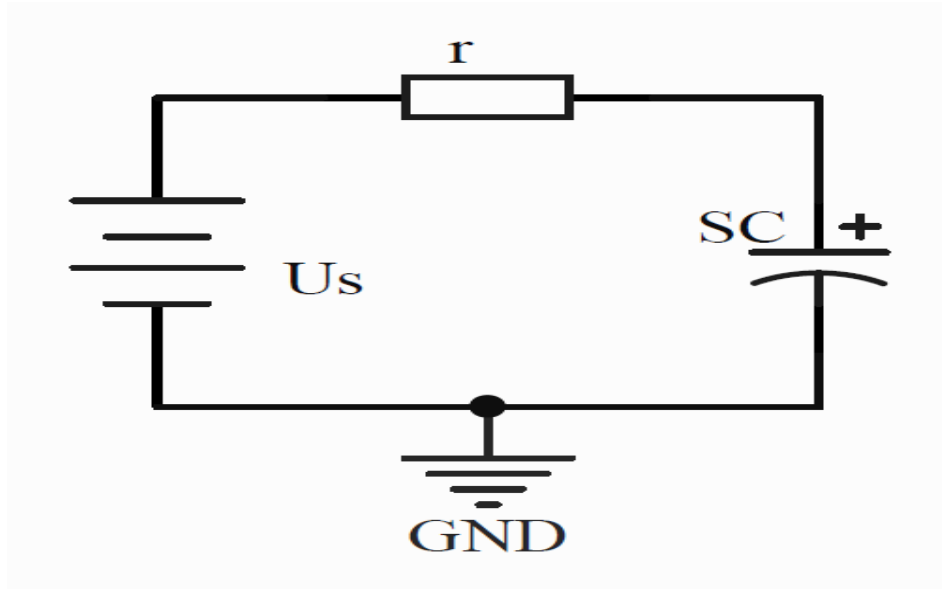


Figure 2.9: Charging an SC directly with a power supply.

The following equations also apply (details are explored in Chapter 4):

$$E_s = \int_0^t i U_s dt = C U_s^2 \left(1 - e^{-\frac{t}{rC}}\right) \quad (2.3),$$

$$E_c = \frac{1}{2} C U_c^2 = \frac{1}{2} C U_s^2 \left(1 - e^{-\frac{t}{rC}}\right)^2 \quad (2.4), \text{ and}$$

$$E_r = \int_0^t i^2 r dt = \frac{1}{2} C U_s^2 \left(1 - e^{-\frac{2t}{rC}}\right) \quad (2.5).$$

When time ( $t$ ) becomes bigger than the  $5rC$  time constant,  $E_c$  then equals  $E_r$ . This means that half of the total energy is wasted and dissipates on the resistor,  $r$ . However, if a resistive load,  $R_x$ , is connected in series with capacitor (as in Figure 2.10a), almost all of this wasted energy is used to power the load instead. This significantly increases system efficiency.

Based on the simple principles elucidated in Equations 2.2–2.5, using a single SC or an array of SCs in the series path to store and release energy (as in Figure 2.10), an SC-based efficiency improvement technique suitable for linear regulators was designed.

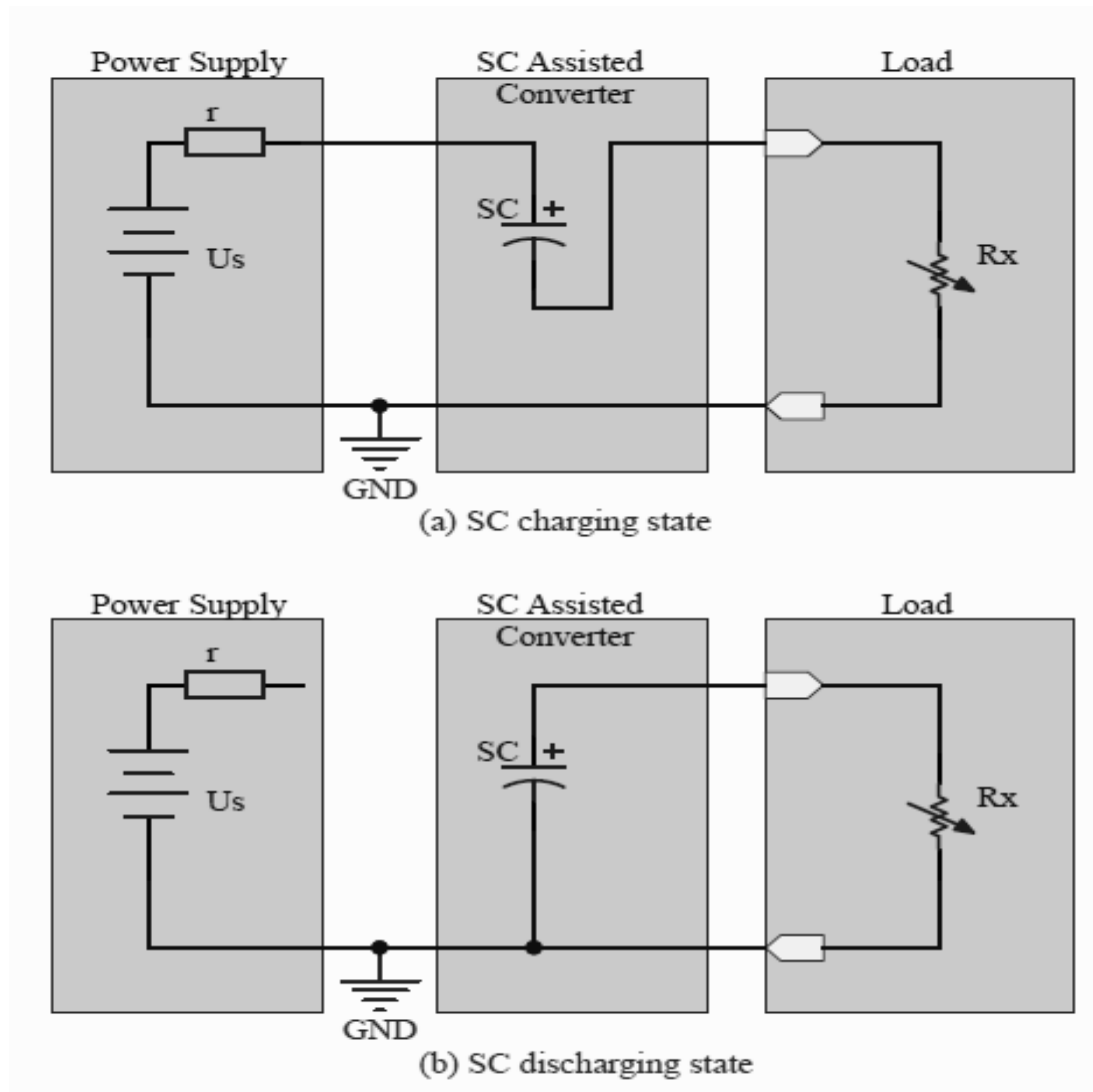


Figure 2.10: The basic concept of SC (supercapacitor) energy storage and recovery: (a) minimising the series element dissipation, and (b) releasing stored energy.

### 2.3.1.2.1 Basic SCALDO Concepts

Figure 2.11 illustrates the basic concepts of SCALDO. In Figure 2.11 (a), an SC ( $C_{SC}$ ) with a large capacitance (of the order of farads) is able to pass current for a reasonable period of time when it is charged by a power supply ( $V_P$ ). In this phase, SC acts as a voltage dropper in the loop. It is used to store energy and to prevent the  $V_{in}$  from climbing too high.

The operation is switched to the next phase (Figure 2.11 b) after the SC is charged to a certain voltage level ( $V_{in}$  drops to the minimum allowable voltage  $V_{in}^{\min}$ ). Then, the SC acts as a power supply, releasing its stored energy to an LDO and  $R_L$ . This discharging process lasts for a reasonable period of time.

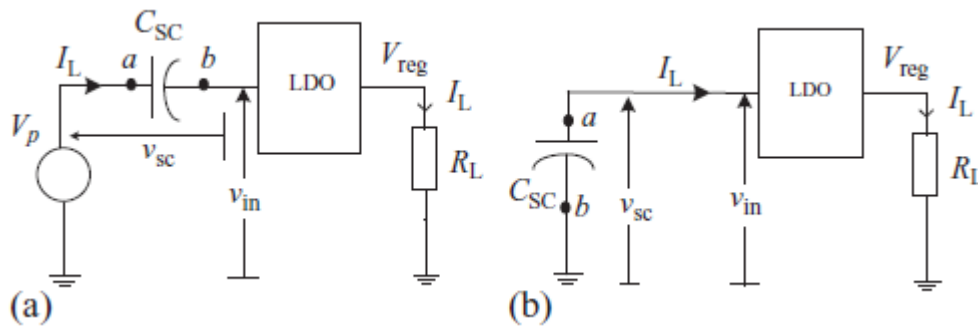


Figure 2.11: The concept of SC energy storage and recovery: (a) charging SC (b) discharging SC [1]

This basic SCALDO concept can be applied in a situation that requires conversion of a 12 V unregulated power supply ( $V_P$ ) to a 5 V regulated output ( $V_{reg}$ ). Figure 2.12 shows the steady state of operation in a real circuit with controlled switches assembled according to Figure 2.11. The load is a constant-current sink (load current  $[I_L] = 200 \text{ mA}$ ).

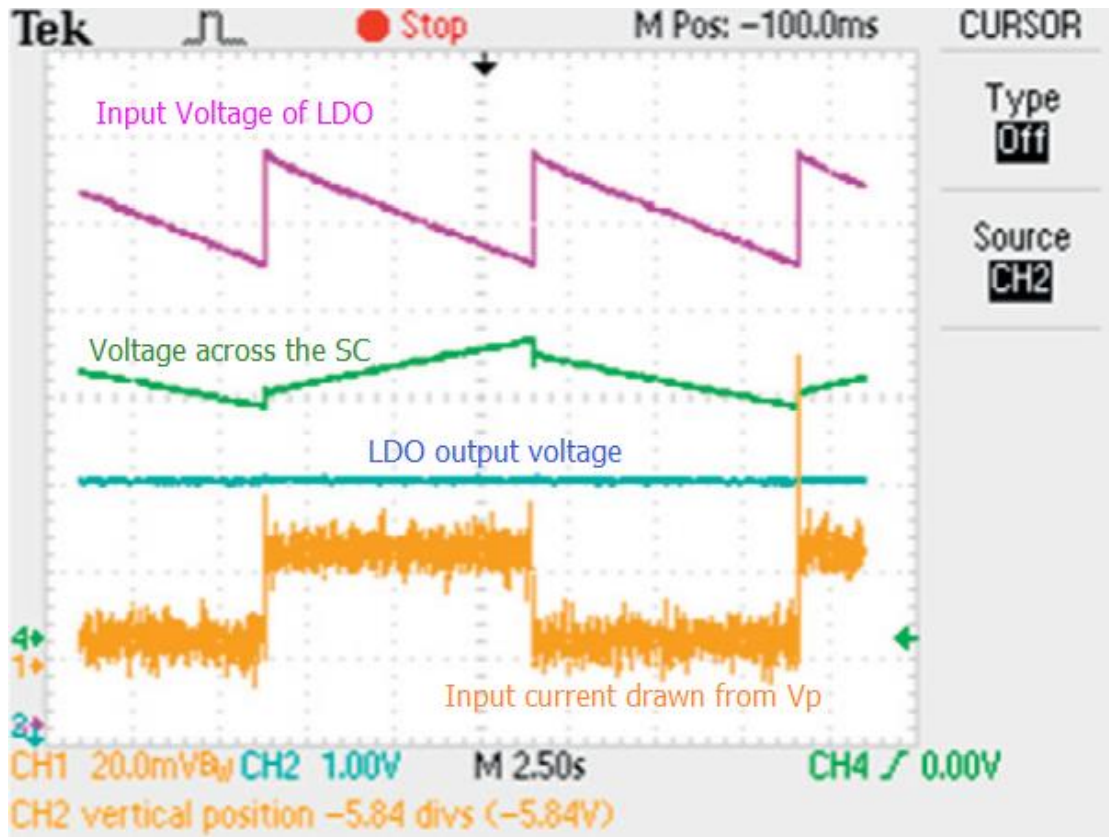


Figure 2.12: Oscilloscope waveforms of 12-to-5 V SCALDO regulator [1]

### 2.3.1.2.2 General SCALDO Concepts

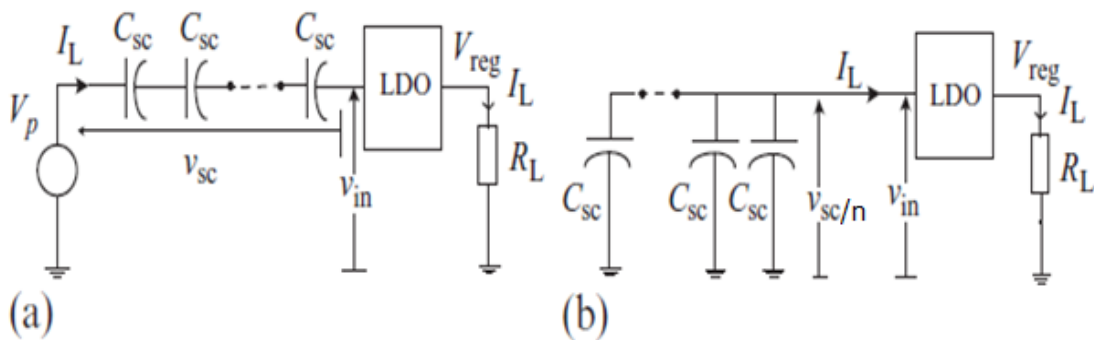


Figure 2.13: The concept of SCALDO for  $V_p > 2V_{in}^{min}$ : (a) charging  $n$  capacitors in series with LDO and  $R_L$ , thus minimising the series element dissipation, and (b) discharging  $n$  capacitors in parallel and releasing stored energy [1].

As shown in Figure 2.13 (a),  $V_{in}^{\min}$  is the minimum input voltage required for the LDO regulator. An array of  $n$  ideal series SCs is placed in series with the input of the LDO regulator. Each of the SCs has a voltage of  $V_{sc}/n$ , also equal to

$$\frac{V_P - V_{in}}{n} \quad (2.6).$$

As in Figure 2.13 (b), the voltage value of each SC should be larger than  $V_{in}$ . Therefore, the following formula can be obtained:

$$\frac{V_P - V_{in}}{n} > V_{in} \quad (2.7).$$

By rearranging this inequality, it can be shown that the number of the SCs ( $n$ ) needed should be smaller than the value of

$$\frac{V_P - V_{in}}{V_{in}} \quad (2.8).$$

Note that  $n$  represents the number of SCs required. Therefore, it should be rounded down to an integer.

Things are different in the case where

$$V_P < 2V_{in}^{\min}. \quad (2.9).$$

Figure 2.14 illustrates the SCALDO regulator concept derived from Equation 2.9.



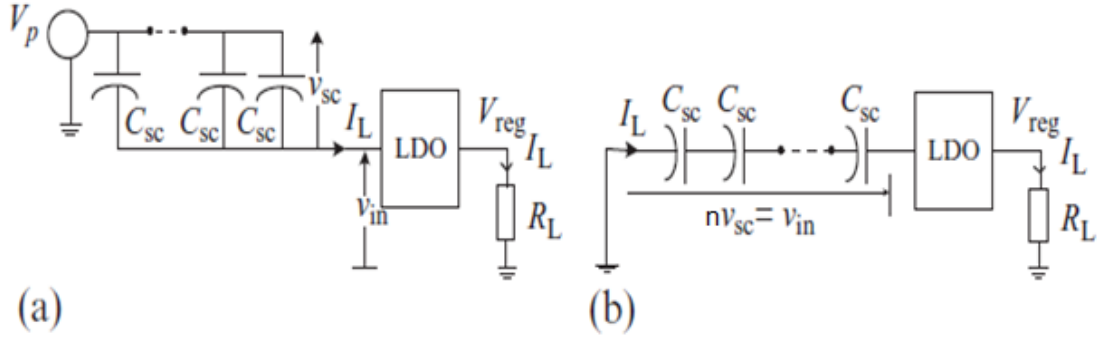


Figure 2.14: The concept of the supercapacitor-assisted low dropout (SCALDO) regulator defined by  $V_P < 2V_{in}^{min}$ : (a) charging an  $n$  parallel capacitor array with LDO and  $R_L$ , thus minimising the series element dissipation, and (b) discharging  $n$  capacitors in series, releasing stored energy [1].

As in Figure 2.14 (a),

$$V_{sc} = V_P - V_{in} . \quad (2.10).$$

In Figure 2.14 (b), the following equation also applies:

$$n \times V_{sc} > V_{in} \quad (2.11).$$

By combining these two formulas together, it becomes apparent that the number of SCs should be higher than the value of

$$\frac{V_{in}}{V_P - V_{in}} \quad (2.12).$$

Note that  $n$  represents the number of SCs. Therefore, it should be rounded up to an integer.

### 2.3.1.2.3 The LDO-removed Scenario

In this research, an SC-assisted power converter was needed to power a 12 V household LED lighting system. The LDO can be removed due to the characteristics (mentioned in detail in Chapter 4, Section 4.2) that LED provides light with a constant illuminance over a voltage range of 5.3 V to > 17 V. Therefore, removing the LDO has little influence on the illuminance of an LED. Meanwhile, energy dissipating on the LDO is also minimised. From the above, in designing the SC-assisted power converter for the DC microgrid system used in this research, it was better to remove the LDO.

## 2.4 Energy Storage Devices

The Ragone plot (Figure 2.15) illustrates the differences in energy density versus (vs.) power density of some typical energy storage devices. All energy storage devices have their own characteristics and are suitable for particular types of electronic equipment.

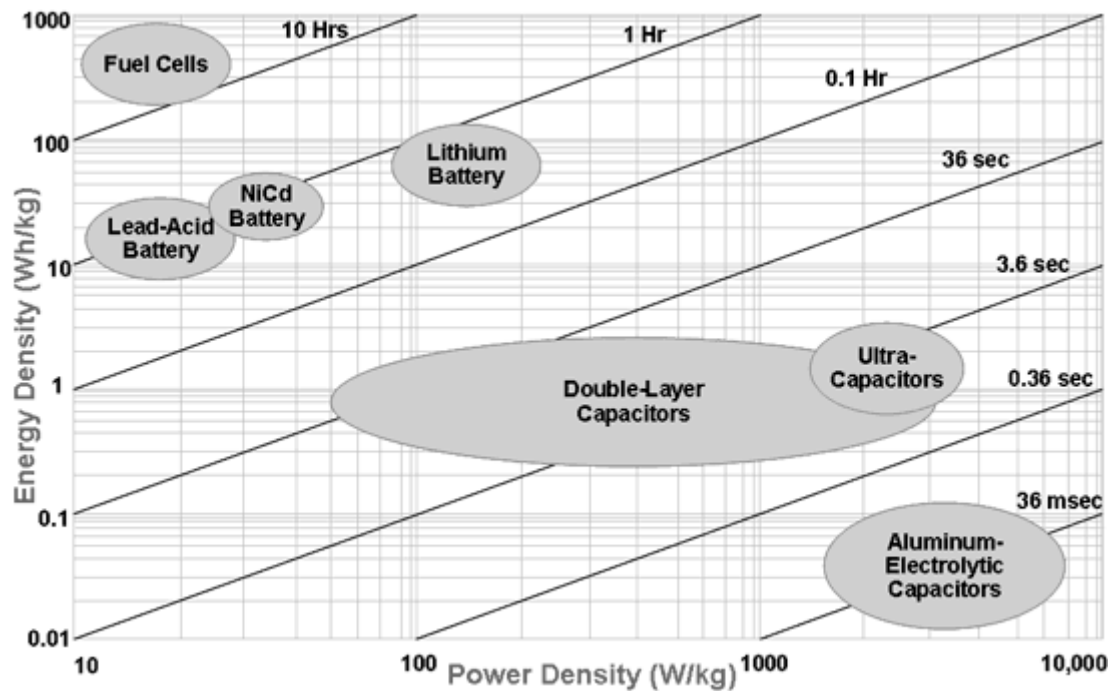


Figure 2.15: The Ragone plot [14].

## 2.4.1 Batteries

Just like a fuel cell, a battery also consists of two electrodes: the cathode and the anode. They are isolated by a separator and are soaked in electrolyte to accelerate chemical reactions. Batteries can be broadly divided into two groups: primary batteries (these batteries are designed to be used once and discarded) and secondary batteries (rechargeable batteries). As shown in Figure 2.16, all batteries (including primary batteries and secondary batteries) can be designed in different sizes and shapes and have different characteristics.



Figure 2.16: Different kinds of batteries.

Primary batteries, also known as non-rechargeable batteries, play an important role, especially when charging is impractical or impossible, such as in military combat, rescue missions and forest-fire services [15]. These batteries are usually cheaper than rechargeable batteries. Compared with primary batteries, secondary batteries offer lower energy density and higher self-discharge rates. However, rechargeable batteries certainly help to save a lot of money in the long run, because they can be used hundreds or even thousands of times if they are used properly. In addition, rechargeable batteries also help to protect the environment as well as conserve resources, since fewer batteries need to be manufactured, while they can be used over and over again.

Common rechargeable chemistries are based on variations of lead–acid, nickel-based and lithium-based systems mainly, while limited zinc-based systems and

rechargeable alkaline batteries are also available [1]. Table 2.2 depicts the basic characteristics of the major chemistries used in battery manufacture.

Parameter	Units/conditions	Sealed lead acid	NiCd	NiMH	Li-Ion	Li-polymer	Li-iron phosphate	Rechargeable alkaline
Average cell voltage	V	2.0	1.2	1.2	3.6	1.8-3.0	3.2-3.3	1.5
Relative cost	NiCd = 1	0.6	1	1.5-2.0				0.5
Internal resistance		Low	Very low	Moderate	High	High	High	
Self-discharge	%/month	2-4%	15-25%	20-25%	6-10%	18-20%		0.3%
Cycle life	Cycles to reach 80% of rated capacity	500-2000	500-1000	500-800	1000-1200		1500-2000	<25
Overcharge tolerance		High	Med	Low		Very low		Med
Internal resistance		Low	Very low	Moderate		High (coke electrode) Highest (graphite electrode)		
Energy by volume (volumetric energy density)	watt-hour/liter	70-110	100-150	200-350	200-330	230-410	200	220
Energy by weight (gravimetric energy density)	watt-hour/kg	30-45	40-60	60-80	120-160	120-210	100	80

Table 2.2: Rechargeable battery chemistry characteristics [1].

## 2.4.2 Superconducting Magnetic Energy Storage

Superconducting magnetic energy storage (SMES) is a technology that stores electricity from the grid within the magnetic field of a coil, composed of superconducting wire, with near-zero loss of energy [16].

The SMES is a grid-enabling device that stores and discharges large quantities of power almost instantaneously. The system is capable of releasing high levels of power within a fraction of a cycle to replace a sudden loss or dip in line power [16]. Strategic injection of brief bursts of power can play a crucial role in maintaining grid reliability, especially with today's increasingly congested power lines and the high penetration of renewable energy sources, such as wind and solar [16].

A typical SMES consists of two parts — a cryogenically cooled superconducting coil and a power conditioning system — which are motionless, thus providing higher reliability than many other power storage devices [16]. Figure 2.17 illustrates a typical SMES system. Ideally, once the superconducting coil is charged, the current does not decay, and the magnetic energy can be stored indefinitely [16].

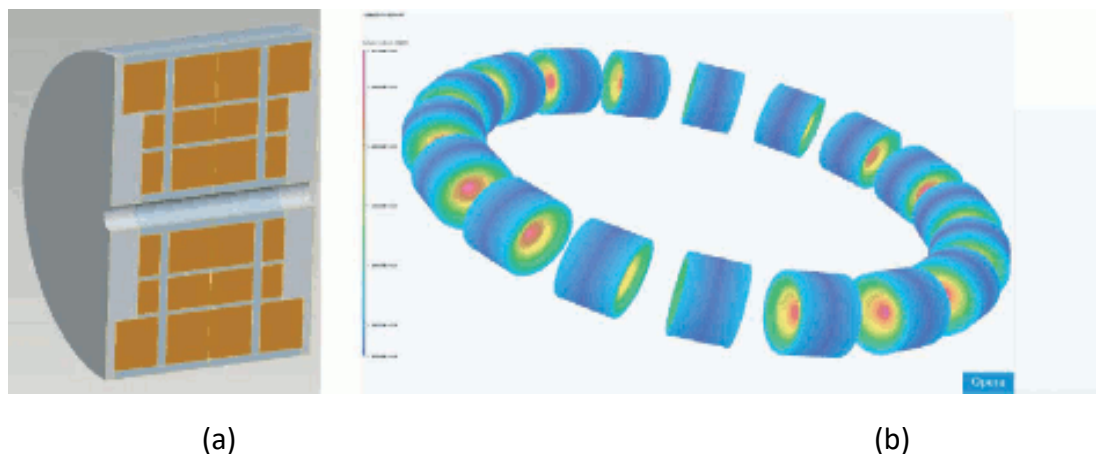


Figure 2.17: The typical superconducting magnetic energy storage (SMES) (a) the SMES coil blocks inside a mechanical structure, and (b) the magnetic field superimposed over the SMES system.

There are many benefits in using an SMES system. First and foremost, it improves power quality and provides carryover energy during momentary power outages and voltage sags. Second, it improves load levelling between renewable energy sources (i.e., solar, geothermal and wind) and the transmission and distribution network.

## 2.4.3 Supercapacitors (SCs)

Supercapacitors are a new technology developed for energy storage. They are governed by the same fundamental equations as conventional capacitors. They are

also known as ultracapacitors or electric double-layer capacitors. Figure 2.18 shows a series of Maxwell SCs. Some of these models were selected as voltage droppers in for the current research project. Their main characteristics are discussed in detail in Chapter 4.



Figure 2.18: Supercapacitors (SCs).

In contrast to commonly used capacitors, SCs come with very low voltage capability, usually in the range of 2 V to <16 V. However, their capacitance values range from about 0.1 F to >5,000 F [1]. Supercapacitors usually have very low internal resistance (in the form of equivalent series resistance [ESR]) compared to rechargeable batteries. In addition, their ESR is relatively constant over its discharge period or the calendar life. Even a small SC, such as one with a 0.6 F value, indicates a constant internal resistance of less than 100 mΩ, while the AA energiser cell has an internal resistance that keeps increasing with the depth of discharge [1].

## 2.5 DC Loads

Electricity is generated in two forms: AC and DC. Each form has its pros and cons in the way it is and how it can be used. Its ease of transport over long distances is the most important advantage of AC electricity. However, for independent island systems (microgrids), this advantage is not important, because the electricity does not move very far to get to where it is used.

Until now, there has been no way to store AC power effectively, although AC generators are more efficient. Basically, most electronic components and everything running on batteries uses DC, and almost all ultra-low voltage systems use DC as well.



With more and more advanced DC technologies applied to appliances, such as the brushless DC (BLDC) motor, DC microgrids and DC loads are constantly improving.

### 2.5.1 Light-emitting Diode (LED) Loads

Light-emitting diodes are an emerging form of lighting used to replace conventional lamps. Previously, LEDs were used as indicator lights only. Nowadays, LEDs can be found in televisions, automotive front and tail lighting, household lighting and so on. The power levels of 1 W, 4 W and 5 W are very common in LEDs. Higher power levels (up to 100 W) are also available. The power conditioning used for LED lighting is different from other conventional lighting, such as incandescent lamps, fluorescent lamps or high-intensity discharge (HID) lamps, both in terms of control and power sources [17]. Modern LED lamps use low voltages from 1.3 V–24 V, and the starting voltage is very low, while fluorescent and HID lamps require hundreds of volts and HID lamps require tens of thousands volts to start. I selected the TCP brand LED lamps (5 W and 12 V white light, Figure 2.19) as the main DC loads in the present research. These lamps' brightness remains constant over a wide voltage range. Lamp data and characteristics are discussed in detail in Chapter 4.



Figure 2.19: TCP brand light-emitting diode (LED) lamps used as DC loads in the current research project.



## 2.5.2 White-ware Loads

Today, almost all whiteware runs on AC. However, most whiteware appliances can be manufactured to run on DC power instead. Some whiteware, such as washing machines, dryers, electric fans and air conditioners, which have motors inside, rectify AC for internal circuits and components. These appliances can also run on DC power directly, because DC motors are already available. This is particularly valid for the inverter-driven latest appliances.

The core components for these appliances are their DC motors. It is said that the invention of the AC induction motor was the deciding factor in the 19th Century battle between AC and DC [18]. However, researchers have still tried to improve DC motors over time. Nowadays, DC motors enjoy many advantages, including good speed–torque characteristics and ease of variable-speed control. With the advent of power electronics (especially the thyristor) in the late 1960s, the use of squirrel cage induction in variable-speed applications starting emerging [18]. This type of motor is robust and virtually maintenance free, as compared to its brush counterpart.

Nowadays, with the further development of BLDC motors, they have again become the ideal choice for many applications. Generally speaking, a BLDC motor is considered to be a high-performance motor capable of providing large amounts of torque over a vast speed range [19]. All BLDC motors are a derivative of the most commonly used DC motor, the brushed DC motor, and they share the same torque and speed performance curve characteristics [19]. The major difference between the two is the use of brushes. The BLDC motor does not have brushes and must be electronically commutated.

# **Chapter 3**

## **Hamilton Illuminance Field Measurements and the Use of a PV Simulator and Associated Software**



## 3.1 Introduction

In the current research, a DC-to-DC converter for a DC microgrid was designed to convert electrical input to a DC output of approximate 12 V. The DC power generator can be any kind of generator, as described in Chapter 2, Section 2.2 “DC Generators”. At the UoW, a suitable solar panel attached to the outside wall (facing north) of the C Block laboratories is available. Therefore, this solar panel was selected as a DC power supply for the research. A PV simulator is also available in the university laboratory, which was used as a replacement for the solar panel, because the panel is small and is only able to provide very low output power. Besides, I found that the wall-attached solar panel was highly influenced by real-time outdoor conditions, while the PV simulator inside the laboratory was not influenced by any environmental factors and could simulate all types of daylight conditions. In order to use this PV simulator properly, data about local Hamilton weather conditions should be collected to create similar and representative weather patterns for the PV simulator. It was necessary to obtain baseline illuminance data from the NIWA website [20] prior to taking field measurements using the solar panel, because a basic understanding of historic Hamilton conditions aided field data collection from the solar panel under difficult-to-predict, variable environmental conditions. Figure 3.1 is a block diagram depicting the process I followed, as described in this chapter.

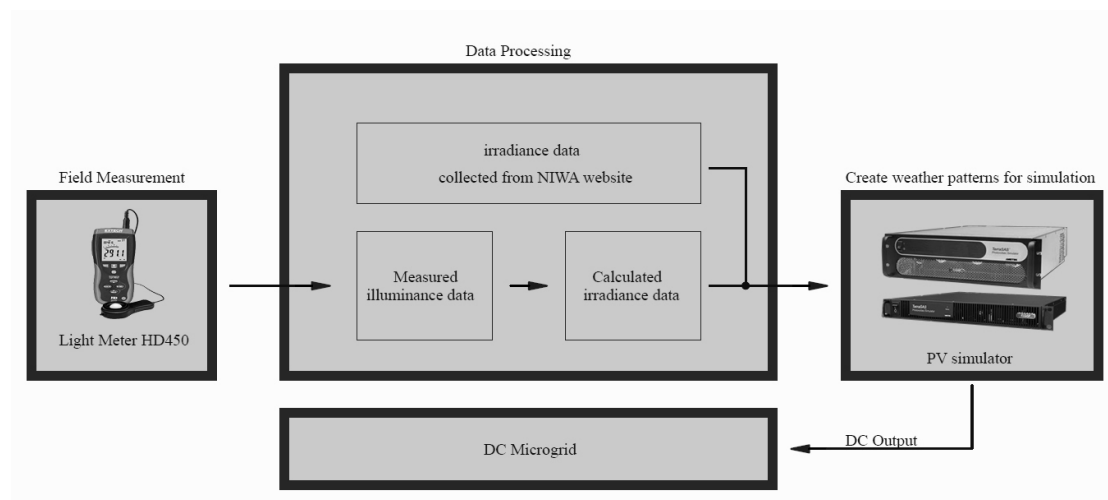


Figure 3.1: A block diagram of equipment and data processing

## 3.2 Waikato Climate and Weather

The Waikato region exhibits a wide range of climates due to the variety of landscapes in the region. It can be very windy in exposed areas, but low-elevation

inland parts of the region are more sheltered. Mountain ranges cause rainfall anomalies, which are directly related to elevation [21]. However, rainfall is plentiful all year round. In general, rainfall in winter is slightly greater than that in summer. A gradient of bright sunshine is observed from the east to the west, with more sunshine in the east than the west of the Waikato region.

### **3.2.1 Wind**

Northerly or westerly air flows are common over most of the Waikato region, although as in all areas of New Zealand, the specific prevailing and strong wind direction in any locality is determined largely by local topography [21]. Some local sites, such as Mt. Te Aroha and Port Taharoa, have a higher percentage of strong winds than more sheltered sites, such as Hamilton.

Spring is generally the windiest season throughout the region. Summer and autumn are the seasons in which the greatest number of light wind days are recorded [21].

### **3.2.2 Rainfall Distribution**

Rainfall patterns in the Waikato region relate to elevation and exposure to prevailing air flows. Areas with high annual rainfall of over 2,000 mm (the Coromandel Ranges, the Central Plateau south of Lake Taupo and the hill country west of Te Kuiti) provide a stark contrast to areas that receive around 1,100 mm of rain per year, including the area east of Hamilton and the Hauraki Plains, as well as sites east of Taupo [21].

### **3.2.3 Air Temperature**

In general, the Waikato region is characterised by relatively warm temperatures in the summer (20–25 °C mean daily maximum temperature) and relatively cold temperatures during the winter (0–8 °C mean daily minimum temperature) [21]. Median annual average temperature in the Waikato region varies with elevation and latitude. Low-lying areas around the Hauraki Plains and north of Hamilton have a mean annual temperature of around 14 °C, whereas the area around Taupo has a mean annual temperature of around 11 °C, and higher elevation areas in Tongariro National Park and the Kaimanawa Ranges have a mean annual temperature of < 8 °C [21].

### **3.2.4 Sunshine and Solar Radiation**

In the Waikato region, a gradient of bright sunshine is observed from the east to the west. The Coromandel Ranges and the ranges to the south receive the most sunshine hours per year ( $> 2,100$  h) [21]. Sunshine hours are also high for the area east of Taupo (around 2,025 h). This declines to 1,950 h near Hamilton and Tokoroa, and the lowest bright sunshine hours received in the Waikato region are experienced in the hill country around Te Kuiti (around 1,800 h) [21].

Solar radiation records for Waikato are available on many websites, but only a few websites have records from  $> 10$  years ago. In order to find enough information about Hamilton climate and weather (especially sunshine and solar radiation) for the current research, some data from the NIWA website was therefore used as a reference (Figure 3.2).

However, more detailed information about illuminance under typical sunlight conditions was still needed to progress the research (Figures 3.3–3.6). Therefore, I used the UoW solar panel to take initial field measurements of illuminance under four conditions: a sunny day, a cloudy day, a day of light rain and a day of heavy rain. These data are shown in the following sections. Data were collected using a light meter HD450 at the UoW in December, 2016.

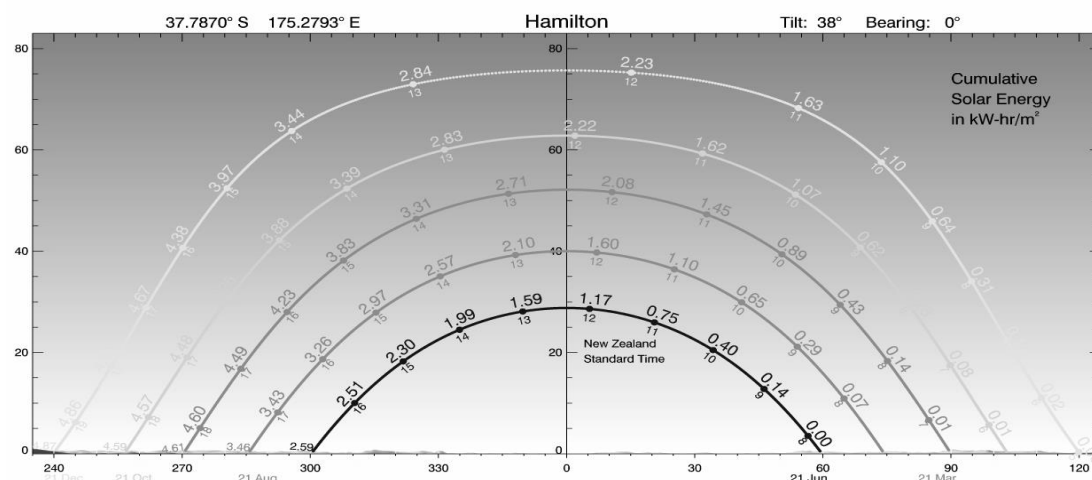


Figure 3.2: Hamilton cumulative solar energy.

Source: The NIWA website. Internet: <https://solarview.niwa.co.nz/>

Figures 3.3–3.6 show real-time Hamilton illuminance values derived from the UoW solar panel first described in Section 3.1, "Introduction". With these data, Hamilton's irradiance data can be ascertained by converting illuminance to irradiance. From these real-time solar panel measurements for a sunny day, a cloudy day and a rainy day, some similar patterns of output were created, and these patterns were used to simulate different outputs from solar panels in the laboratory, where I used a PV simulator under more controlled situations.

### 3.2.4.1 Sunny Day Illuminance

On a sunny day, there was sufficient sunlight to provide energy to power loads. Starting from around 5 a.m., the illuminance increased gradually, and it reached its zenith at noon, at around 25,000 lux. Thereafter, it decreased. The illuminance dropped to 0 lux between 8 p.m. and 9 p.m., and no light could be detected after 9 p.m. until the next morning. The illuminance curve of a sunny day (Figure 3.3) therefore looks vaulted. The curve is smooth, illustrating the lack of severe fluctuation during the day.

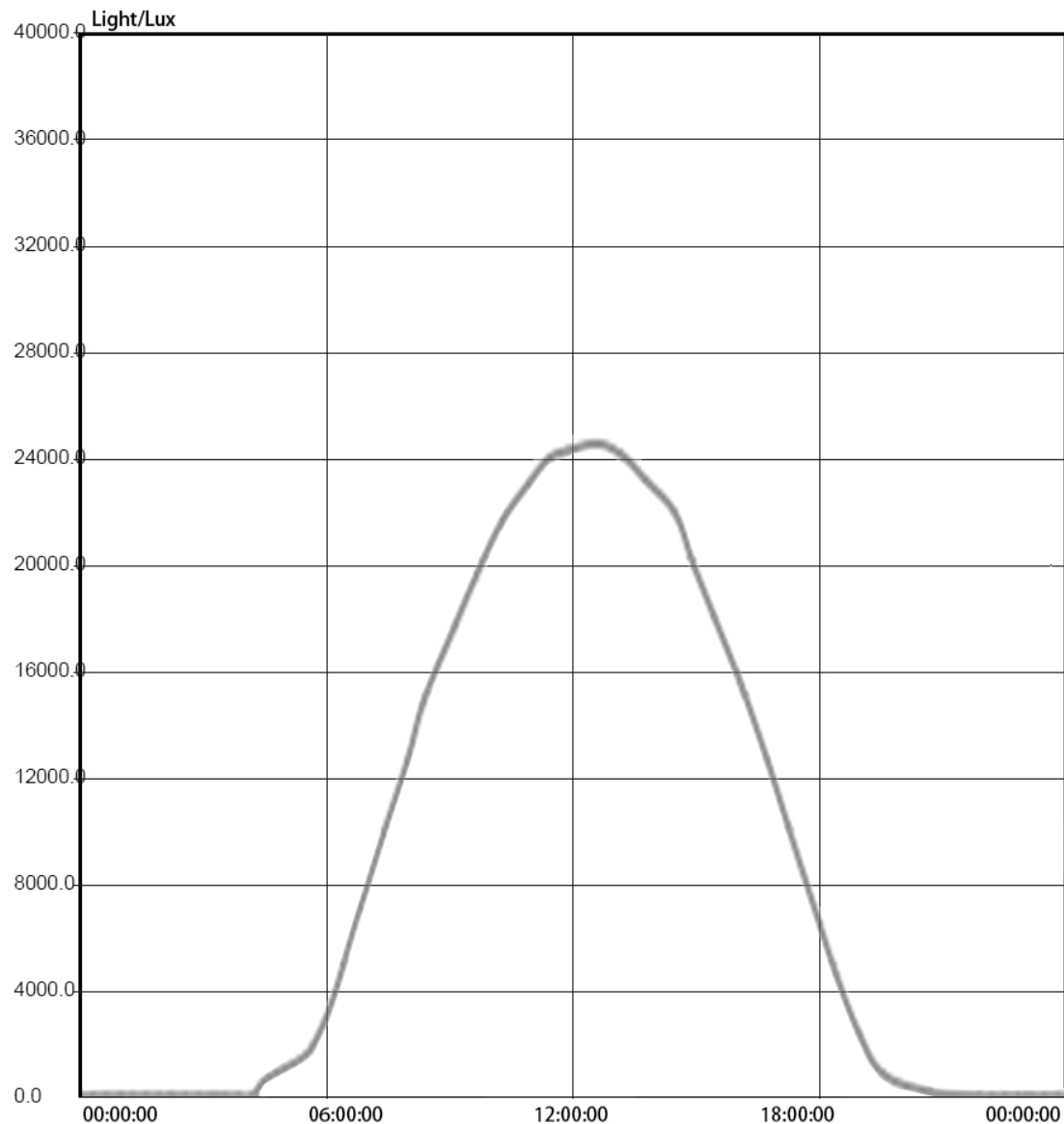


Figure 3.3: Sunny day illuminance at the University of Waikato (UoW) in Hamilton.

### 3.2.3.2 Cloudy Day Illuminance

During cloudy day measurements, the ground was often hidden from the sun by clouds. Illuminance patterns depended on wind speed and how many clouds there were in the sky. The maximum illuminance value on a cloudy day was approximately equal to the maximum value on a sunny day. However, the illuminance fluctuated sharply and quickly during the cloudy day. The total amount of sunlight was less than on a sunny day. Yet, the illuminance values were still much higher than illuminance values on a rainy day (Figure 3.4).



Figure 3.4: Cloudy day illuminance at the University of Waikato (UoW) in Hamilton.



### 3.2.3.3 Rainy Day Illuminance

On a rainy day, there was also some illuminance fluctuation in the daytime. However, this fluctuation was not as sharp and quick as illuminance fluctuations on a cloudy day. The peak illuminance value was approximately 25 % lower than on both sunny and cloudy days (Figure 3.5). This value was even lower when it rained heavily (Figure 3.6). Clearly, sunlight was deficient on rainy days compared with both sunny and cloudy days.



Figure 3.5: Rainy day illuminance (light rain) at the University of Waikato (UoW) in Hamilton.

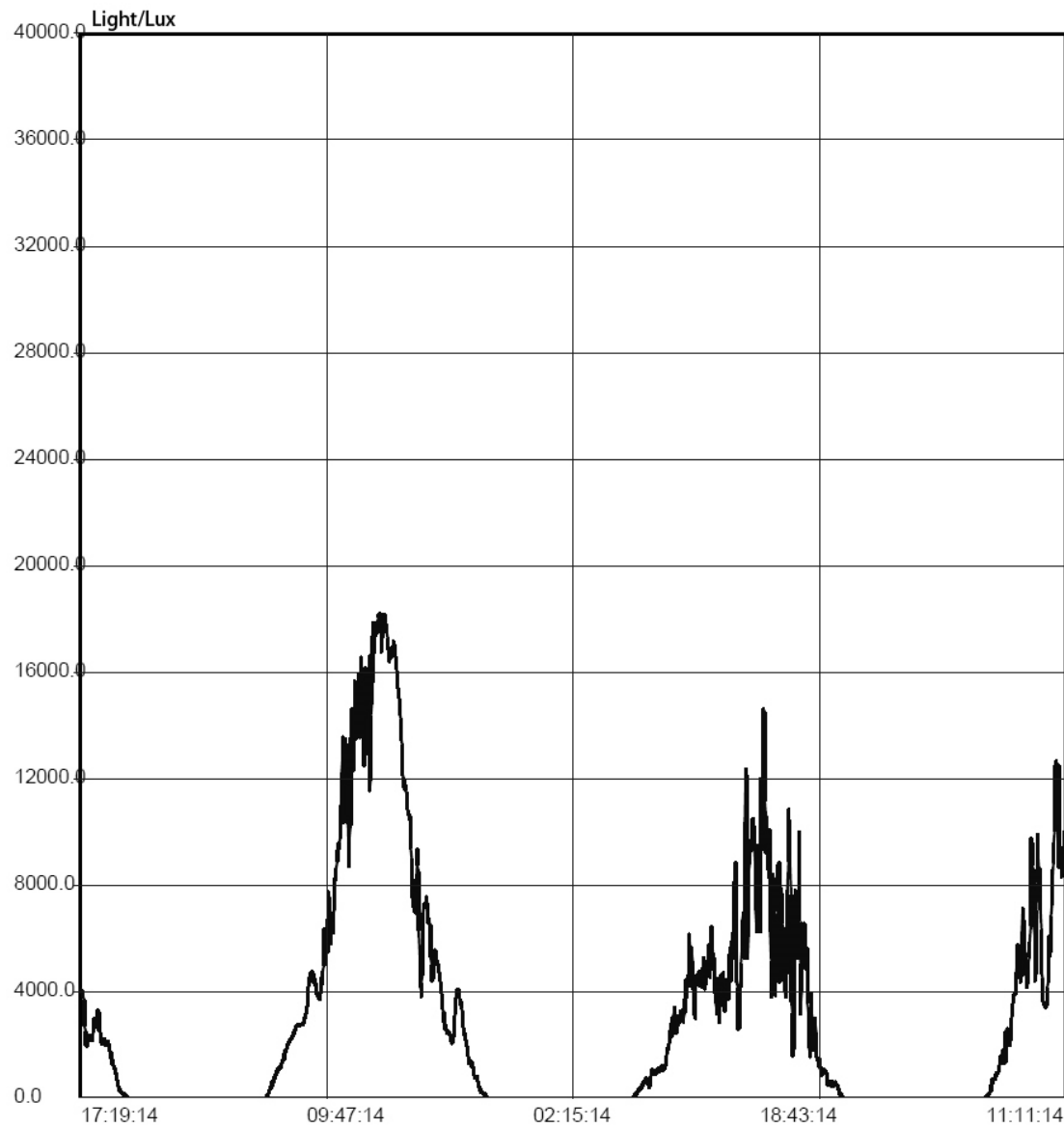


Figure 3.6: Rainy day illuminance (heavy rain) at the University of Waikato in Hamilton.

### 3.3 Illuminance-to-Irradiance Conversion

In photometry, illuminance is the total luminous flux incident on a surface, per unit area. It is a measure of how much the incident light illuminates the surface, wavelength-weighted by the luminosity function to correlate with human brightness perceptions [22]. In SI units, the illuminance is measured in lx or lux,

$$(lux = cd \bullet sr \bullet m^{-2}) \quad (3.1).$$

Illuminance has often been called “brightness”, but this nomenclature leads to confusion with other words such as “luminance”. Therefore, I attempt to avoid using the word “brightness” when describing quantitative measurements.

Solar irradiance is the power per unit area received from the sun in the form of electromagnetic radiation in the wavelength range of the measuring instrument [22]. Irradiance may be measured in space or at the Earth's surface after atmospheric absorption and scattering [22]. It is measured perpendicular to the incoming sunlight. Total solar irradiance (TSI), is a measure of the solar power over all wavelengths per unit area incident on the Earth's upper atmosphere [22].

The unit of illuminance is lux (SI alternative symbology, lx), and  $lux = lm/m^2$ , while irradiance is measured in  $W/m^2$ . Therefore, converting lux to  $W/m^2$  and converting lumen to watts are equivalent.

The power,  $P$  in watts (W) is equal to the luminous flux,  $\Phi_v$  in lumens (lm), divided by the luminous efficacy,  $\eta$  in lumens per watt (lm/W):

$$P = \frac{\Phi_v}{\eta} \quad (3.2).$$

Luminous efficacy can be calculated by using the following formula:

$$\eta = \frac{\Phi_v}{\Phi_e} = \frac{\int_0^\infty K(\lambda) \Phi_{e,\lambda} d\lambda}{\int_0^\infty \Phi_{e,\lambda} d\lambda} \quad (3.3),$$

Where  $\Phi_v$  is the luminous flux,  $\Phi_e$  is the radiant flux,  $\Phi_{e,\lambda}$  is the spectral radiant flux and  $K(\lambda)$  is the spectral luminous efficacy.

On a sunny day, the wavelength of light changes slightly. Therefore,  $K(\lambda)$  can be treated as a constant. In this case, the integration of the denominator and numerator is a constant and the result is a constant. Therefore, from Equation 3.2,

$$\Phi_V = P \times \eta \quad (3.4)$$

Where Luminous flux,  $\Phi_V$  is in proportion to the power,  $P$ . Therefore, the illuminance is in proportion to the irradiance.

However, cloudy or rainy conditions affect outcomes. Rapid flow of clouds makes the light spectrum change quickly. The spectral luminous efficacy,  $K(\lambda)$ , changes slightly in a short period but not for a long time. This changes  $\eta$  to a non-constant. However, the most important analysis involves elucidating the features of irradiance on cloudy and rainy days, rather than creating irradiance curves that are identical with illuminance curves. Indeed, having tested Hamilton's illuminance, the local characteristics of these three kinds of weather are known variables.

- During a sunny day, there is sufficient sunlight during the day to power loads. The illuminance curve is smooth and it reaches the highest point at noon.
- On a cloudy day, sunlight is sufficient to power loads sometimes, but sometimes it is not; the illuminance curve fluctuates quickly.

During a rainy day, there is also some illuminance fluctuation during the day, but it is not so marked as on cloudy days. However, unfortunately, the illuminance is not generally sufficient to power loads.

By applying illuminance-to-irradiance conversion formulae to the current research project, I created similar patterns of irradiance that represented a typical sunny day (Figure 3.7), an average cloudy day (Figure 3.8) and a typical rainy day (Figure 3.9) in Hamilton.

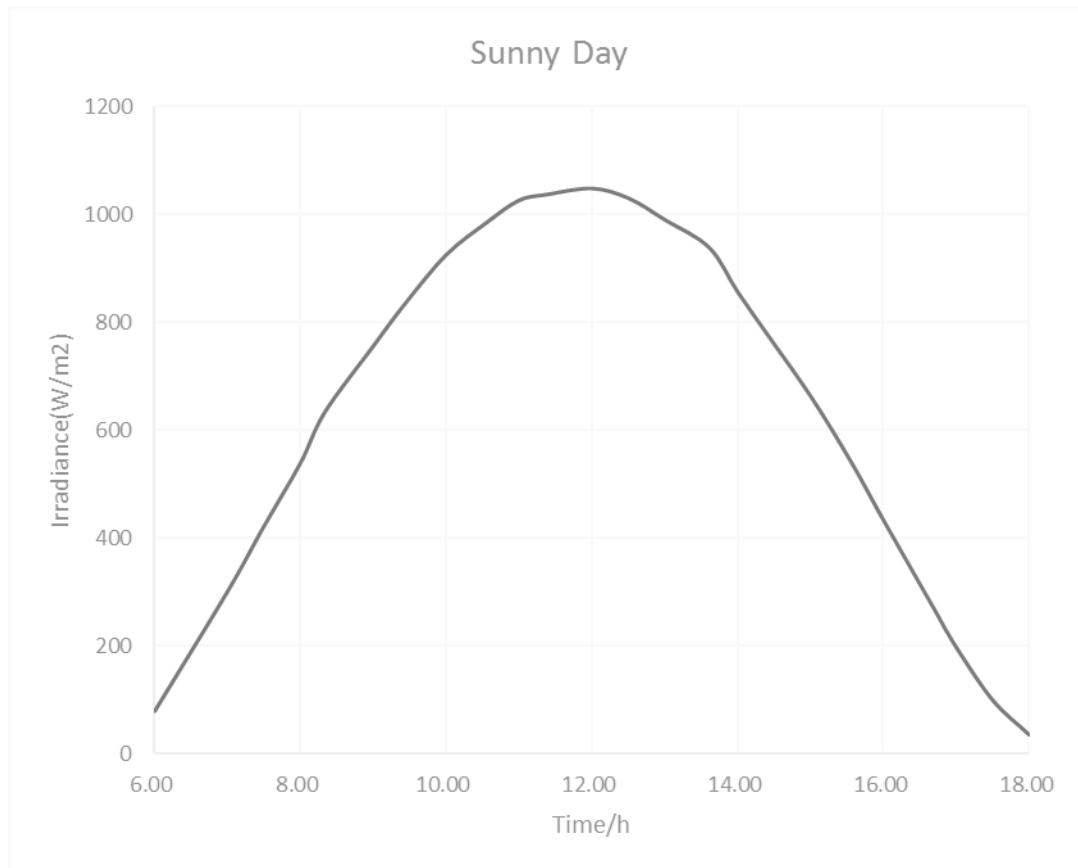


Figure 3.7: The calculated average sunny day irradiance curve for Hamilton.

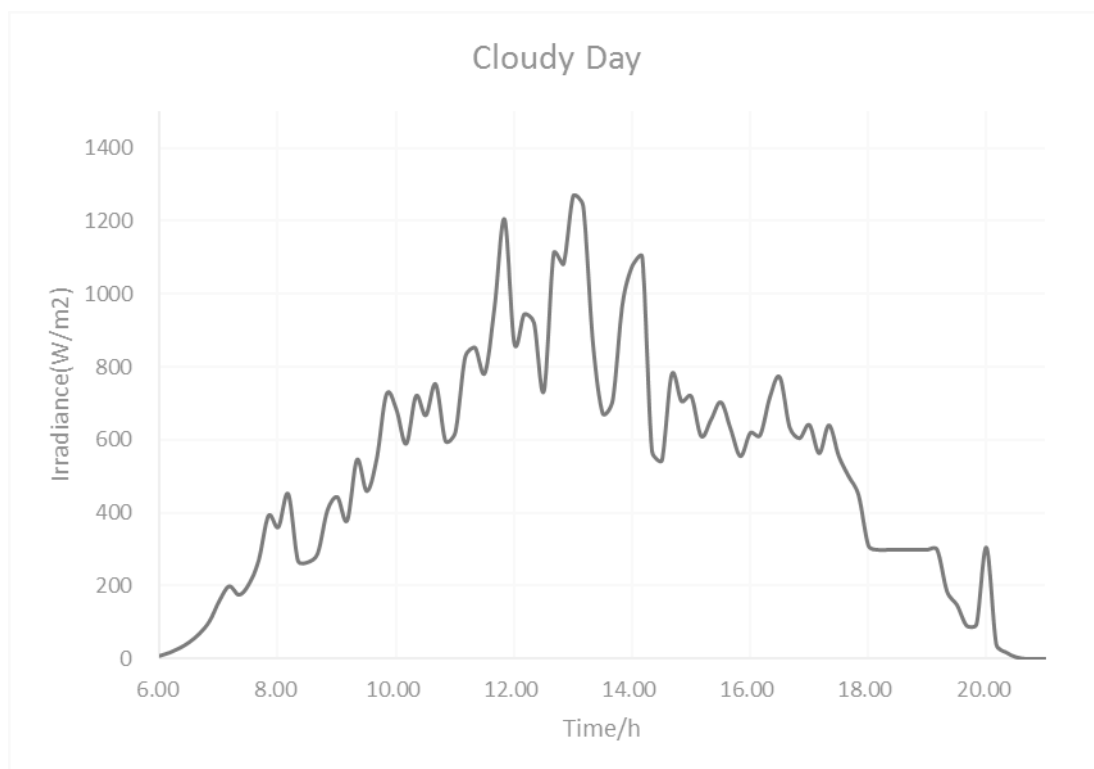


Figure 3.8: The average calculated cloudy day irradiance curve for Hamilton.

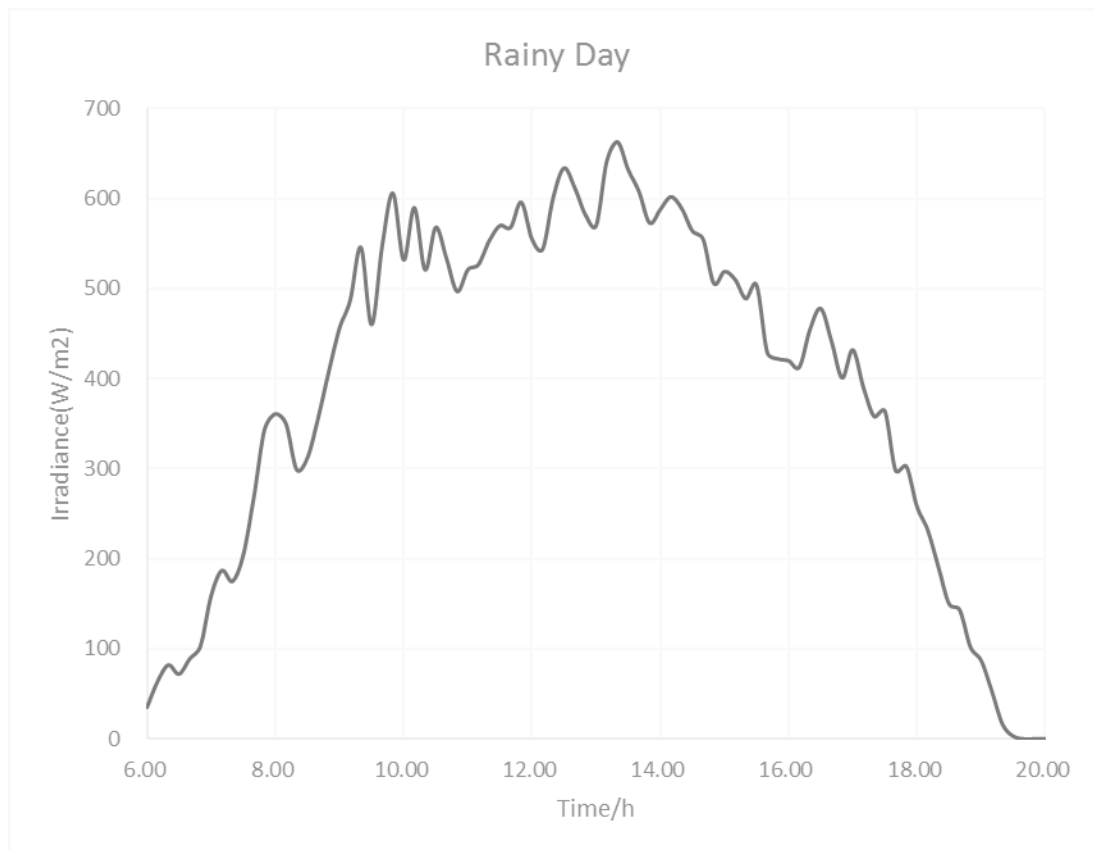


Figure 3.9: The average calculated rainy day irradiance curve for Hamilton.

## 3.4 The Photovoltaic (PV) Simulator and Associated Software

### 3.4.1 Model, Manufacturer and Main Specifications

The ETS600X is a PV simulator produced by AMETEK Inc. Its open-circuit voltage is 600 V, its short-circuit current is 8.3 A and its maximum output power at fill factor 0.85 is 4.25 kW.

Although this PV simulator has only one output channel, it is good enough as a power supply for a DC microgrid running a 12 V household LED lighting system with a peak power requirement of approximately 50 W.

### 3.4.2 Photovoltaic (PV) Simulator Operation

The PV simulator is controlled by the software TerraSAS™. This programmable PV simulator can be treated as a power supply. Just like other DC power supplies, this simulator has two connectors on the back chassis for input and ground.

### 3.4.2.1 Demonstration Mode

The demonstration (demo) mode simulates a TerraSAS™ system with 24 low-voltage PV simulators (distributed control system [DCS] 80 V, 15 A) [23]. The software can run on any computer (whether an actual PV simulator is connected or not), and this mode can be used for training or demonstration purposes. The steps I followed were as per manufacturer recommendations. Initiate the PV simulator to work in demo mode [23] as depicted in Figure 3.10 below.



Figure 3.10: A screenshot of TerraSAS™ in demonstration mode.

Although there are 24 channels in demo mode, they can all run but cannot all be demonstrated at the same time. Only one channel can be shown on the screen at a time. But for the purposes of my research, one channel was enough.

For the purposes of my research, one of the most useful functions in demo mode was to check the irradiance profiles and PV curves created by users. This function enabled me (the user) to create these files without actually running a physical PV simulator. In normal mode, if a PV simulator is not detected, the software itself will stop running automatically. Therefore, users cannot simulate or work with software with the machine in a normal mode.

3.4.2.2 Power supply (P/S) mode

P/S mode allows the disabling of the current–voltage (I–V) curve controller and the driving of the power converter directly, with a programmable voltage and current reference [23]. Figure 3.11 is a screenshot of the system settings window, which allows the user to place one or more channels in P/S mode. The output tile (circled in red in Figure 3.12) turns yellow to show the different operating mode. In this window, the user can switch the PV simulator between constant voltage mode and simulation mode.

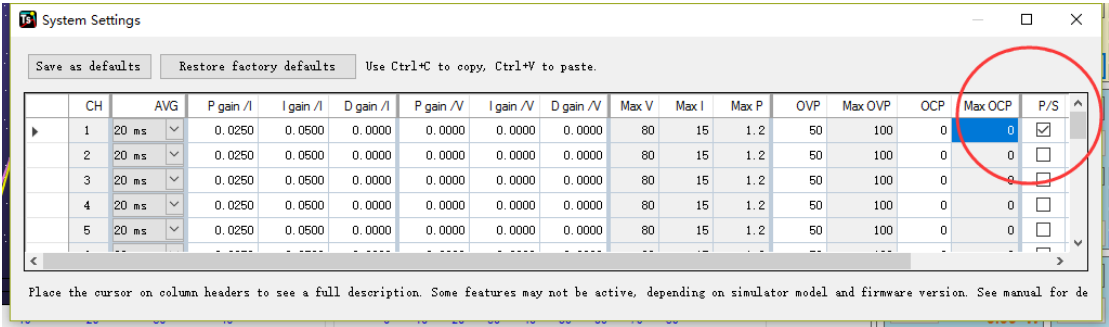


Figure 3.11: Switching modes on the photovoltaic (PV) simulator.

If an I–V curve is assigned to the yellow tile (shown in the upper right circle of Figure 3.12), “Isc” (meaning “short circuit current”) sets the current reference, and “Voc” (meaning “open circuit voltage”) sets the voltage reference. All other points can be ignored. When clicking the [PGM] (meaning “program”) button (shown in the lower right circle of Figure 3.12), the dialogue allows the users to program both voltage and current [23]. The blue lines in the middle circuit is the I–V characteristics of this power supply.



Chapter 3: Hamilton Illuminance Field Measurements and the Use of a PV Simulator and Associated Software

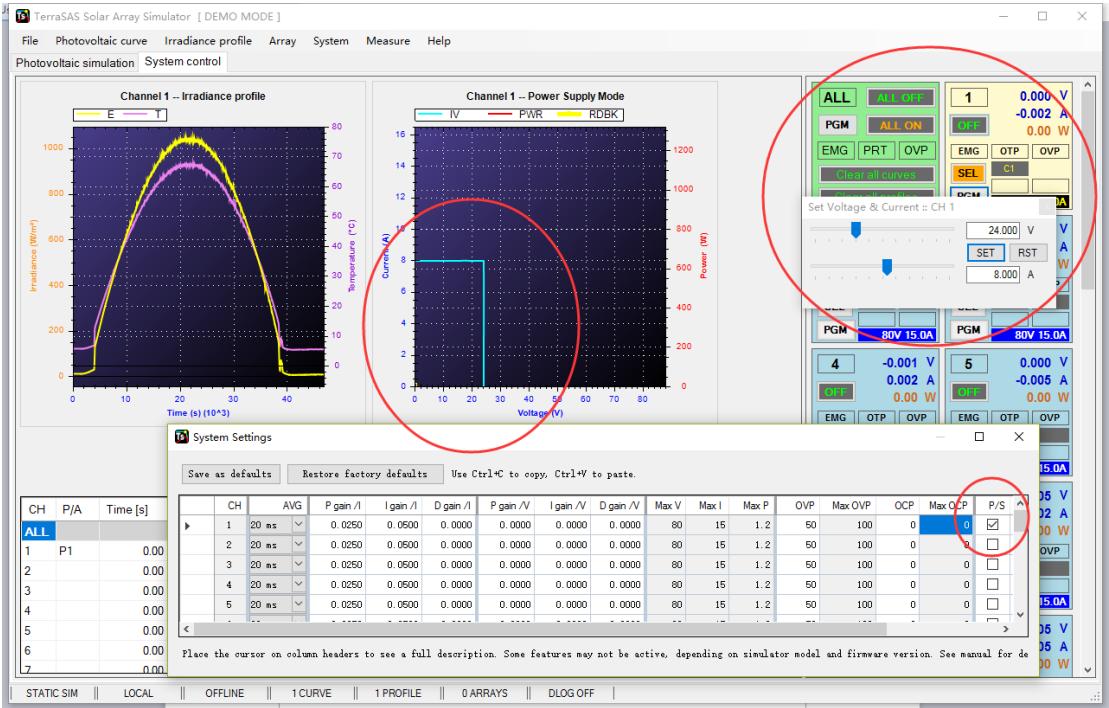


Figure 3.12: The open-circuit voltage reference and short-circuit reference settings.

3.4.2.3 Simulation Mode

After loading irradiance profiles and photovoltaic curves, users can start simulating as per the sample simulation show in Figure 3.13. This feature enables users to get different outputs that are similar to the real outputs given by solar panels.

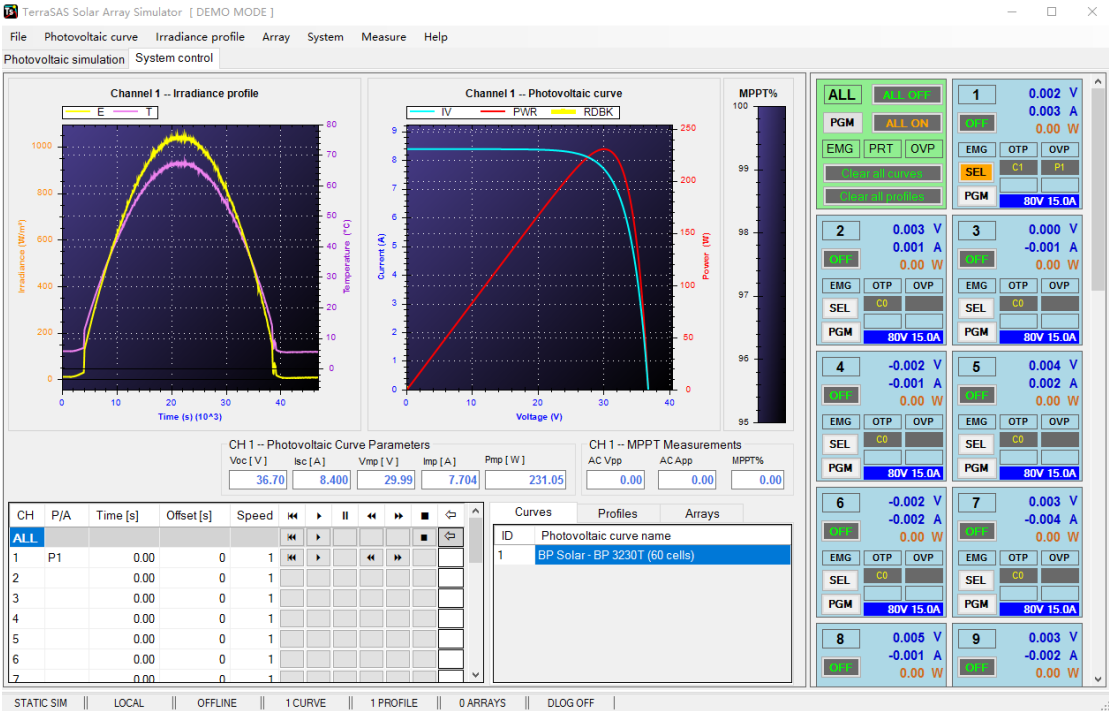
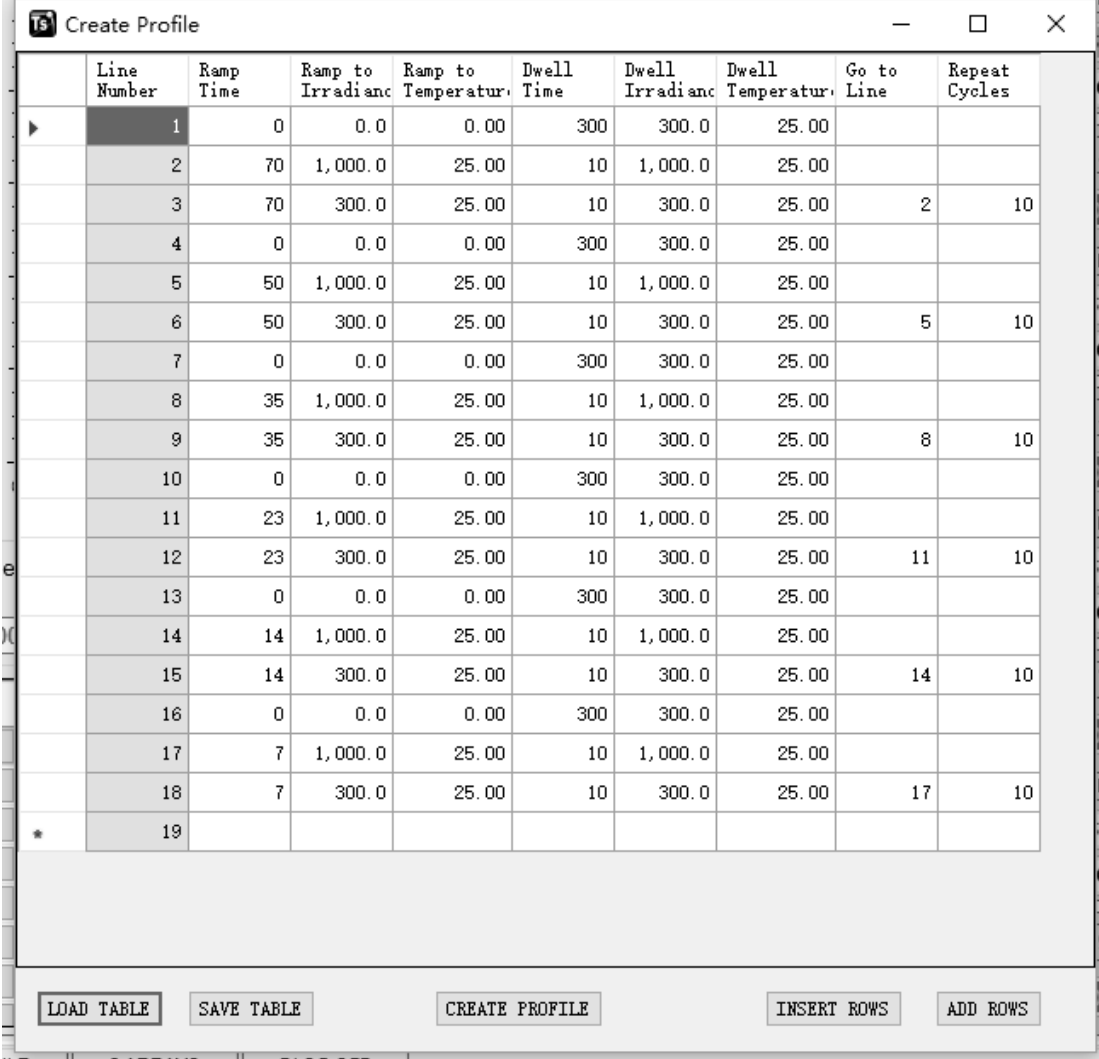


Figure 3.13: A screenshot of a sunny day simulation.

### 3.4.3 Creating Irradiance Profiles by Coding

The window shown in Figure 3.14 is a table used to create irradiance profiles for simulation (via Profile > Create). The sample table shown (Figure 3.14) was used in this research to create irradiance profiles for irradiance testing (Figure 3.15).



Line Number	Ramp Time	Ramp to Irradiance	Ramp to Temperature	Dwell Time	Dwell Irradiance	Dwell Temperature	Go to Line	Repeat Cycles
1	0	0.0	0.00	300	300.0	25.00		
2	70	1,000.0	25.00	10	1,000.0	25.00		
3	70	300.0	25.00	10	300.0	25.00	2	10
4	0	0.0	0.00	300	300.0	25.00		
5	50	1,000.0	25.00	10	1,000.0	25.00		
6	50	300.0	25.00	10	300.0	25.00	5	10
7	0	0.0	0.00	300	300.0	25.00		
8	35	1,000.0	25.00	10	1,000.0	25.00		
9	35	300.0	25.00	10	300.0	25.00	8	10
10	0	0.0	0.00	300	300.0	25.00		
11	23	1,000.0	25.00	10	1,000.0	25.00		
12	23	300.0	25.00	10	300.0	25.00	11	10
13	0	0.0	0.00	300	300.0	25.00		
14	14	1,000.0	25.00	10	1,000.0	25.00		
15	14	300.0	25.00	10	300.0	25.00	14	10
16	0	0.0	0.00	300	300.0	25.00		
17	7	1,000.0	25.00	10	1,000.0	25.00		
18	7	300.0	25.00	10	300.0	25.00	17	10
*	19							

LOAD TABLE    SAVE TABLE    CREATE PROFILE    INSERT ROWS    ADD ROWS

Figure 3.14: A screenshot of an irradiance profile sample table used to create an irradiance profile.

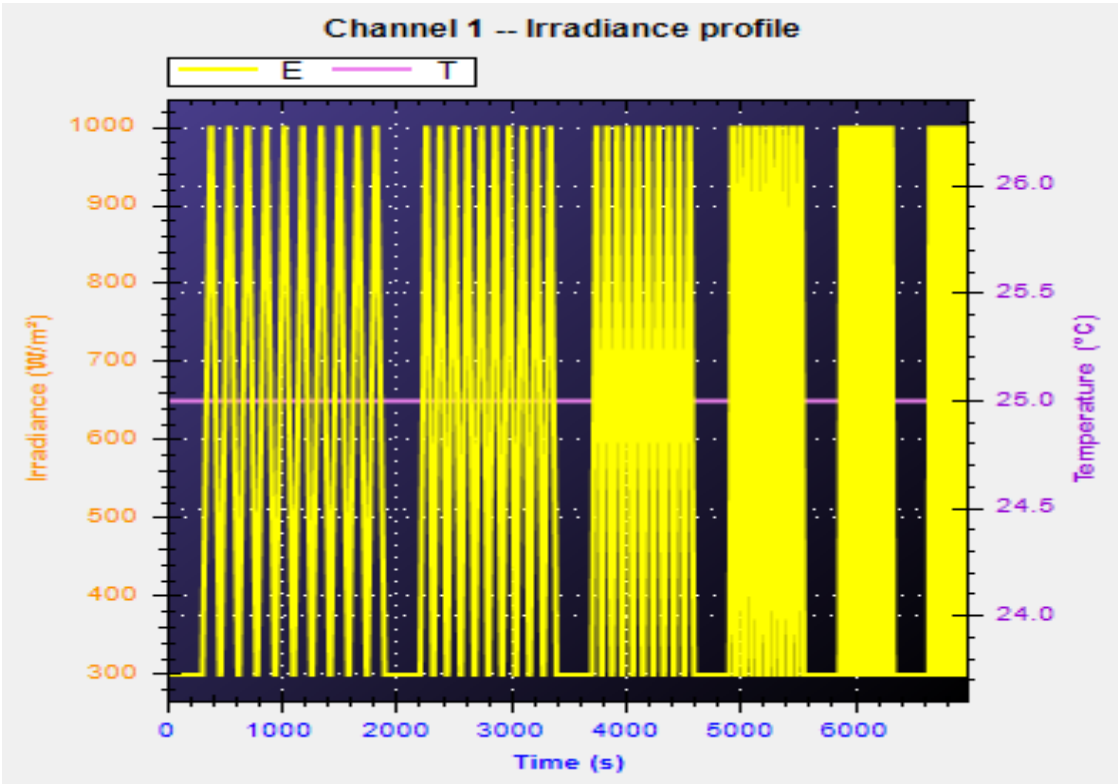


Figure 3.15: A sample of irradiance profile testing.

As shown in the Figure 3.15 sample irradiance profile test, there are two curves (a purple line and a yellow pattern), which represent irradiance and temperature, respectively. In the “Create Profile Window” on line 2, the ramp time was 70 s, the ramp-to-irradiance was 1,000 lm, the dwell time was 10 s and dwell irradiance was 1,000 lm. These times indicated that 70 s was required for irradiance to rise from 0 to 1,000 lm and that irradiance was maintained at 1,000 lm for 10 s. I found that every single line required one line of code. The temperature could be set in the same way.

Based on the sample code creations, I then created the following Hamilton irradiance profiles (discussed in Sections 3.4.3.1–3.4.3.4). I collected the data used for creating these patterns by light meter, summarised them and then converted them from illuminance to irradiance, using methods described earlier in this chapter.

### 3.4.3.1 A Simulated Sunny Day in Hamilton

The following Figures (Figures 3.16–3.18) are the irradiance profiles I created for Hamilton. They simulate a sunny day, a cloudy day and a rainy day, respectively. Table 3.1 shows the code I used to create a sunny day’s irradiance profile. The codes for Hamilton’s cloudy and rainy day irradiance profiles are shown in Appendix [F].

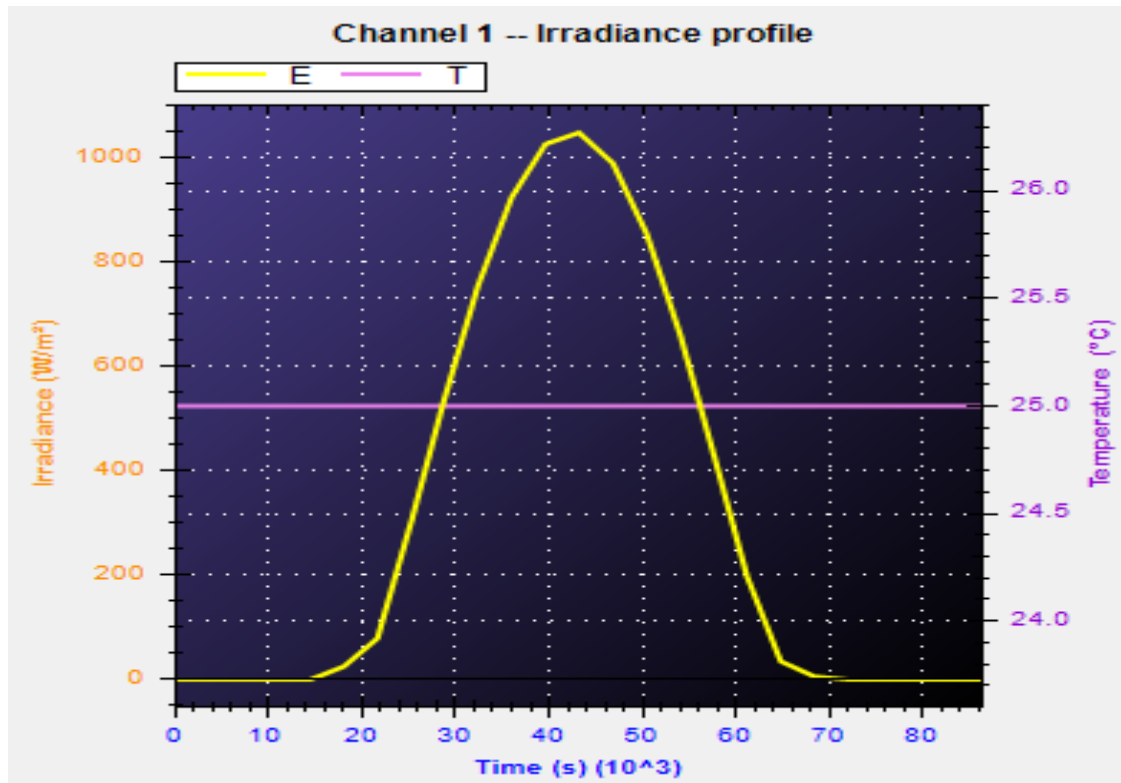


Figure 3.16: A simulated sunny day irradiance profile I created for Hamilton.

Table 3.1: A table used to create the Hamilton sunny day irradiance profile.

Line number	Ramp time	Ramp-to-irradiance	Ramp-to-temperature	Dwell time	Dwell irradiance	Dwell temperature	Go to line	Repeat cycles
1	0	0	25	3600	0	25	0	0
2	0	0	25	3600	0	25	0	0
3	0	0	25	3600	0	25	0	0
4	0	0	25	3600	0	25	0	0
5	3590	25	25	10	25	25	0	0
6	3590	79	25	10	79	25	0	0
7	3590	301	25	10	301	25	0	0
8	3590	539	25	10	539	25	0	0
9	3590	756	25	10	756	25	0	0
10	3590	925	25	10	925	25	0	0
11	3590	1026	25	10	1026	25	0	0

Chapter 3: Hamilton Illuminance Field Measurements and the Use of a PV Simulator and Associated Software

<b>Line number</b>	<b>Ramp time</b>	<b>Ramp-to-irradiance</b>	<b>Ramp-to-temperature</b>	<b>Dwell time</b>	<b>Dwell irradiance</b>	<b>Dwell temperature</b>	<b>Go to line</b>	<b>Repeat cycles</b>
<b>12</b>	3590	1048	25	10	1048	25	0	0
<b>13</b>	3590	990	25	10	990	25	0	0
<b>14</b>	3590	856	25	10	856	25	0	0
<b>15</b>	3590	663	25	10	663	25	0	0
<b>16</b>	3590	433	25	10	433	25	0	0
<b>17</b>	3590	197	25	10	197	25	0	0
<b>18</b>	3590	35	25	10	35	25	0	0
<b>19</b>	3590	6	25	10	6	25	0	0
<b>20</b>	3590	0	25	10	0	25	0	0
<b>21</b>	0	0	25	3600	0	25	0	0
<b>22</b>	0	0	25	3600	0	25	0	0
<b>23</b>	0	0	25	3600	0	25	0	0

### 3.4.3.2 A Simulated Cloudy Day in Hamilton

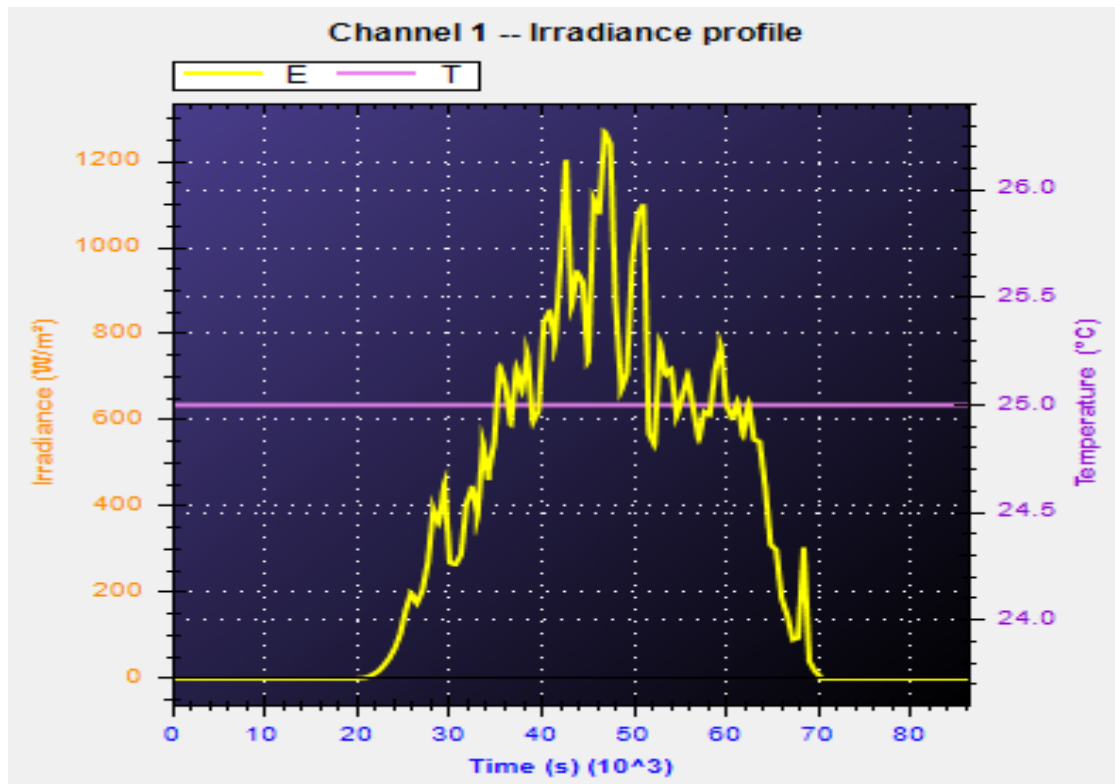


Figure 3.17: A simulated cloudy day irradiance profile I created for Hamilton.

### 3.4.3.3 A Simulated Rainy Day in Hamilton

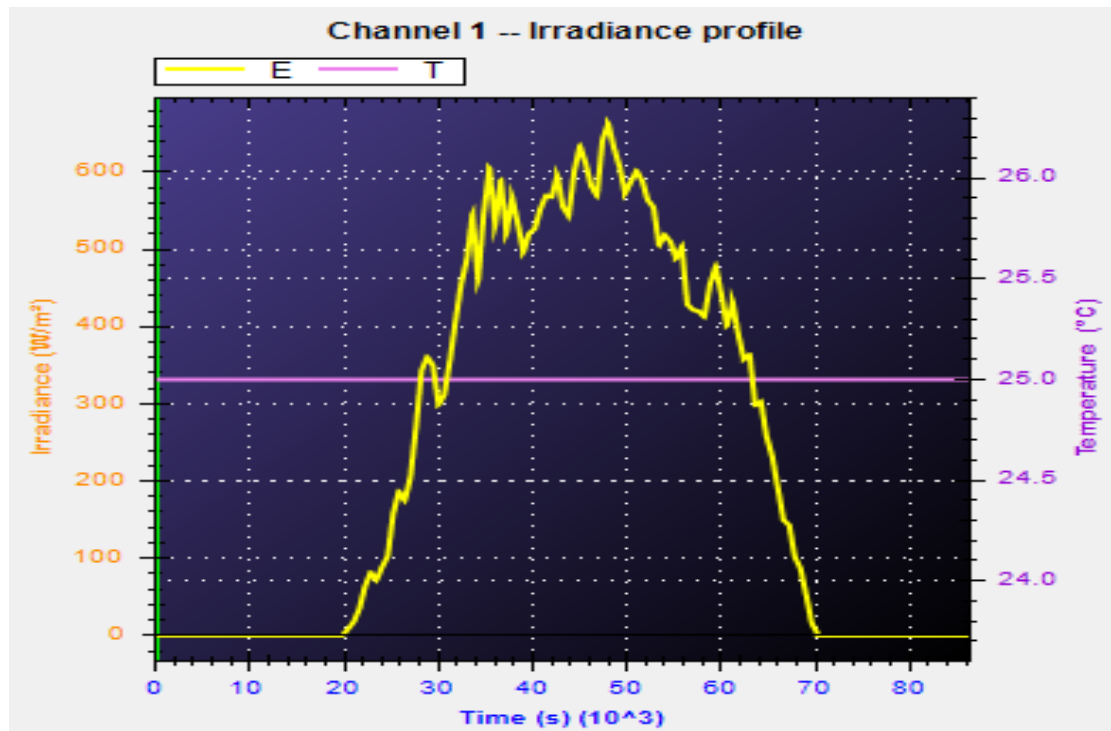


Figure 3.18: A simulated rainy day irradiance profile I created for Hamilton.

### 3.4.4 Photovoltaic (PV) Curve Creation

The TarraSAS™ software enables users to load PV curves generated by different types of solar panels manufactured by different manufacturers. These curves can be created by users as well. In the ‘real world’, one solar panel can be connected in series or in parallel with others. The TarraSAS™ software can also simulate both of these situations. However, due to the limitation that one channel can simulate only one solar panel and that there is just one output channel on the back chassis of the ETS600X PV simulator, users must calculate the Voc and Isc values, and how many watts can be gathered for one panel, to create an ‘equivalent’ solar panel (if more than one solar panel is needed). These solar panel specifications can be entered in the “Settings” window of the TarraSAS™ software program (Figure 3.19). The behaviour of this virtual solar panel can also be demonstrated (Figure 3.20).

**Add Curve (SNL)**

Curve parameters

Voc: 24.000 V    Isc: 8.300 A

Vmp: 21.466 V    Imp: 7.424 A

FF: 0.80    ☒ Use fill factor

Temperature coefficients

$\beta_v$ : -0.360 %/°     $\beta_p$ : -0.500 %/°

Irradiance correction

Voc: 22.322 V    E: 200 W/m²

Name: Curve 24V 8.3A

ADD

Figure 3.19: A screenshot of the window for setting the specifications of a virtual solar panel.

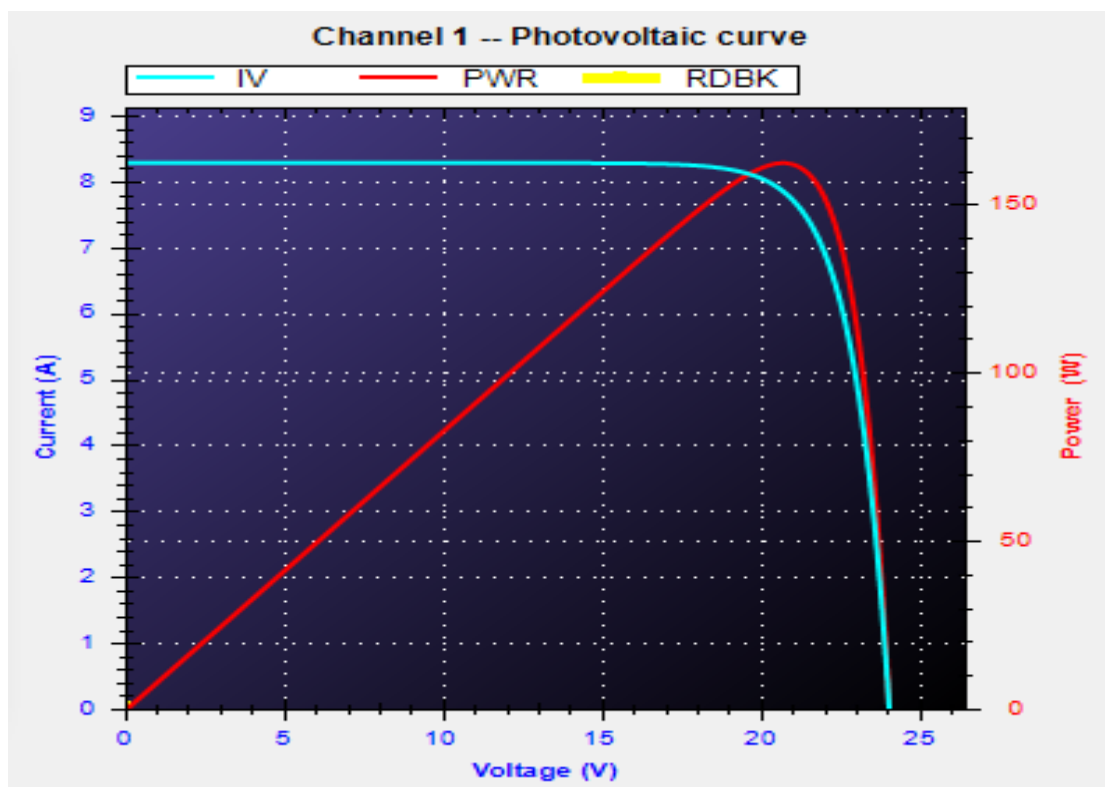


Figure 3.20: A PV curve with an open-circuit voltage of 24 V and a short-circuit current of 8.3 A.





# **Chapter 4**

## **Components Testing**



## 4.1 Supercapacitor (SC) Characteristics

Supercapacitors are very similar to conventional capacitors in terms of their electrical characteristics. Both of them share the same formulae used to calculate their electric charge, stored energy, terminal voltage and other parameters. Compared with conventional capacitors, the biggest advantage inherent in an SC is its capacitance. Capacitance of an SC can be 1 F, 100 F, 6,500 F or even larger.

### 4.1.1 SC Charging Characteristics

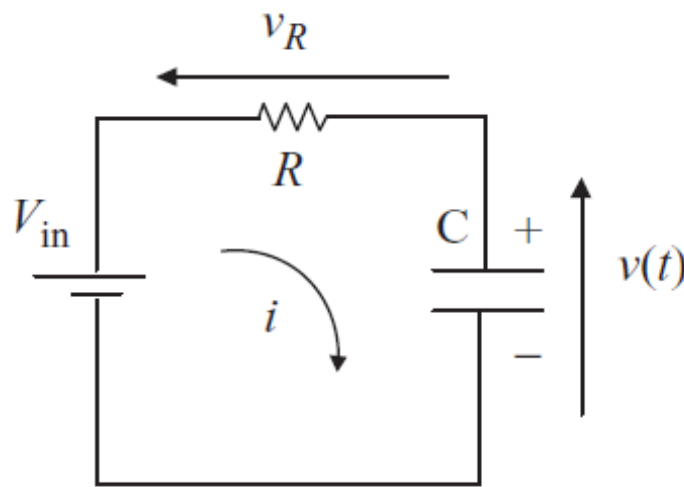


Figure 4.1: Charging a supercapacitor (SC) from a voltage source.

The above circuit diagram (Figure 4.1) shows a typical SC's charging circuit. A constant DC power supply with  $V_{in}$  output voltage is used to charge the SC. The resistance of  $R$  is equal to the value of the loop resistance, plus the internal resistance of the SC and the DC power supply. By solving Kirchhoff's voltage law (Equation 4.1),

$$V_{in} = i(t)R + V_C(t) \quad (4.1),$$

Where

$$i(t) = C \frac{dV_C(t)}{dt} \quad (4.2),$$

The following equation is obtained:

$$V_C(t) = V_{in} + ke^{-\frac{t}{RC}} \quad (4.3).$$

Where k can be any constant.

If the initial voltage of the capacitor  $V_C(t_0)$  is zero,

$$0 = V_{in} + ke^{-\frac{0}{RC}} \quad (4.4),$$

The following equation also applies:

$$k = -V_{in} \quad (4.5).$$

Therefore, the following equation is finally obtained:

$$V_C(t) = V_{in} \left( 1 - e^{-\frac{t}{RC}} \right) \quad (4.6),$$

It then follows:

$$i(t) = \frac{V_{in} - V_C(t)}{R} = \frac{V_{in}}{R} e^{-\frac{t}{RC}} \quad (4.7).$$

The energy stored in an SC is governed by the following equation:

$$E_C(t) = \frac{1}{2} CV_C^2(t) \quad (4.8).$$

By solving Equations 4.6 and 4.8, it is also clear that

$$E_C(t) = \frac{1}{2} CV_{in}^2 \left( 1 - e^{-\frac{t}{RC}} \right)^2 \quad (4.9).$$

The total energy delivered by the power supply,  $E_S$ , and the energy dissipated on the resistor,  $E_R$ , can be calculated by applying Equations 4.10 and 4.11, respectively:

$$E_S = \int_0^t i(t) V_{in} dt \quad (4.10),$$

And

$$E_R = \int_0^t i^2(t) R dt \quad (4.11).$$

By combining results from equations 4.2, 4.10 and 4.11, we obtain the following two equations:

$$E_S = CV_{in}^2 \left( 1 - e^{-\frac{t}{RC}} \right) \quad (4.12),$$

And

$$E_R = \frac{1}{2} CV_{in}^2 \left( 1 - e^{-\frac{2t}{RC}} \right) \quad (4.13).$$

If an SC is charged (Figure 4.2) for a long time, which means  $t$  is larger than the 5RC time constant, the value of the energy stored in the SC will be approximately equal to that of the energy dissipation on the resistor. This means that approximately half of the total energy is wasted. Figure 4.3 illustrates this charging process.

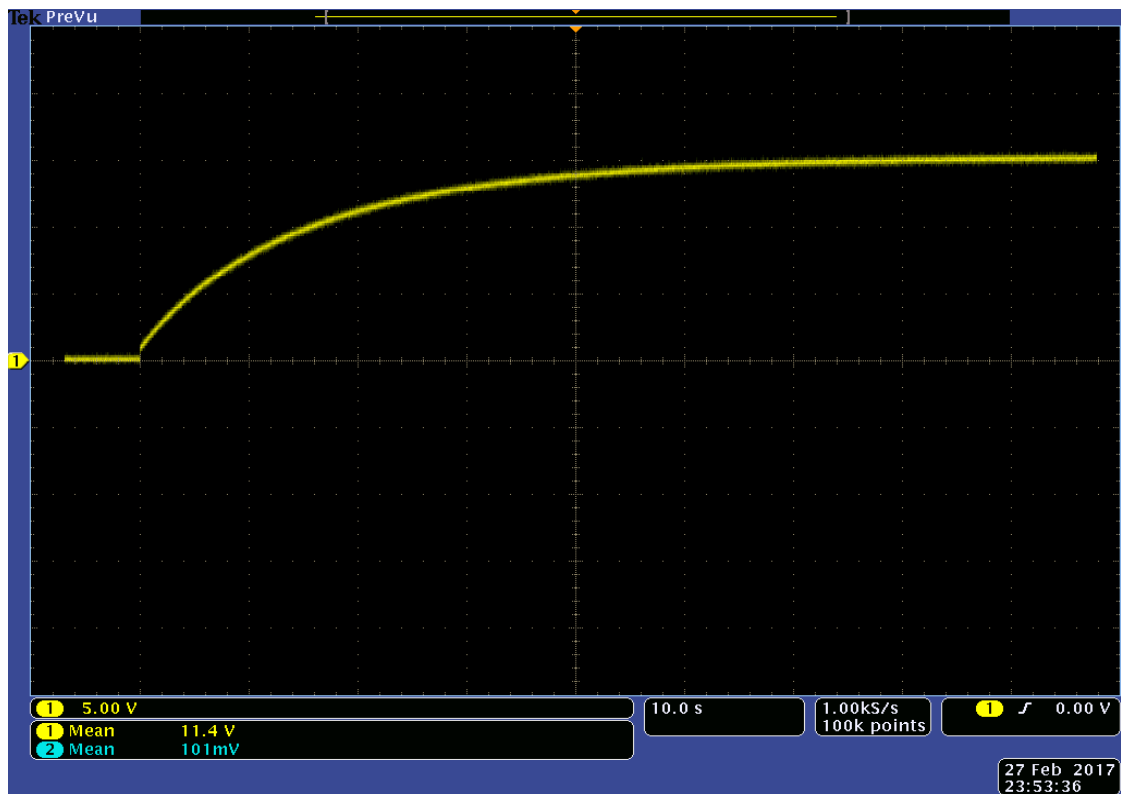


Figure 4.2: Charging curve of a 2.5 F supercapacitor (SC). Note that  $V_{in}$  is 15 V. A small resistor is connected in series in the loop to make sure that the loop current will not exceed the maximum current limit of the power supply.

In Figure 4.2, it is obvious that the terminal voltage of the SC rises exponentially from 0 to the value that approximately equals the source voltage. The loop current also drops exponentially from  $\frac{V_{in}}{R}$  to 0 at around  $t = 5RC$ . Figure 4.3 depicts the energy distribution over time in a SC charging process.

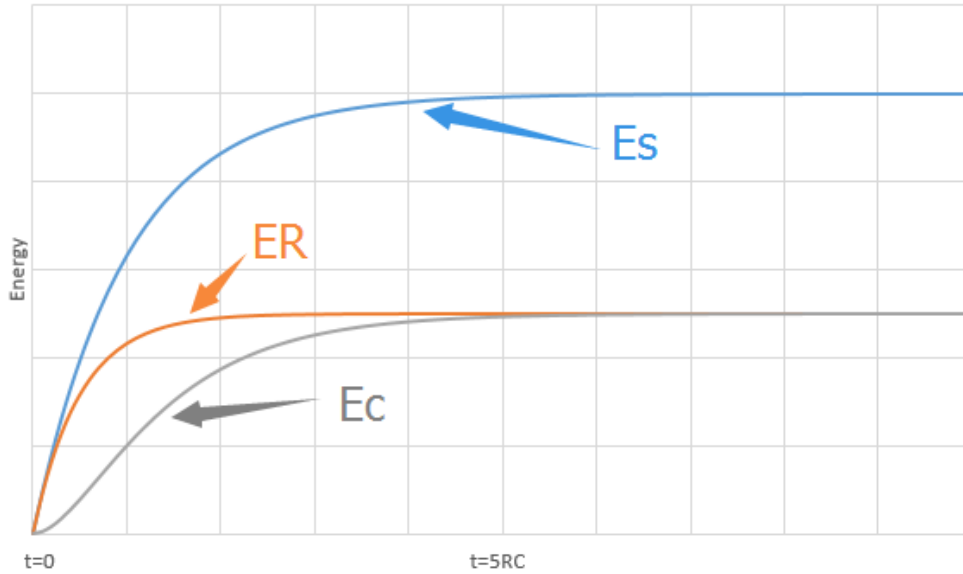


Figure 4.3: The energy distribution over time in a supercapacitor (SC) charging process (constant  $V_{in}$ ).

The energy dissipation,  $E_R$ , occurs on the resistor  $R$  in Figure 4.1; is the total energy delivered from the power source is shown as  $E_s$ , and  $E_c$  is the energy stored in the SC. The scenario depicted in Figure 4.1 and related discussion only apply to the case of a capacitor having a zero charge from the beginning of the process.

#### 4.1.1.2 Charging Efficiency Improvement

As discussed in the previous section, it is clear that a non-negligible amount of energy will dissipate on the loop resistor when an SC is charged by a power source directly. However, if a resistive load (i.e., an LED lamp; Figure 4.4) is connected in series into the loop, most of the wasted energy can be used to power this load instead, and this redirection of energy improves the efficiency of the system significantly.

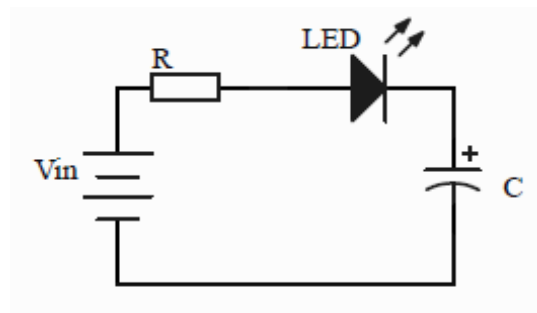


Figure 4.4: Charging a supercapacitor (SC) by using a constant voltage source and with a resistive load (a light-emitting diode [LED]) connected.



Efficiency is described by Equation 4.14:

$$Eff = \frac{E_{LED} + E_C}{E_S} * 100\% \quad (4.14).$$

As shown in figure 4.5, because an LED is a nonlinear component, capacitor voltage,  $V_C$ , does not work exponentially any more. Figure 4.6 illustrates the energy distribution over time as this process takes place. Thus, useful energy ( $E_{LED}$  [LED energy] and  $E_C$  [capacitor energy]) accounts for a major proportion of the total energy ( $E_S$ ). This addition of an LED greatly increases efficiency.



Figure 4.5: Time versus (vs.) terminal voltage of the supercapacitor (SC) when it is charging and discharging, with a light-emitting diode (LED) load connected.

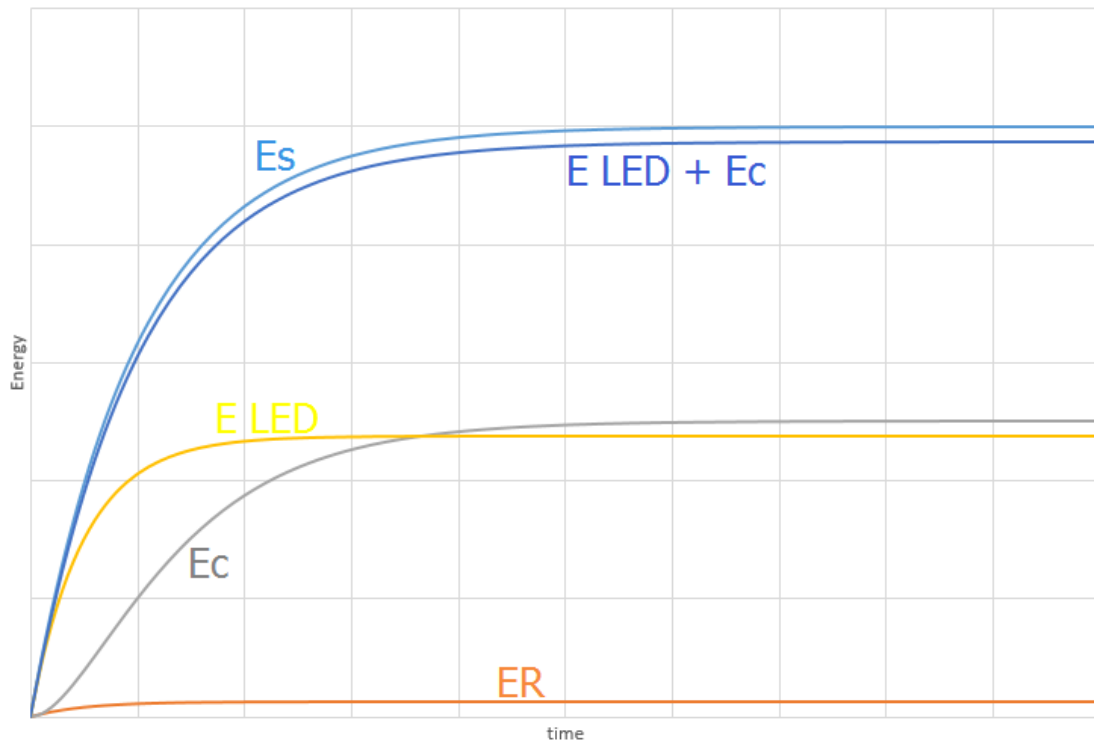


Figure 4.6: Energy distribution over time as charging progresses.

Figure 4.4 shows the energy dissipation,  $E_R$ , on the resistor,  $R$ ; the total energy delivered from the power source is denoted by  $E_s$ , and  $E_c$  is the energy stored in the SC. The energy dissipation in the LED is denoted as  $E_{LED}$ . Note, Figure 4.4 only applies in the situation where the capacitor has a zero charge at the beginning of the process.

### 4.1.2 SC Discharging Characteristics

Figure 4.7 shows a typical circuit used to measure the discharging characteristics of an SC.

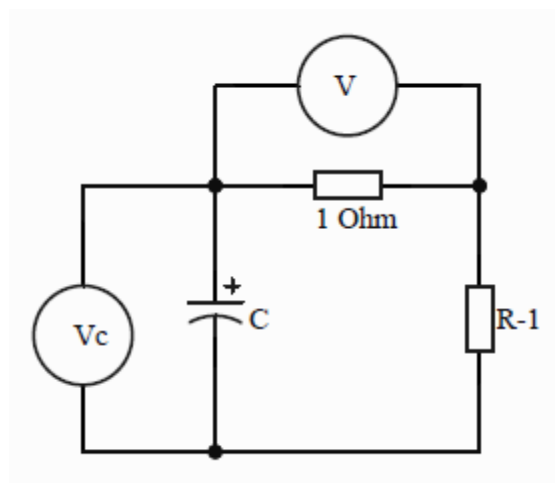


Figure 4.7: Discharging a supercapacitor (SC).

Assume that the SC has been fully charged to its rated voltage before being discharged. The total resistance of this circuit is  $R$ . A volt-meter is connected in parallel with a  $1\ \Omega$  resistor. The value shown on its screen is also the value of the loop current. Another volt-meter yields the real-time reading of the SC's terminal voltage. From Kirchhoff's voltage law, it is clear that the following equation then applies:

$$V_C(t) = i(t)R \quad (4.15)$$

By solving Equations 4.12 and 4.15, it becomes apparent that further SC discharging characteristics can be elucidated:

$$V_C(t) = V_C e^{-\frac{t}{RC}} \quad (4.16),$$

$$i(t) = \frac{V_C(t)}{R} = \frac{V_C}{R} e^{-\frac{t}{RC}} \quad (4.17),$$

$$E_C(t) = \frac{1}{2} C V_C^2(t) = \frac{1}{2} C V_C^2 e^{-\frac{2t}{RC}} \quad (4.18),$$

And

$$E_R(t) = E_C - E_C(t) = \frac{1}{2} C V_C^2 \left( 1 - e^{-\frac{2t}{RC}} \right) \quad (4.19).$$

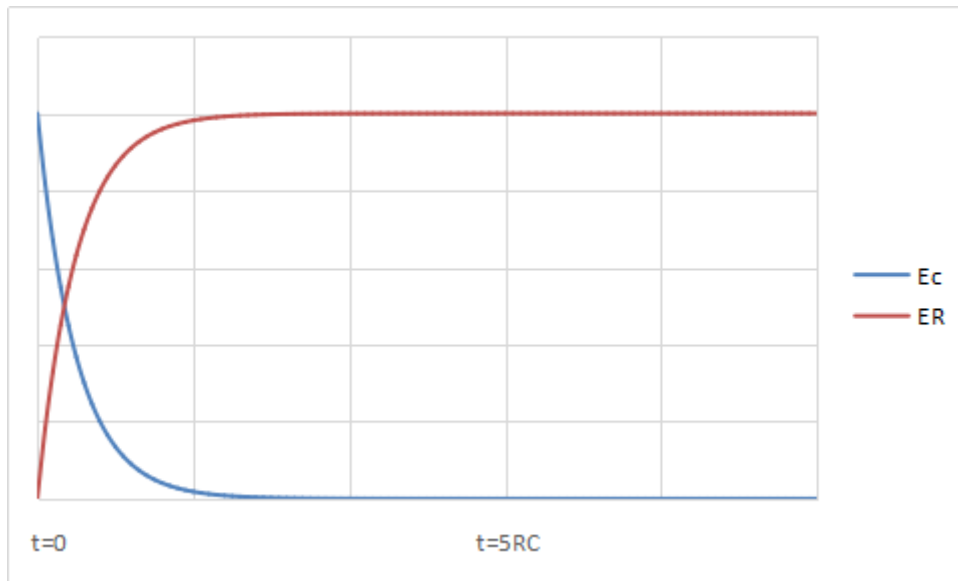


Figure 4.8: The energy distribution over time during a supercapacitor (SC) discharging process.

Figure 4.7 shows the energy dissipation,  $E_R$ , on the resistor,  $R$ , and  $E_C$  is the energy stored in the SC. Figure 4.7 only applies when a capacitor has a zero charge at the beginning of the process.

A typical RC circuit and an oscilloscope (V) used to measure the terminal voltage of capacitor,  $C$ , is shown in Figure 4.9. Figure 4.10 is an example measurement of a typical RC circuit as it discharges. The terminal voltage of the SC decreases exponentially, just as described by Equation 4.16.

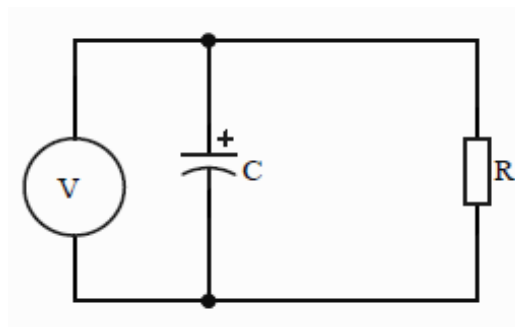


Figure 4.9: A circuit diagram of a typical discharging resistor–capacitor (RC) circuit.

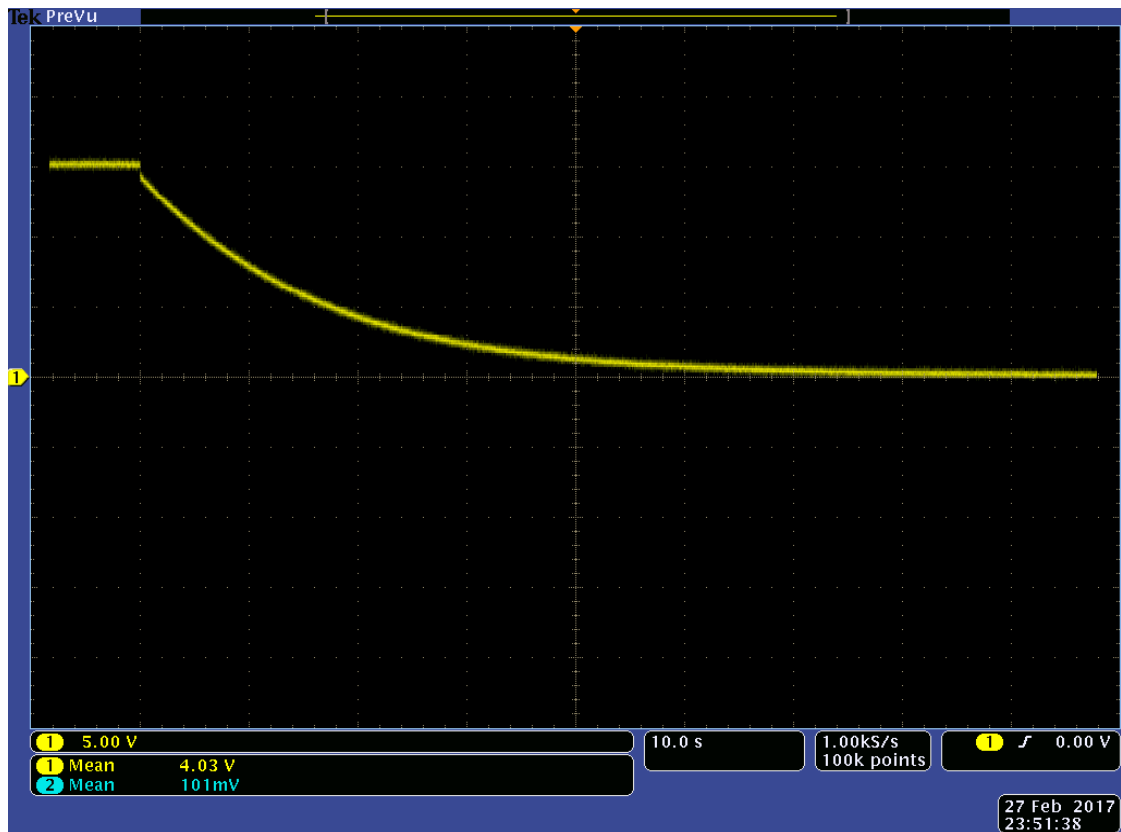


Figure 4.10: The discharge curve of a 2.5 F supercapacitor (SC).

### 4.1.3 Equivalent Series Resistance Measurements

The equivalent circuit of a normal SC is depicted in Figure 4.11. Such an SC consists of an equivalent series resistance ( $ESR$ ), a leakage resistance ( $R_{leakage}$ ) and capacitance ( $C$ ). Due to technological developments,  $ESR$  can now be minimised to around  $10\text{ m}\Omega$ . Because the leakage resistance ( $R_{leakage}$ ) is very large, SC can be considered an open circuit over a short period of time. Figure 4.12 shows a commonly accepted way to measure  $ESR$ .

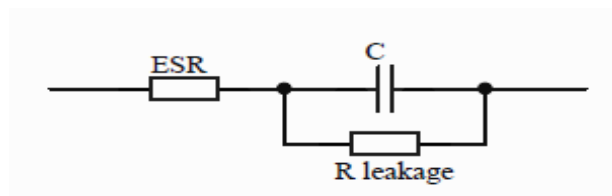


Figure 4.11: The equivalent circuit of a supercapacitor (SC).

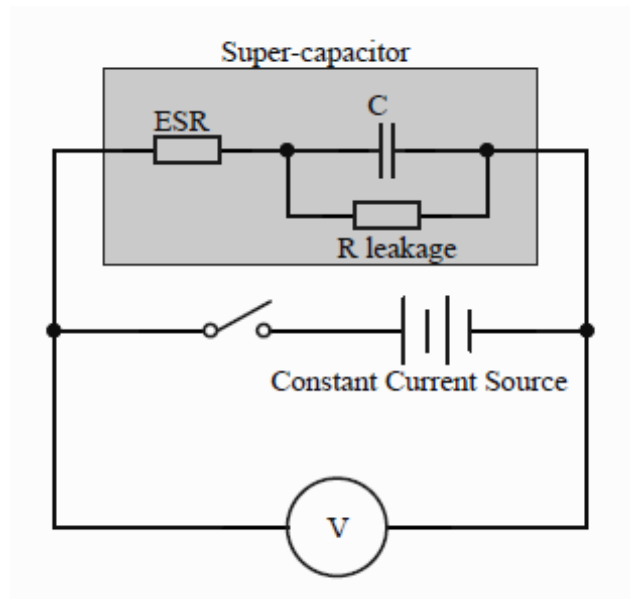


Figure 4.12: A circuit diagram of ESR measurement.

An SC is powered by a constant-current source. The terminal voltage of the SC consists of ESR voltage ( $V_{ESR}$ ) and capacitor voltage ( $V_C$ ):

$$V_1 = V_{ESR} + V_C \quad (4.20).$$

If the current source is disconnected suddenly, the volt-meter measures the SC's  $V_{OC}$ . Thus,  $V_{OC}$  equals  $V_C$  in these circumstances:

$$V_2 = V_C \quad (4.21).$$

Therefore, there will be a voltage drop after disconnecting the SC from the current source. This phenomenon can be monitored by an oscilloscope (Figure 4.13).

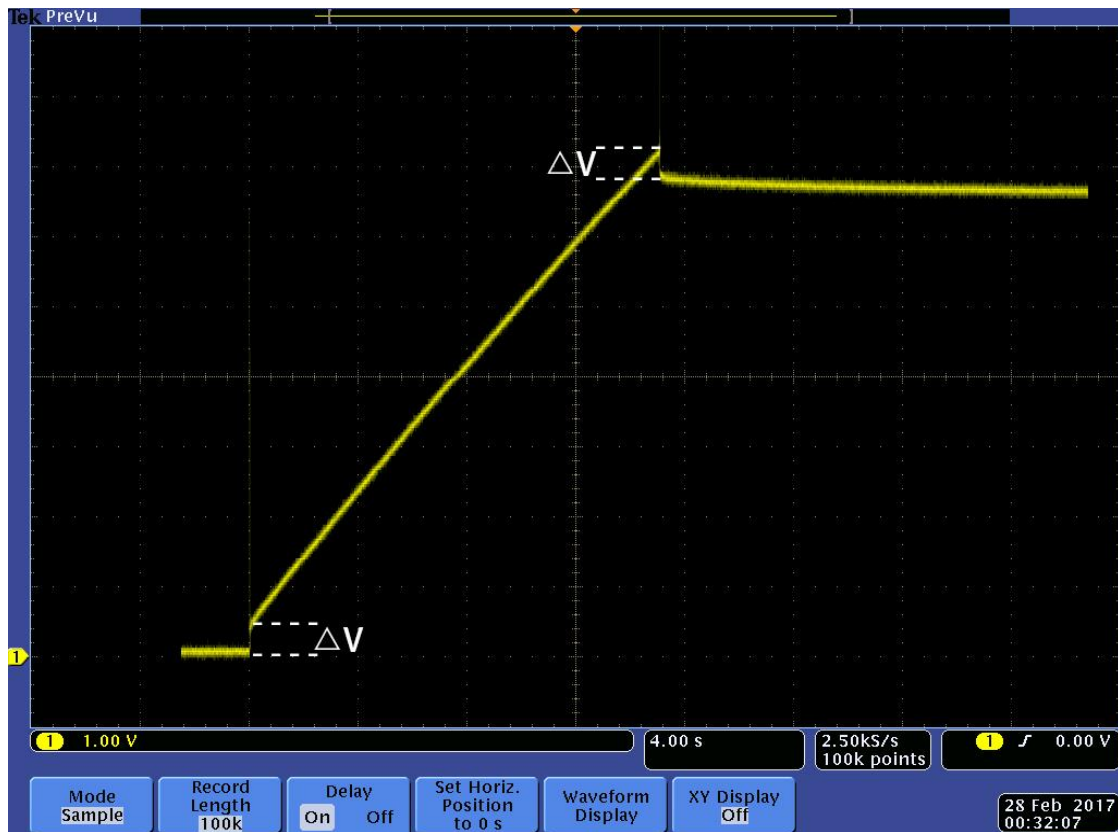


Figure 4.13: A voltage drop occurs after removing the current source suddenly.

The voltage drop in these circumstances can be described by the following equation:

$$\Delta V = |V_1 - V_2| = V_{ESR} \quad (4.22).$$

It then follows that:

$$ESR = \frac{V_{ESR}}{I} = \left| \frac{V_1 - V_2}{I} \right| \quad (4.23),$$

Where  $I$  is the current provided by the current source.

## 4.2 Light-emitting Diode (LED) Lamp Testing

Light-emitting diode lamp arrays are used as resistive loads in DC microgrid systems. The I–V curve of a TCP brand LED lamp and its luminous properties are shown in Figure 4.14. This LED lamp is non-polar and can be powered by bi-directional current.

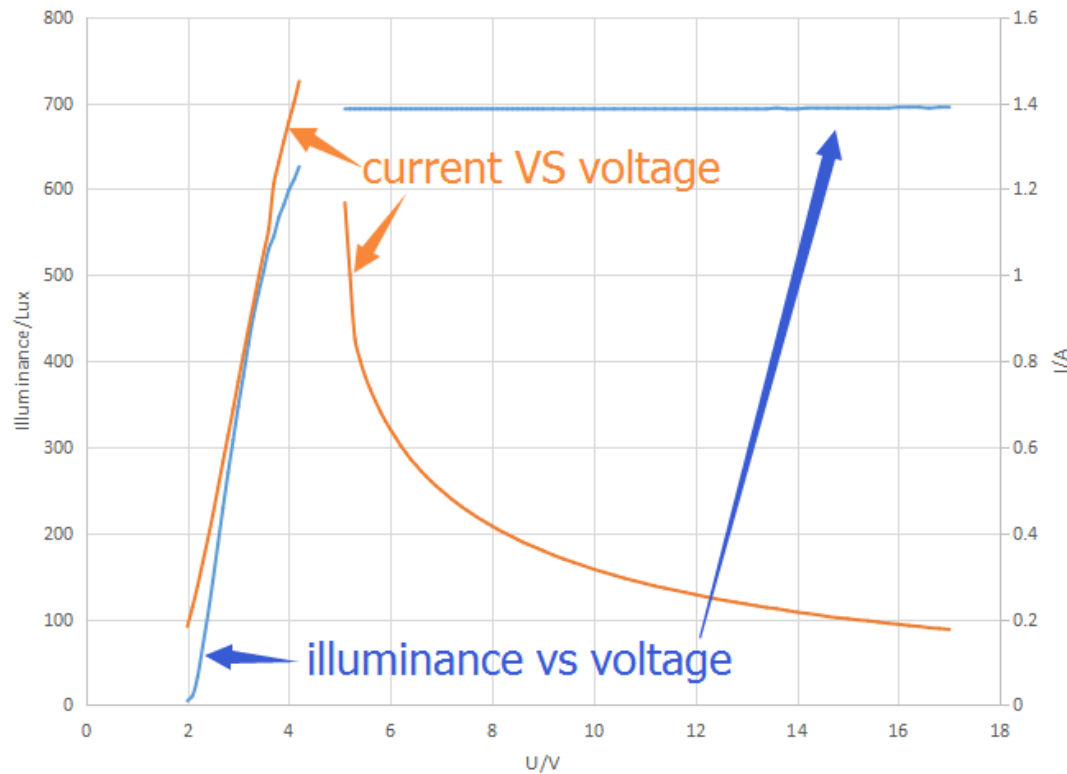


Figure 4.14: A line graph showing the performance of a single TCP brand LED. (the discontinuity was resulted in an unstable working condition for LED over a input voltage range from 4.2 V to 5.3 V)

An input of  $> 5.3$  V should be provided to LED lamps to guarantee they provide light with a constant illuminance. However, an LED lights up with an input voltage of  $> 2$  V. It becomes brighter with higher-input voltages. The LED lamp flashes and does not work properly between 4.2 V and 5.3 V. illuminance remains unchanged at an input voltage ranging from 5.3 V to  $> 17$  V. If this voltage input range is exceeded, LED lamps still work but may burn out quickly.

To light up an LED (TCP brand LED MR16, 5 W, 12 V), a large initial current is needed. The testing circuit required is shown in Figure 4.15, and the test results from the current research are shown in Figures 4.16 and 4.17.



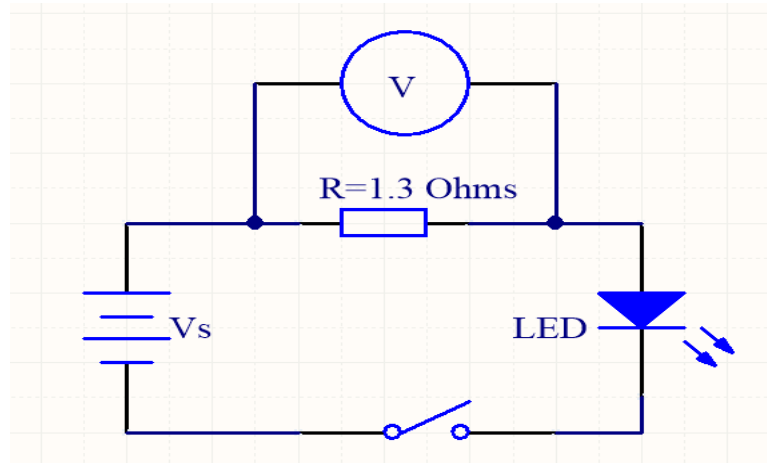


Figure 4.15: A circuit diagram of a light-emitting diode (LED) performance test.

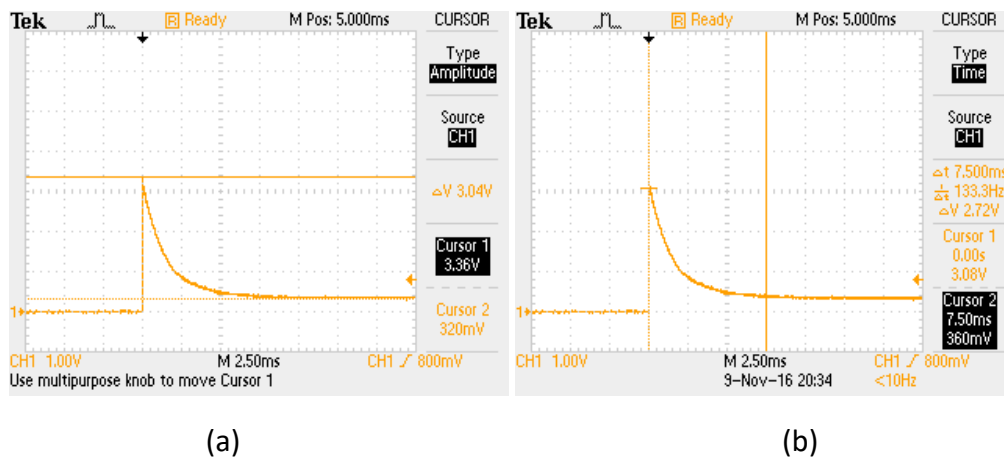
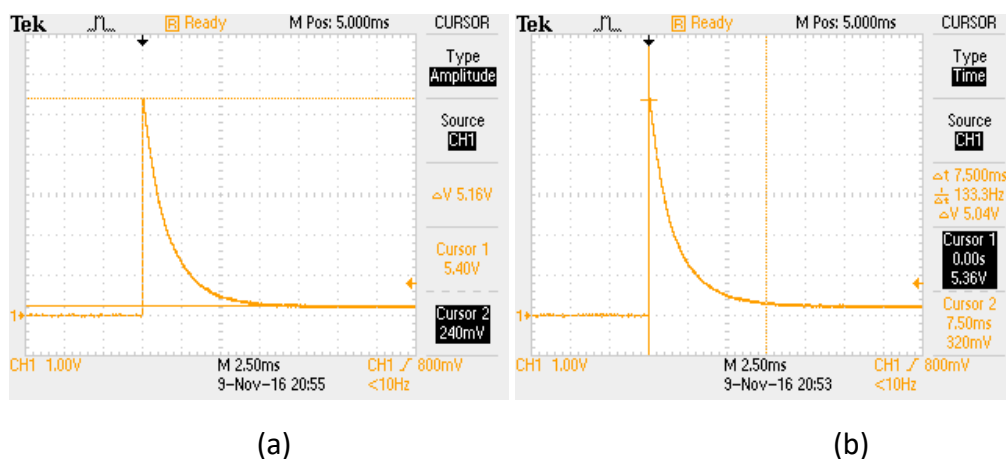
Figure 4.16: A diagram showing the moment a TCP brand LED is turned on (MR16; 5 W,  $V_s = 12 \text{ V}$ ): (a) voltage measurement; and (b) time measurement.Figure 4.17: A diagram showing the moment when a TCP brand LED is turned on (MR16; 5 W,  $V_s = 18 \text{ V}$ ): (a) voltage measurement; and (b) time measurement.

Figure 4.16 (a) & (b) and Figure 4.17 (a) & (b) are screenshots of the exact moment when a TCP brand MR16, 5 W, 12 V LED lamp was turned on. These figures illustrate that the initial current required for lighting up an LED was quite large. However, the LED required a smaller initial current if it was powered by a higher input voltage. In other words, the TCP brand 5 W MR16 LED lamp required a high initial input power to light up. The time period for lighting up was very short and lasted no longer than 10 ms.

As described in Chapter 2 (Figure 2.7), due to the delay inherent in the PID algorithm, the PV simulator used in the current research was unable to output the needed power within 10 ms. However, adding a capacitor in parallel with the power supply solved this problem, because the capacitor was able to provide an instant large current to the LED.



# **Chapter 5**

## **Circuit Design and System Implementation**



## 5.1 Introduction

The complete SC-assisted power converter for a DC microgrid system consists of a control circuit and a switch circuit. The control circuit can be further divided into two parts: a voltage sampling circuit and a driver circuit for MOSFET switches.

Figure 5.1 is a simplified circuit diagram of the complete DC microgrid system with SC-assisted power converter designed for this project. Table 5.1 provides a brief description of the switches' operation. In Figure 5.1, P-channel MOSFETs are used as switches  $S_{11}$  and  $S_{21}$ , while N-channel MOSFETs are used as switches  $S_{12}$  and  $S_{22}$ . The main aim of this switch circuitry is to achieve the symmetrical working of two system portions, or halves. However, if both halves (left and right) are charging or discharging at the same time, the power supply (the PV or solar panels) works discontinuously. Indeed, when both SC banks are being charged, the power supply always outputs approximately twice the power needed for each load, while if both SC banks are discharging, no energy comes from the PV, which results in a waste of solar energy if sunlight is available. Therefore, a good switch circuit routine should be able to keep both halves of the system operating at the same time but in different stages (one half charging and the other half discharging). In other words, if the left portion of the system is powered by the PV or solar panels and SC bank 1 is being charged, the right portion of the system should disconnect from the PV and run by discharging SC bank 2, and *vice versa*.

The whole system was set up, as shown in Figure 5.2, to evaluate the performance of the experimental solar-powered DC microgrid, and Figure 5.3 illustrates the final implementation of this DC microgrid system.

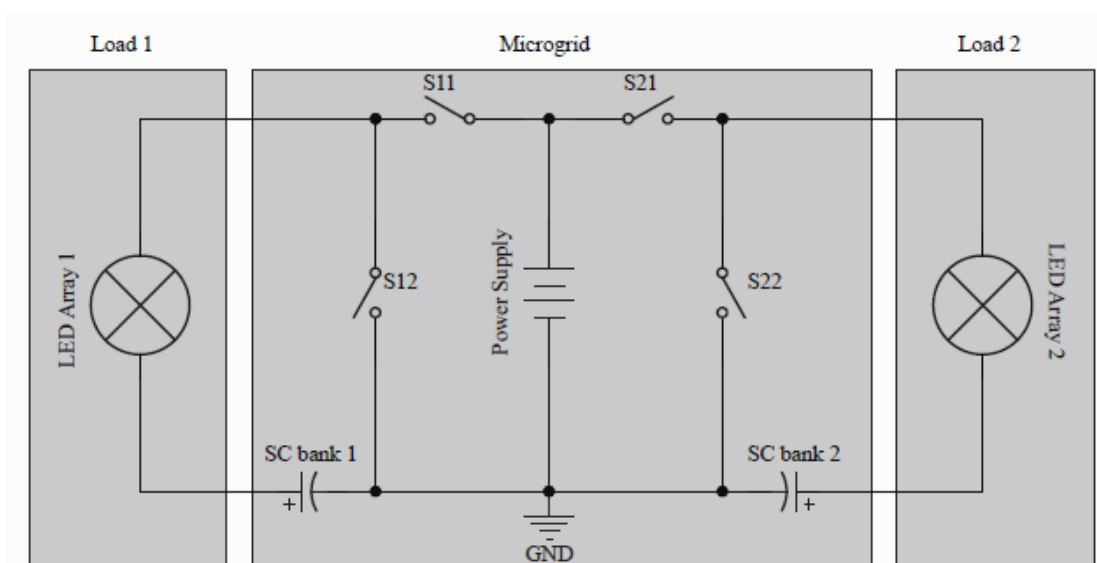


Figure 5.1: Circuit diagram of the complete DC microgrid system.

Table 5.3 Switch operation.

	<b>C1C2</b>	<b>C1D2</b>	<b>D1C2</b>	<b>D1D2</b>
<b>Switch 11</b>	on	on	off	off
<b>Switch 12</b>	off	off	on	on
<b>Switch 21</b>	on	off	on	off
<b>Switch 22</b>	off	on	off	on
In this table, C = charge; D = discharge;				

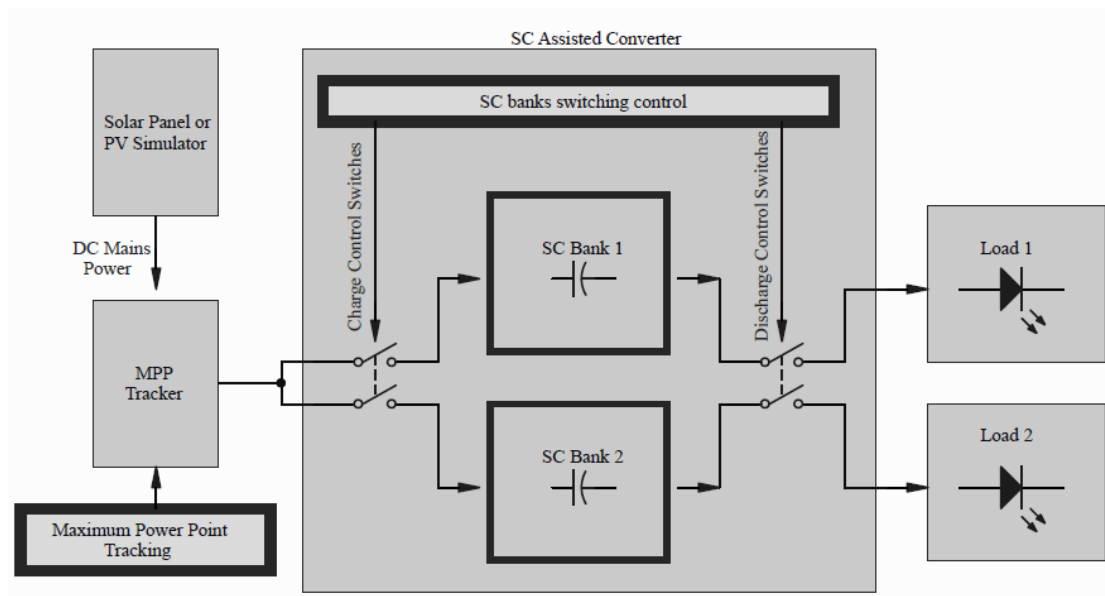


Figure 5.2: A block diagram of a DC microgrid system.

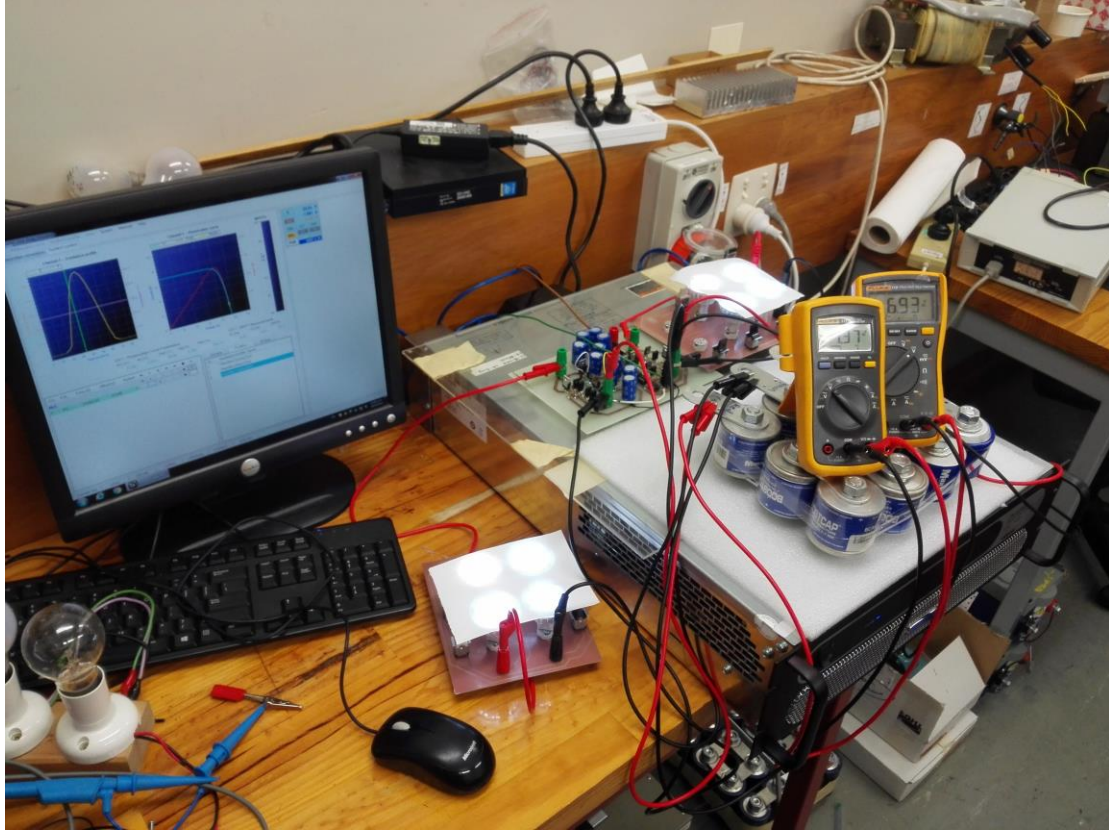


Figure 5.3: Photo of the complete DC microgrid System with 12V LED loads.

## 5.2 Control Circuit Design and Implementation

### 5.2.1 Sampling circuit

There are three analogue-to-digital converters (ADCs) integrated into the microcontroller PIC16F684 (manufactured by Microchip Technology Inc.). they can be used to measure the real-time source voltage and terminal voltages of two SC banks. The ADC converts an analogue input signal into a 10-bit binary digital representation of that signal via successive approximation. Then, this result is stored in the ADC result low (ADRESL) and ADC result high (ADRESH) registers of the microcontroller. The ADC voltage reference is software-selectable to either  $V_{DD}$  (Voltage Drain Drain) or a voltage applied to the external reference pins [24]. In my code, a 5 V  $V_{DD}$  was selected as a voltage reference. Therefore, the resolution of each 10-bit ADC was:

$$5V \times \frac{1}{1024} \approx 4.88mV \quad (5.1)$$



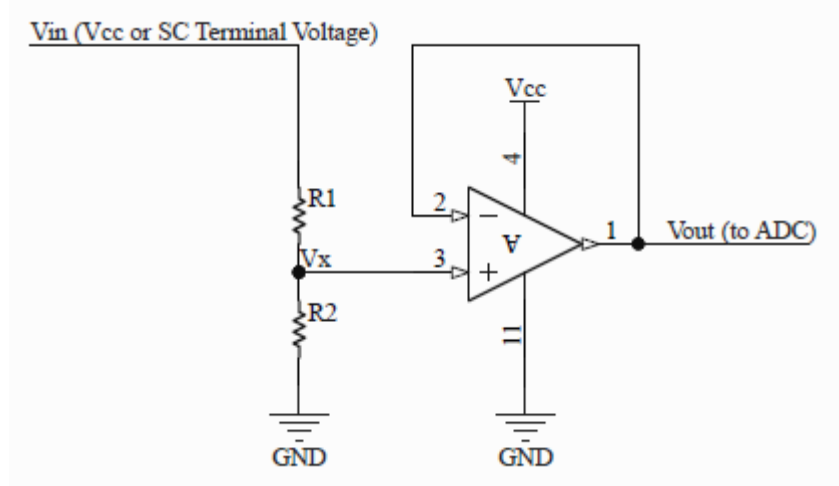


Figure 5.4: The diagram for the sampling circuit.

Figure 5.4 shows sampling circuit structure for the DC microgrid system. This type of circuit is used to sample the source voltage or terminal voltage of each SC bank. The source voltage (PV simulator output) can be up to 25 V. The  $V_x$  in Figure 5.4 should not be bigger than 5 V when  $V_{in}$  is 25 V. Therefore:

$$V_x = V_{in} \times \frac{R_2}{R_1 + R_2} < 5 \Rightarrow \frac{R_1}{R_2} > \frac{V_{in} - 5}{5} \quad (5.2).$$

The voltage divider in Figure 5.4 consists of  $R_1$  and  $R_2$ . The voltage signal,  $V_x$ , is fed to the ADC via an operational amplifier (OP-AMP), which acts as a voltage follower in this circuit.  $V_x$  should not be fed to the ADC directly. An equivalent circuit with the OP-AMP removed is shown in Figure 5.5.

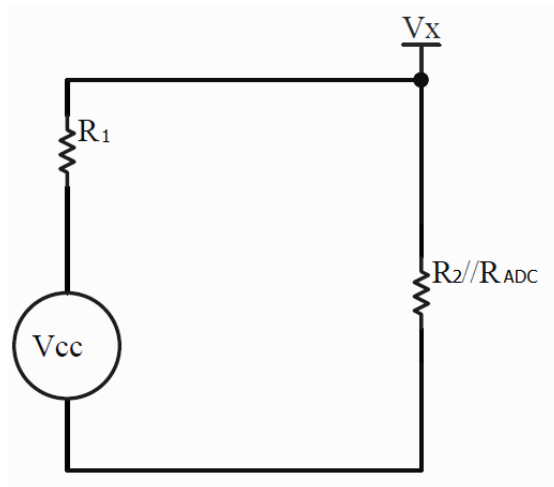


Figure 5.5: Equivalent circuit with the OP-AMP removed.

The value of  $R_{ADC}$  ranges from 10 k $\Omega$  to 56 k $\Omega$  [24]. Take a 25 k $\Omega$   $R_{ADC}$  as an example. If a 10 k $\Omega$   $R_1$  and a 1.8 k $\Omega$   $R_2$  are selected as voltage dividers for sampling 24 V source voltage,  $V_x'$  in Figure 5.5 becomes:

$$V_x' = V_{CC} \times \frac{R_2 // R_{ADC}}{R_1 + R_2 // R_{ADC}} = 3.594V \quad (5.3).$$

However,  $V_x$  in figure 5.4 should be:

$$V_x = V_{CC} \times \frac{R_2}{R_1 + R_2} = 3.661V \quad (5.4).$$

The error is calculated thus:

$$V_E = |V_x' - V_x| = 0.067V = 67mV \quad (5.5).$$

The error,  $V_E$ , is approximately 14 times that of the 4.88 mV resolution. If larger values for  $R_1$  and  $R_2$  are selected, this error becomes even larger (by applying function [24]). However, if the resistances, of  $R_1$  and  $R_2$ , are too small, the steady-state current from source to ground via  $R_1$  and  $R_2$  can be large. This leads to a low-efficiency system. Therefore, because of its advantageous characteristics, the operational amplifier (OP-AMP) was selected as a voltage follower connected between the voltage divider ( $R_1$  and  $R_2$ ) and the analogue-to-digital converter (ADC). The OP-AMP's advantages are that it has an infinite input resistance and a zero output resistance (ideally). Therefore, it was used to increase input resistance and to reduce output resistance. The voltage divider and the ADC were isolated by the OP-AMP (Figure 5.6).

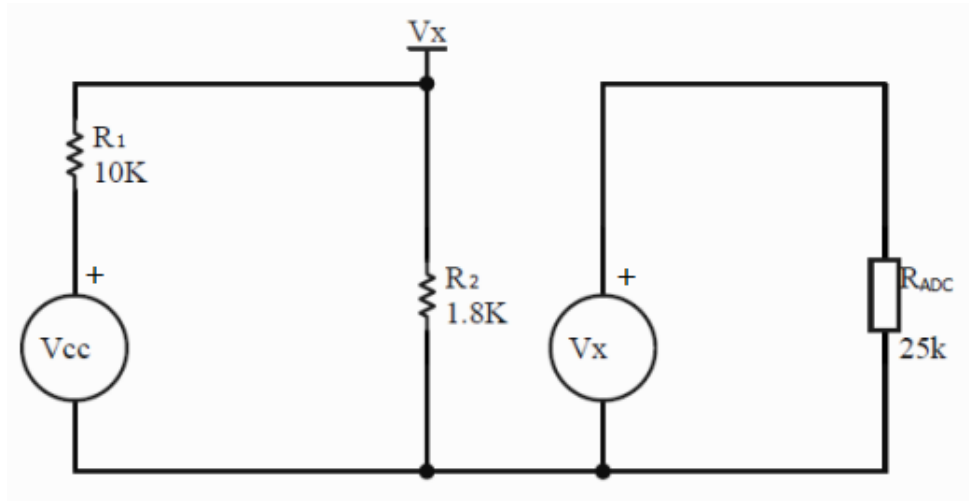


Figure 5.6: Equivalent circuit after adding an OP-AMP

In this design, the resistance values of  $R_1$  and  $R_2$  selected for sampling source voltage ( $V_{cc}$ ) or SC terminal voltages ( $V_{sc}$ ; up to 15 V) were obtained by using inequality 5.2. Table 5.1 shows the chosen values of  $R_1$  and  $R_2$  after performing the necessary calculations.

Table 5.1: Resistance selection for sampling source and terminal voltages.

	For sampling $V_{cc}$	For sampling $V_{sc}$
$R_1$	10k $\Omega$	10k $\Omega$
$R_2$	1.8k $\Omega$	4.7k $\Omega$

Figure 5.7 shows the input and output waveform of the sampling circuit. The yellow curve represents the input signal and the blue curve represents the response of the input signal. This response can be measured by ADCs.

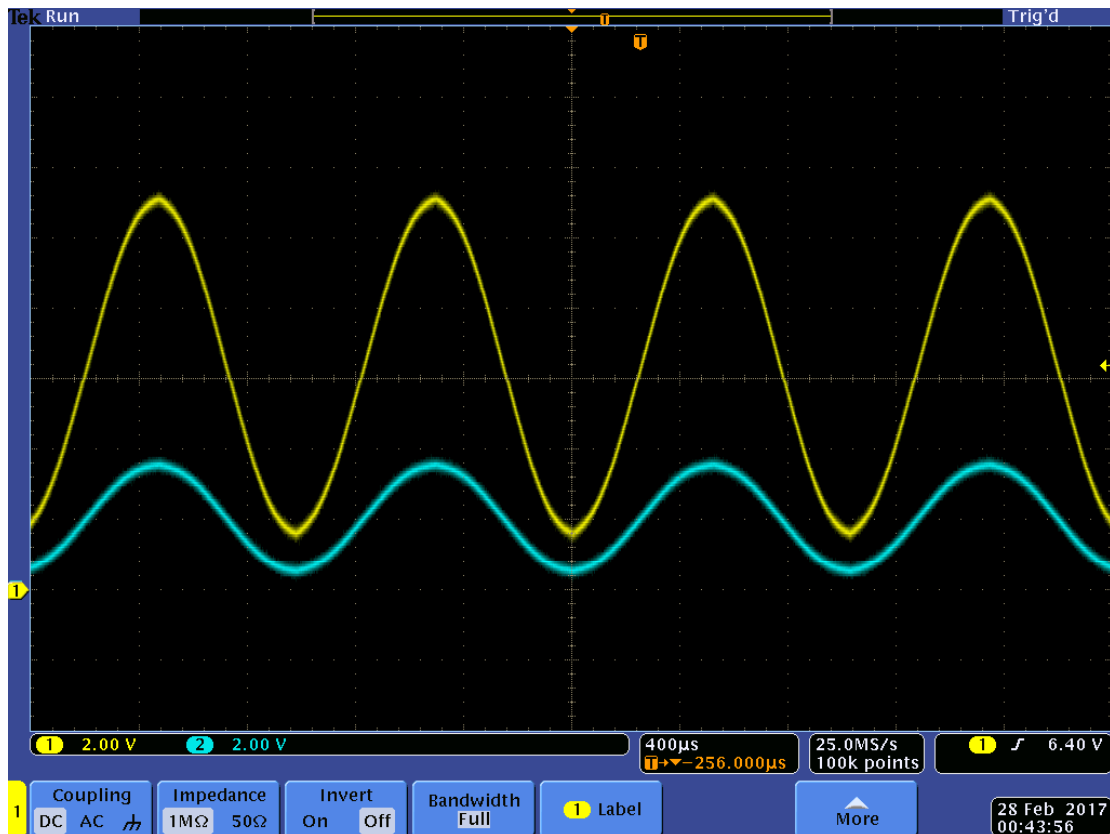


Figure 5.7: Response of the sampling circuit.

## 5.2.2 The Metal-Oxide Semiconductor Field Effect Transistor (MOSFET) Driver Circuit

The DC microgrid application designed in the current project contained an SC-assisted, high-efficiency converter. This converter was a switch circuit controlled by a microcontroller and driven by MOSFET drivers. Figure 5.8 illustrates one part of the switch circuit I used. The circuit was powered by a PV when switch 1 ( $S_1$ ) was on and switch 2 ( $S_2$ ) was off. By disconnecting  $S_1$  and connecting  $S_2$ , the SC discharged. One of the optional components for both switches (Figure 5.8) was a power MOSFET transistor. I was able to use the P-channel power MOSFET as  $S_1$ , while the N-channel power MOSFET operated as  $S_2$ .

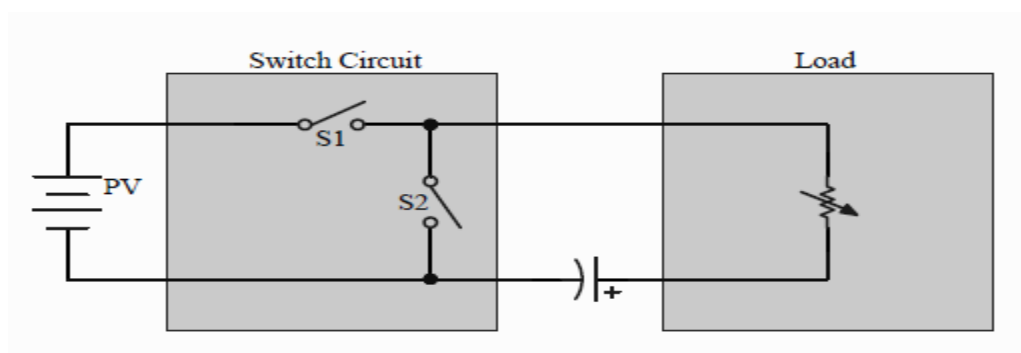


Figure 5.8: A schematic drawing of a switch circuit with a load and a supercapacitor (SC).

### 5.2.2.1 The Metal-Oxide Semiconductor Field Effect Transistor (MOSFET)

A MOSFET is a semiconductor device that is often used as an electric switch in a circuit. The major advantage of the MOSFET transistor is that it uses low power for switching on or off, and the dissipation of power in terms of loss is therefore very small.

There are two types of MOSFET: the N-channel MOSFET and the P-channel MOSFET. They have three terminals, namely the source, the gate and the drain. In an N-channel MOSFET, the channel is made of an N-type semiconductor, so the charges are free to move along the channel and are negatively charged (electrons). In a P-channel device, the free charges that move from end-to-end are positively charged (holes) [25]. When the MOSFET is used as a switch, its basic function is to control the drain current via the gate voltage.

An equivalent circuit model of a typical N-Channel MOSFET (Figure 5.9) is often used for the analysis of MOSFET switching performance. The performance of a MOSFET is determined by the time required to establish voltage changes across capacitances. In Figure 5.9, the distributed resistance of the gate is denoted by  $R_G$ , and  $L_D$  and  $L_S$  denote drain and source lead inductances, respectively. Both  $L_D$  and  $L_S$  are a few tens of nanohenries (nH) each.

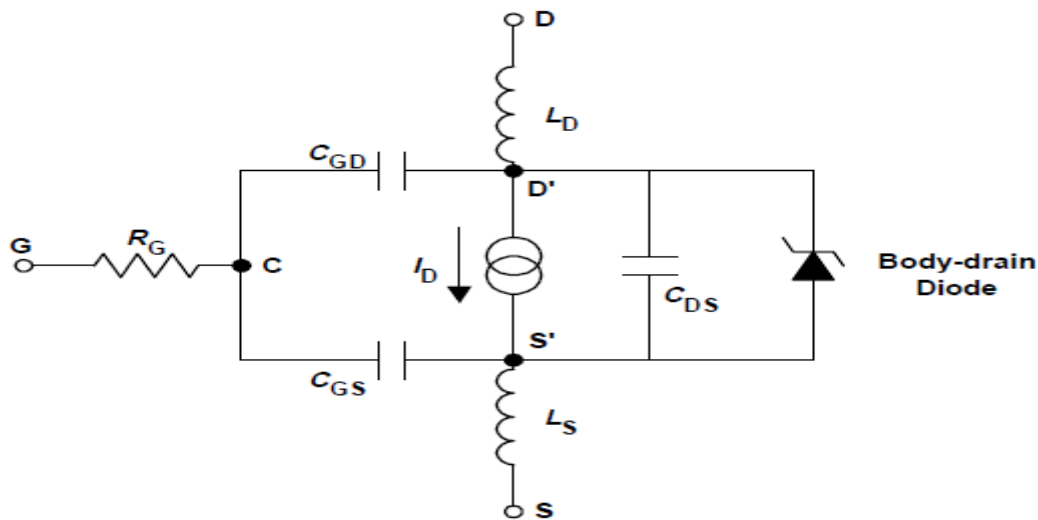


Figure 5.9: A metal-oxide semiconductor field effect transistor (MOSFET) equivalent circuit.

Typical values of input capacitance ( $C_{iss}$ ), output capacitance ( $C_{oss}$ ) and reverse transfer ( $C_{rss}$ ) capacitance are usually provided in datasheets. The datasheet capacitances are defined as

$$C_{iss} = C_{GS} + C_{GD}, \quad (5.6),$$

$C_{DS}$  shorted,

$$C_{rss} = C_{GD} \quad (5.7),$$

And

$$C_{oss} = C_{DS} + C_{GD} \quad (5.8).$$

The nonlinear function of voltage,  $C_{GD}$ , is the most important parameter because it provides a feedback loop between the circuit output and input.  $C_{GD}$  is also known as the Miller capacitance; it causes the total dynamic input capacitance to become greater than the sum of the static capacitances [26].

Turn-on delay is the time taken to charge the input capacitance of the device before drain current conduction can start. Similarly, turn-off delay is the time taken to discharge the capacitance after the device is switched off.

As shown in Figure 5.10, when the gate is connected to the supply voltage,  $V_{GS}$  starts to increase until it reaches the threshold,  $V_{TH}$ , at which point  $C_{GS}$  begins to charge, and the drain current starts to flow. From time  $t_1$  to time  $t_2$ ,  $C_{GS}$  keeps charging, gate voltage continues to rise and drain current rises proportionally. At time  $t_2$ ,  $C_{GS}$  is completely charged, and the drain current reaches the predetermined current,  $I_D$ , which then remains constant while the drain voltage starts to fall [26]. With reference to the equivalent circuit model of the MOSFET shown in Figure 5.9, it can be seen that with  $C_{GS}$  fully charged at time  $t_2$ ,  $V_{GS}$  becomes constant and the drive current starts to charge the Miller capacitance,  $C_{DG}$  [26]. This continues until time  $t_3$  [26]. Charge time for the Miller capacitance,  $C_{DG}$ , is larger than that for the gate-to-source capacitance,  $C_{GS}$ , due to the rapidly changing drain voltage between time  $t_2$  and time  $t_3$  (current =  $C \cdot dv/dt$ ). Once both  $C_{GS}$  and  $C_{GD}$  are fully charged, gate voltage ( $V_{GS}$ ) starts increasing again until it reaches the supply voltage at time  $t_4$  [26]. The gate charge ( $Q_{GS} + Q_{GD}$ ) corresponding to time  $t_3$  is the bare minimum charge required to switch the device on [26].

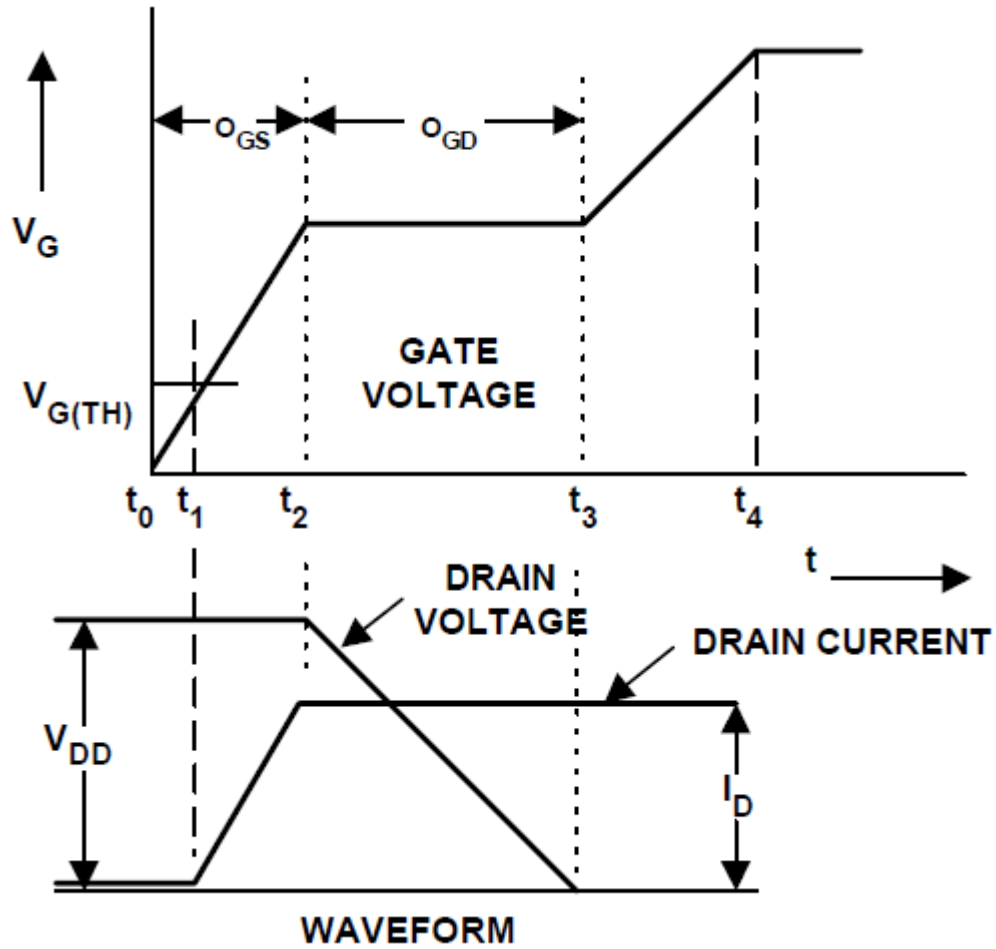


Figure 5.10: Resulting gate and drain waveforms during a gate-charge test.

The advantage of using gate charge in the current project was that I could easily calculate the amount of current required from the drive circuit to switch the device on in a desired length of time, because

$$Q = CV \Rightarrow I = \frac{dQ}{dt} = C \frac{dV}{dt} \quad (5.9).$$

For example, a device with a gate charge of 20 nC can be turned on in 20 ms if 1 mA is supplied to the gate, or it can be turned on in 20 ns if the gate current is increased to 1 A [26].

### 5.2.2.2 Gate Drivers

Figure 5.11 and 5.12 represent the circuit schematics of a P-Channel MOSFET ( $S_1$  in figure 5.8) gate driver and an N-Channel MOSFET ( $S_2$  in figure 5.8) gate driver. When

the circuit is working, either  $S_1$  or  $S_2$  will conduct, and a large current (1.5 A–2 A) will flow via these power MOSFET switches. Therefore, I used a totem-pole circuit, including transistors  $Q_1$  and  $Q_2$ , to provide an instant large current to the grid of  $S_1/S_2$ , which guaranteed that the power MOSFET was turned on / off as quickly as possible.

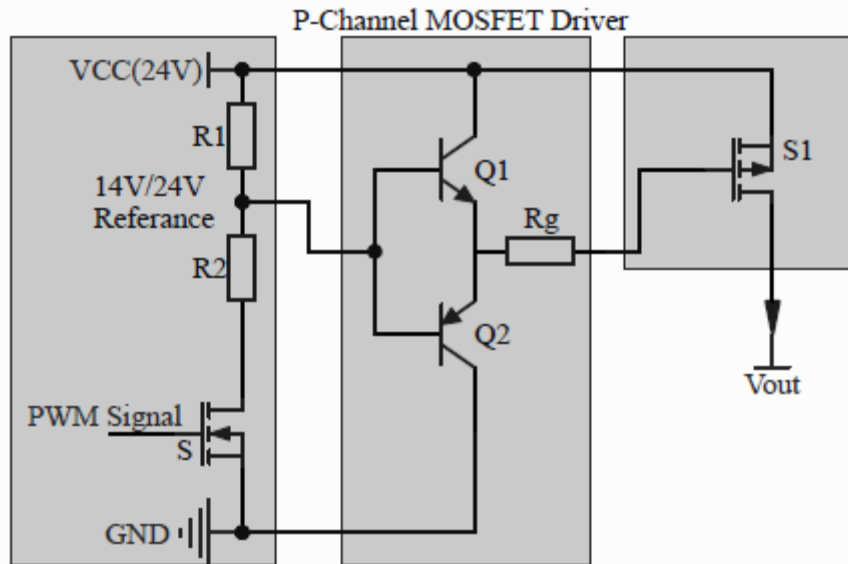


Figure 5.11: A schematic drawing of a P-channel power MOSFET switch 1 ( $S_1$ ) gate driver.

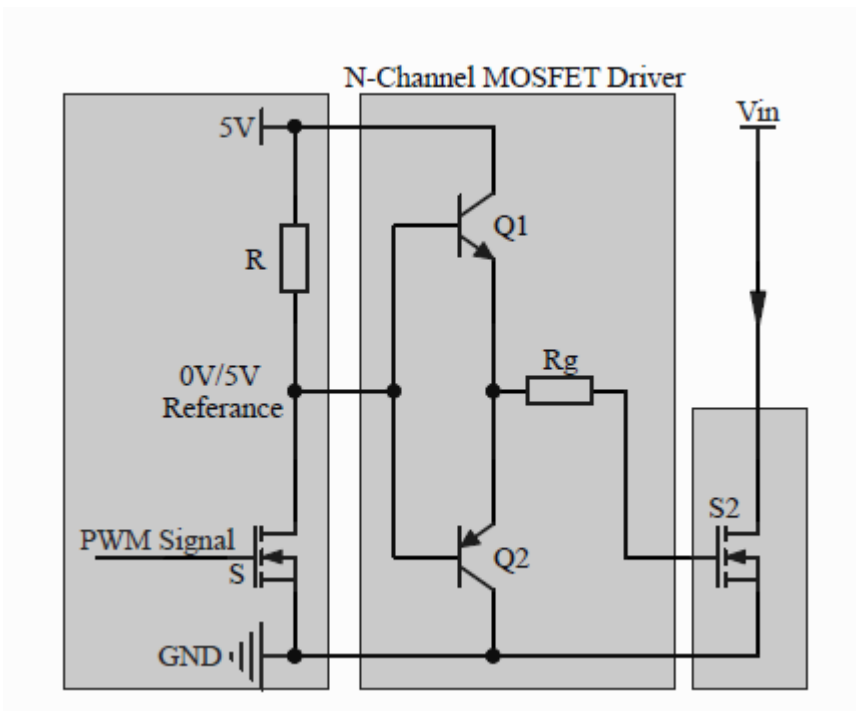


Figure 5.12: A schematic drawing of an N-channel power MOSFET switch 2 ( $S_2$ ) gate driver.



In Figure 5.11, the difference of the voltage reference is 10 V; this parameter is 5 V in Figure 5.12. I checked the input capacitance,  $C_{iss}$ , of both  $S_1$  and  $S_2$  by reviewing their respective datasheets. These capacitances are shown in Table 5.2. By using Equation 5.9, the values of  $I_G$  and  $R_g$  ( $R_g = \Delta V_{Grid}/I_G$ ), can be obtained. Figure 5.13 shows the response of the MOSFET SPP80P06P H under the condition that  $I_D = 1.5$  A and  $V_{GS} = 10$  V.

Table 5.2: the values of  $I_G$  and  $R_g$  for P-Channel [27] and N-Channel [28] metal-oxide semiconductor field effect transistor (MOSFET) drivers.

	P-channel (SPP80P06P H)	N-channel (PSMN80R5-100PS)
$C_{iss}$	4500 pF	9500 pF
$\Delta V_{Grid}$	10 V	5 V
$I_G$	450 mA	475 mA
$R_g$	22 $\Omega$	10 $\Omega$
Delay $\Delta t \leq 100$ ns		

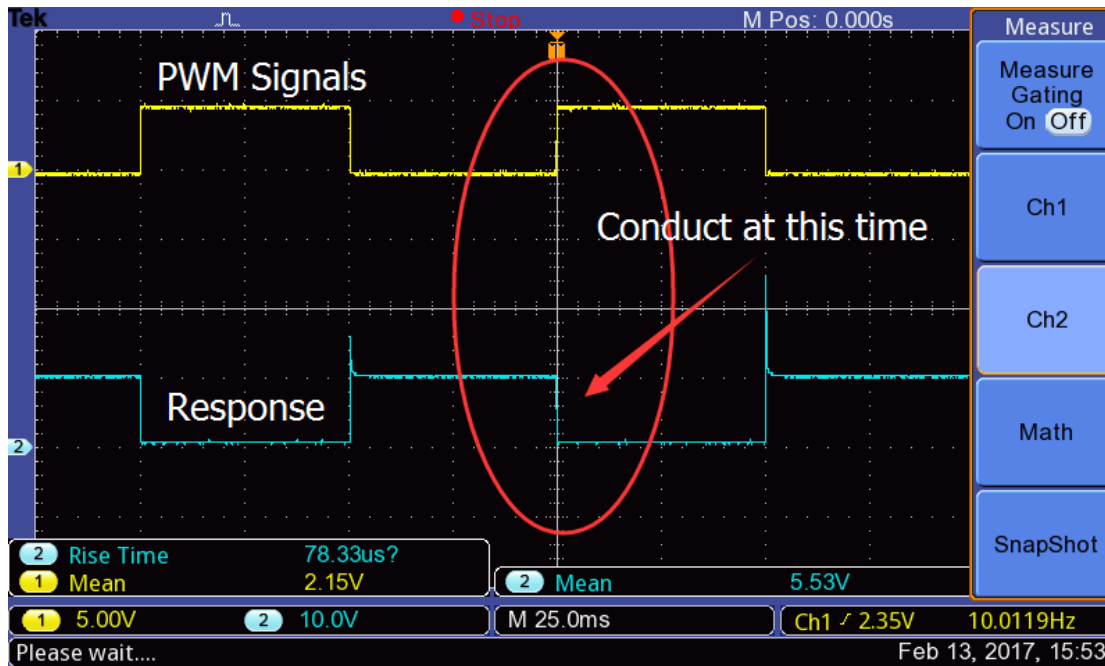


Figure 5.13: The metal-oxide semiconductor field effect transistor (MOSFET) response to a 10 V pulse-width modulation (PWM) input signal via the MOSFET driver.

A small resistor,  $R_g$ , connected to the gate helps to eliminate swings, but this addition causes a delay when turning on the MOSFET. Figures 5.14 and 5.15 show the delay difference when turning on an N-channel MOSFET SPP80P06P H ( $I_D = 1.5$  A;

$V_{GS} = 10$  V) without and with the small resistor, respectively. Times of 59 ns and 881 ns were required to conduct electricity with a  $R_g$  of  $1.5\ \Omega$  and  $10\ \Omega$ , respectively.

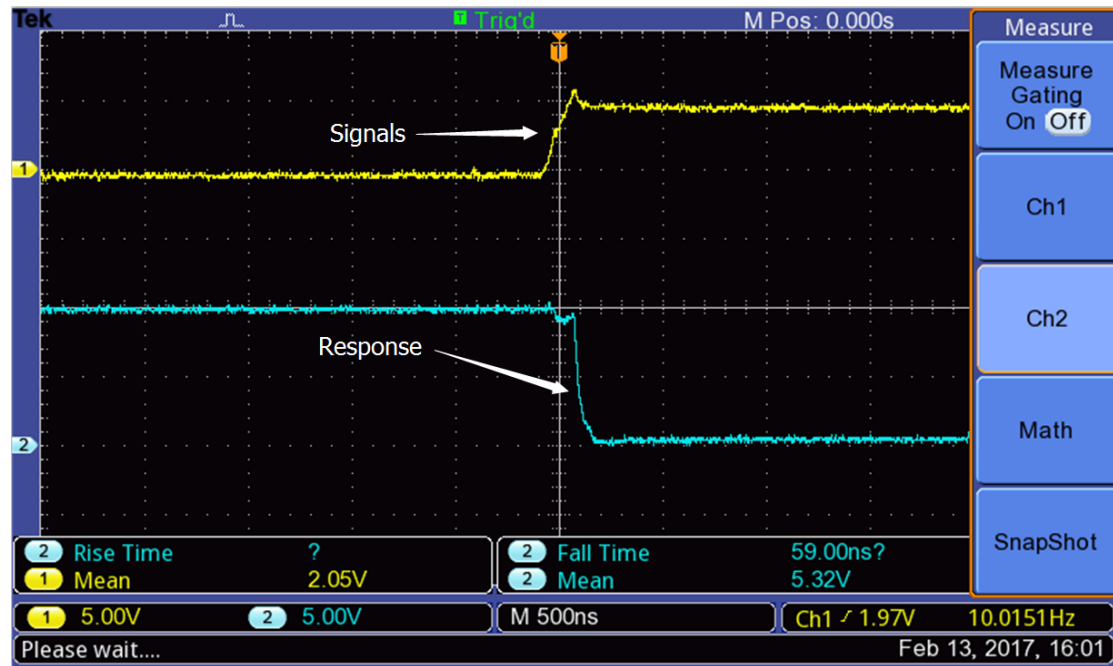


Figure 5.14: The delay (59 ns) in turning on the metal-oxide semiconductor field effect transistor (MOSFET) SPP80P06P H without the small resistor ( $I_D = 1.5$  A;  $V_{GS} = 10$  V;  $R_g = 1.5\ \Omega$ ).

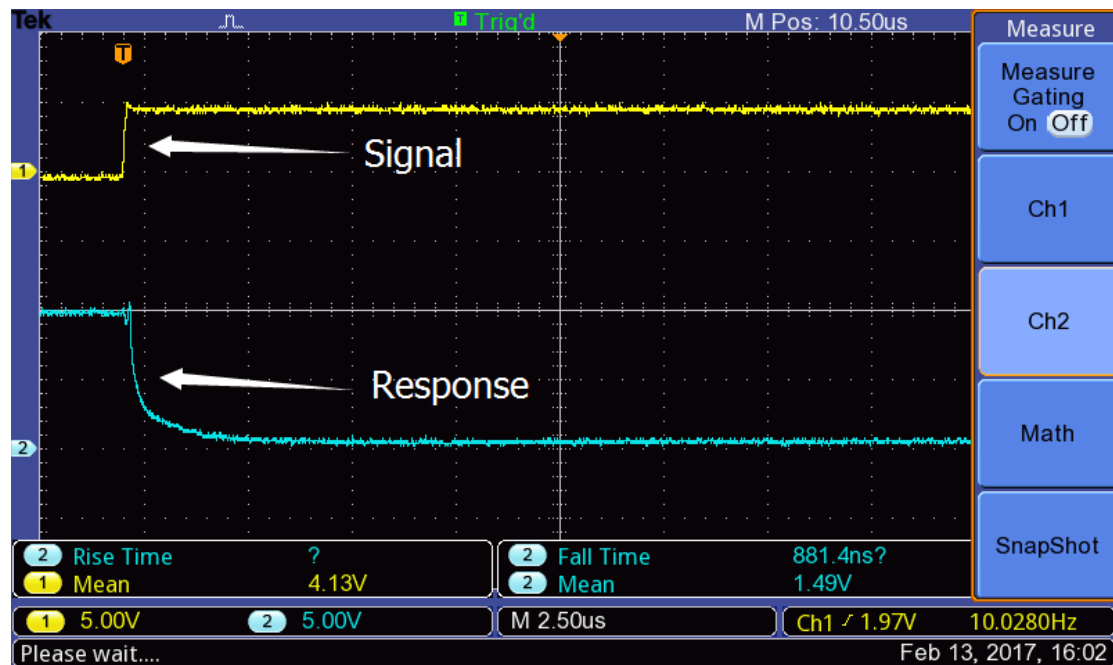


Figure 5.15: The delay (881 ns) in turning on the metal-oxide semiconductor field effect transistor (MOSFET) SPP80P06P H with the small resistor ( $I_D = 1.5$  A;  $V_{GS} = 10$  V;  $R_g = 10\ \Omega$ ).

As illustrated in Figures 5.14 and 5.15, it takes  $< 100$  ns to turn on the MOSFET when a smaller  $R_g$  is selected. In addition, less heat is generated during the off-to-on period. This guarantees that the MOSFET does not burn out quickly.

## 5.3 Switch Circuit Design and Implementation

As mentioned in Section 5.1, the main aim in designing this type of switch circuit (Figure 5.1) was to achieve the symmetrical working of the system's two parts. Figure 5.16 depicts the ideal case of both system parts in terms of the SC banks' terminal voltages. In Figure 5.16, ideally, if the left half (part 1) and the right half (part 2) of the system are identical, when SC bank 1 is charged to 12 V from time  $t_0$  to time  $t_1$  (the blue line),  $V_{c2}$  should also reach 12 V (the red line) at time  $t_1$ . Then, the system starts running at a steady state. From time  $t_1$ , SC bank 1 charges to 13 V at time  $t_2$ , which is 1 V higher than half- $V_s$  ( $0.5 * 24 = 12$  V). On the other hand, SC<sub>2</sub> discharges to 11 V at time  $t_2$ , which is also 1 V but lower than half- $V_s$ . After time  $t_2$ , both parts change their phase: SC bank 1 is discharged while SC bank 2 is charged. Subsequently, they 'meet' again at time  $t_3$  at 12 V. This process maintains until a sudden outage of power supply (reasons may include sunset, a sudden breakdown of the solar panels, a failure in an electronic circuit or similar problem) at time  $t_6$ . Both banks release their stored energy to maintain system running for a period of time.

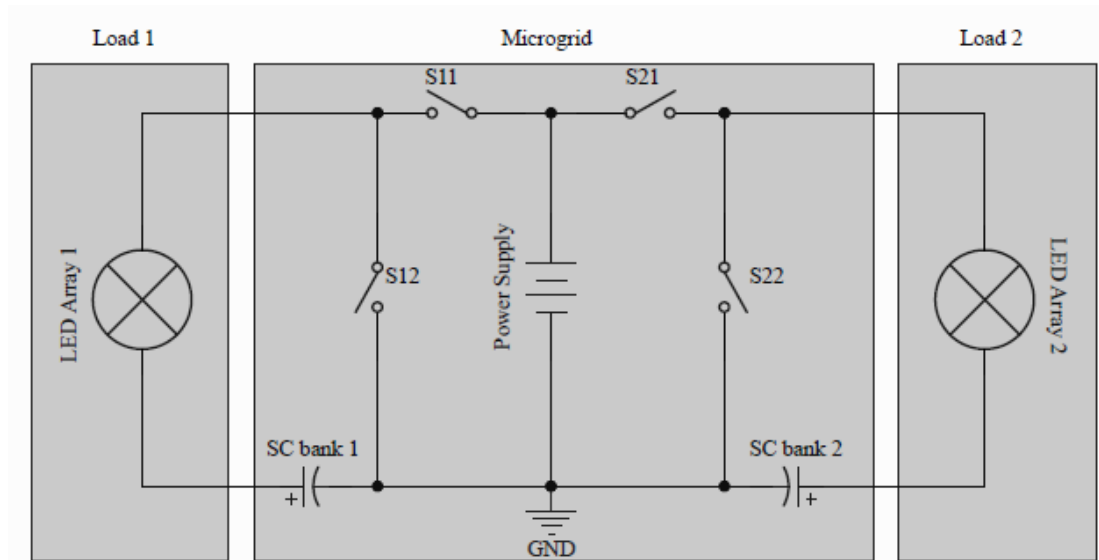


Figure 5.1: Circuit diagram of the complete DC microgrid system.

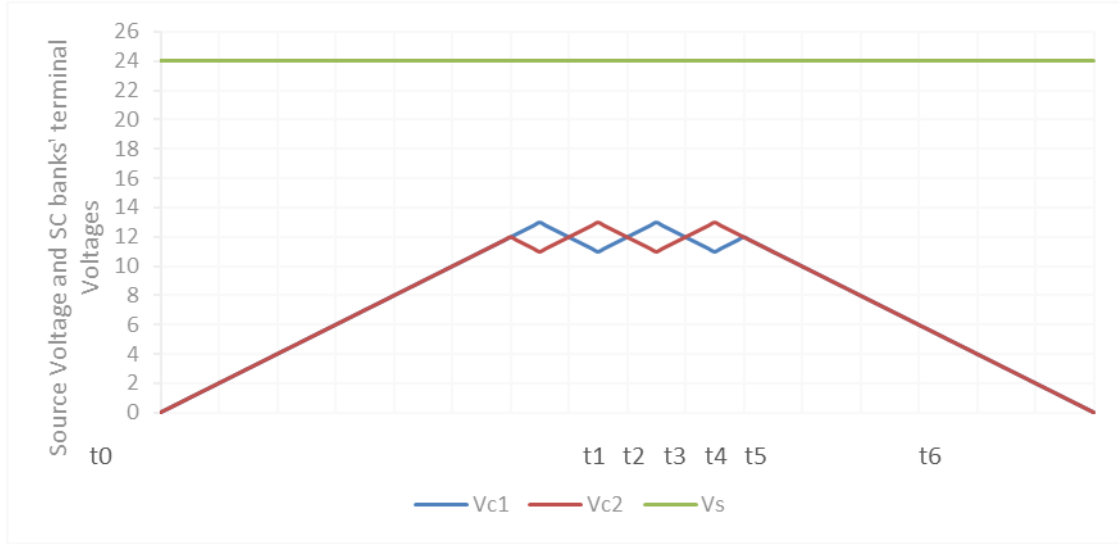


Figure 5.16: The ideal running situation for the DC microgrid.

As shown in Figure 5.16, the voltage drop on an LED array is:

$$V_{LED-1} = V_s - V_c \quad (5.10)$$

When the SC is charged, and:

$$V_{LED-2} = V_c \quad (5.11)$$

When the SC is discharged.

The blue and red lines in Figure 5.16 ( $V_{c1}$  and  $V_{c2}$ ) always 'meet' at 12 V when the DC microgrid system is running at a steady state between time  $t_1$  and time  $t_6$ , and both SC banks are always running within a voltage range of

$$\left( \frac{1}{2} V_s - 1 \right) \quad (5.12),$$

To

$$\left(\frac{1}{2}V_s + 1\right) \quad (5.13).$$

By solving equations 5.10 and 5.11, it can be seen that the voltage drop on LED arrays ranges from

$$\left(\frac{1}{2}V_s - 1\right) \quad (5.14)$$

Volts, to

$$\left(\frac{1}{2}V_s + 1\right) \quad (5.15)$$

Volts.

As mentioned in the last section of Chapter 4 “Light-emitting Diode (LED) Lamp Testing”, LEDs normally emit light with a constant brightness within a voltage range of 5.3 V to 17 V. Therefore, the DC microgrid system, with just a 2 V output fluctuation, is theoretically good and stable enough to convert a 24 V power source to an 11 V–13 V output to run LED arrays.

However, the ideal situation never exists in the ‘real world’. Figure 5.17 is a snapshot of an oscilloscope reading when ran the switch circuit in real time. As can be seen,  $V_{SC1}$  (the SC bank 1 voltage) sometimes dropped more quickly than  $V_{SC2}$  (the SC bank 2 voltage) rose, and *vice versa*. At times  $t_3$  and  $t_5$ , the two SC banks rarely achieved the desired equilibrium voltage level. There was even a short period from time  $t_a$  to time  $t_b$  in which both SC banks were charging at the same time. This non-ideal phenomenon occurred repeatedly because:

1. The components used to construct the two halves of the system were not identical; and/or
2. Sunlight irradiance fluctuations led to variance in source voltage. This variance significantly influenced the two SC banks’ charging speed.

In fact, the period from time  $t_a$  to time  $t_b$  could be shortened but could not be eliminated.

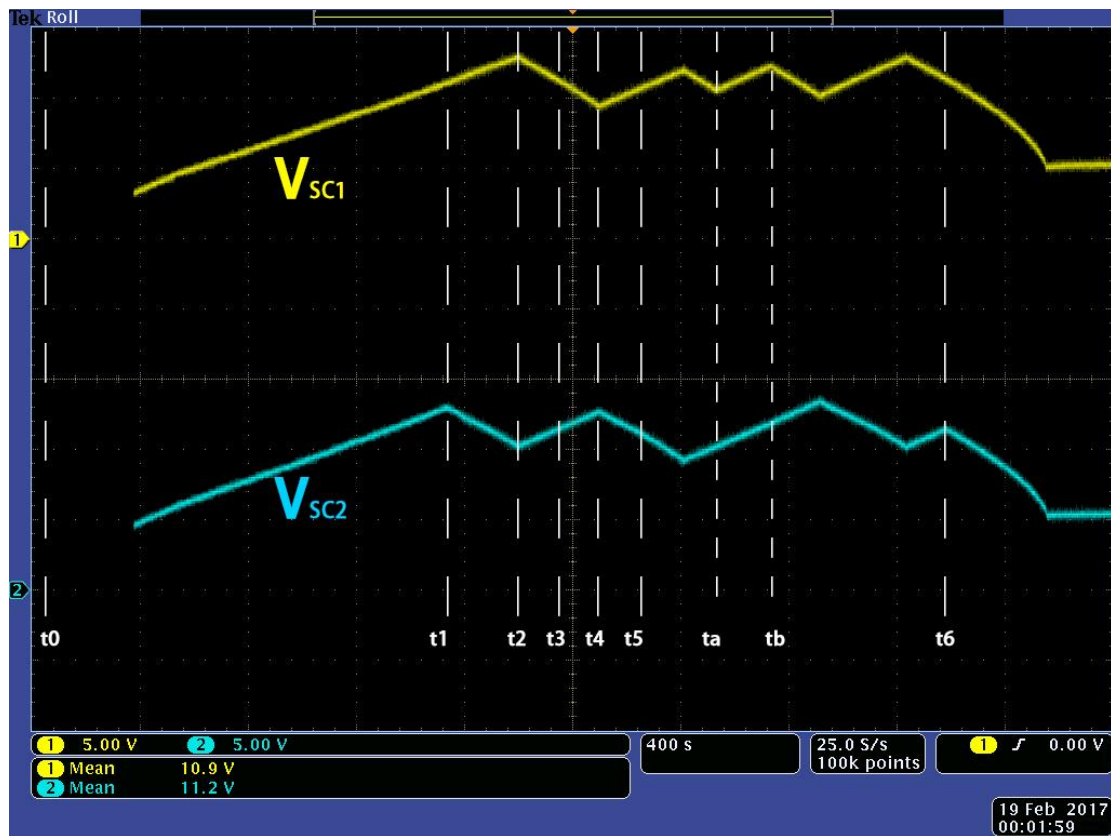


Figure 5.17: 'Real life' oscilloscope reading obtained when running the DC microgrid switch circuit.

In Table 5.4, four stages (stages 6, 7, 10 and 11) are marked by grey shadows because conditions were not good enough for the microcontroller to make decisions. Therefore, more calculations are needed to deal with these non-ideal situations. Figure 5.18 illustrates how the microcontroller ‘made decisions’ when conditions were not good enough.

Table 5.4: Logic table.

Vc	0 V–11 V	11 V–12 V	12 V–13 V	13 V–24 V	SC1	SC2
①	SC1, SC2				C	C
②	SC1	SC2			C	X
③	SC1		SC2		C	D
④	SC1			SC2	C	D
⑤	SC2	SC1			X	C
⑥		SC1, SC2				
⑦		SC1	SC2			
⑧		SC1		SC2	C	D
⑨	SC2		SC1		D	C
⑩		SC2	SC1			
⑪			SC1, SC2			
⑫			SC1	SC2	X	D
⑬	SC2			SC1	D	C
⑭		SC2		SC1	D	C
⑮			SC2	SC1	D	X
⑯				SC1, SC2	D	D
C = charge; D = discharge; X = running state unchanged						

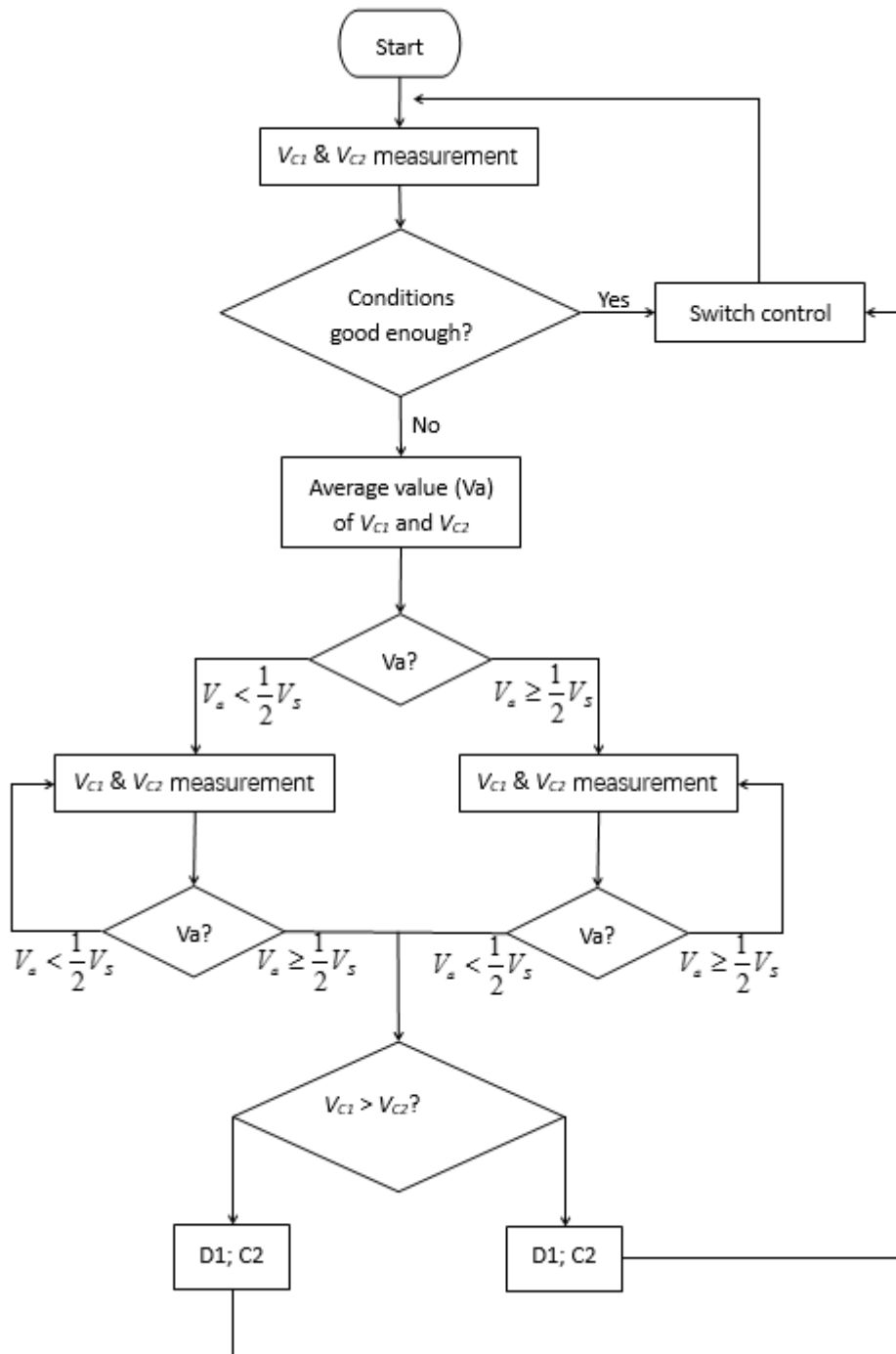


Figure 5.18: A flow chart showing how the microcontroller ‘makes decisions’ in directing DC microgrid operations.



## 5.3 Selection of SC Bank Size

In the current research project, I designed a DC microgrid to run 50 W loads (10 LEDs total, with each half or part of the system running 5 x 5 W LEDs) for a period of time when a sudden power outage occurs.

Assuming that the efficiency of my microgrid is 90% (these data were measured and are shown in Chapter 6), if the LED array is required to emit light for a certain period of time ( $t$ ) after a sudden power failure, the total energy needed for each LED array is  $5 \times 5 \text{ W} \times t = 25 \text{ tW}$ .

All of this energy can be extracted from the SC. Therefore, the energy stored in the SC should be at least

$$E_c * 90 \% \geq 25 \text{ tW} \quad (5.16).$$

In addition,

$$E_c = \frac{1}{2} CV^2 \quad (5.17).$$

Meanwhile, LED lamps work properly between 5.3 V and 17 V. However, it would be better to set a lower voltage range of operation for the  $V_{LED}$  between 11 V and 13 V for safety of the LED lamps. In addition, it would be better to provide at least 6 V to the LED at the time of the power failure. Assume that the power supply is removed when the terminal voltage of the SC is 12 V. Therefore:

$$E_c = \frac{1}{2} C \times 12^2 - \frac{1}{2} C \times 6^2 = 54C \Rightarrow 54C \times 90\% = 25tW \Rightarrow C = \frac{25t}{48.6} \quad (5.18)$$

To address these issues, I prepared Table 5.5, an estimation of approximate capacitance if LED arrays were required to glow for 3 min, 10 min, 30 min or 1 h.

Table 5.5: Capacitance selection for LEDs.

T	3 min	10 min	30 min	1 h
C	100 F	300 F	1,000 F	1,800 F

# **Chapter 6**

## **Results, Conclusions and Future Developments**



## 6.1 Results

DC microgrid system with SC-assisted converter was tested to determine the following behaviours:

- How the output efficiency changed in response to a change in the irradiance at different capacitance conditions.
- How long this system emitted light after a mains power outage.

### 6.1.1 Efficiency of the DC microgrid system

The efficiency tests were carried out on the completed SC-assisted converter system. Figure 6.1 is an oscillograph showing when the system was running at a steady state. The yellow trace and the blue trace show the terminal voltage of SC bank 1 and SC bank 2, respectively (Figure 6.2). Taking the blue trace as an example, during the first stage (Figure 6.2; times  $t_1$ – $t_2$ ), the SC bank 2 was charged from  $V_1$  (at time  $t_1$ ) to  $V_2$  (at time  $t_2$ ). The total energy provided by the power source was partly consumed by the LED lamps and loop resistance; part of the energy was stored in the SC bank 2. During stage two (Figure 6.3; times  $t_2$ – $t_3$ ), the power source was disconnected from the right-hand half (SC bank 2) of the system. At this time, the SC bank 2 released its stored energy to the loop to keep the LED lamps 2 glowing until the terminal voltage of the SC bank 2 dropped back to  $V_1$  (at time  $t_3$ ).

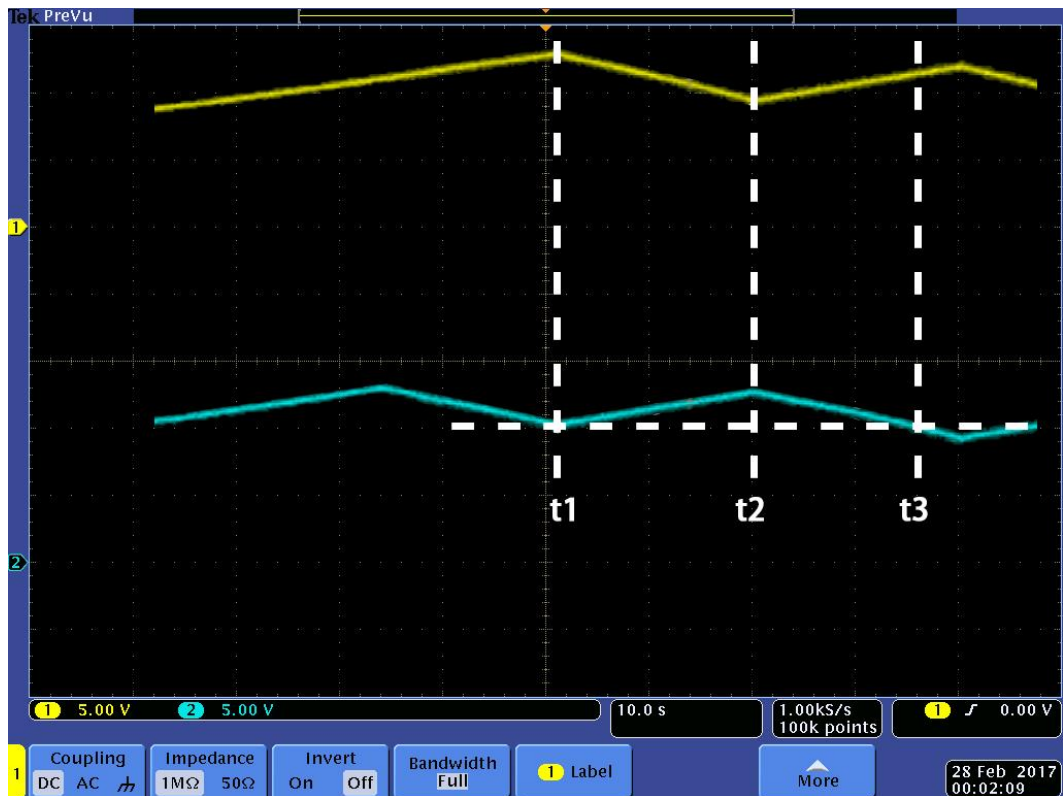


Figure 6.1: The terminal voltage of one of the supercapacitor (SC) banks (blue trace), when the system was running at a steady state.

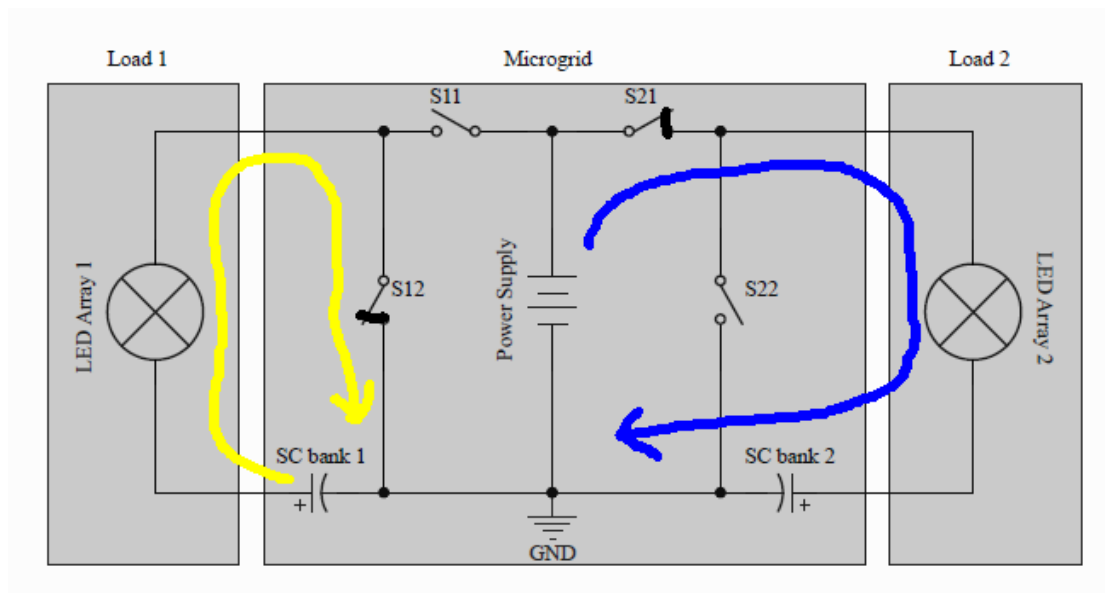


Figure 6.2: Stage 1,  $t_1$ – $t_2$ , as the SC bank 2 (blue) charged.

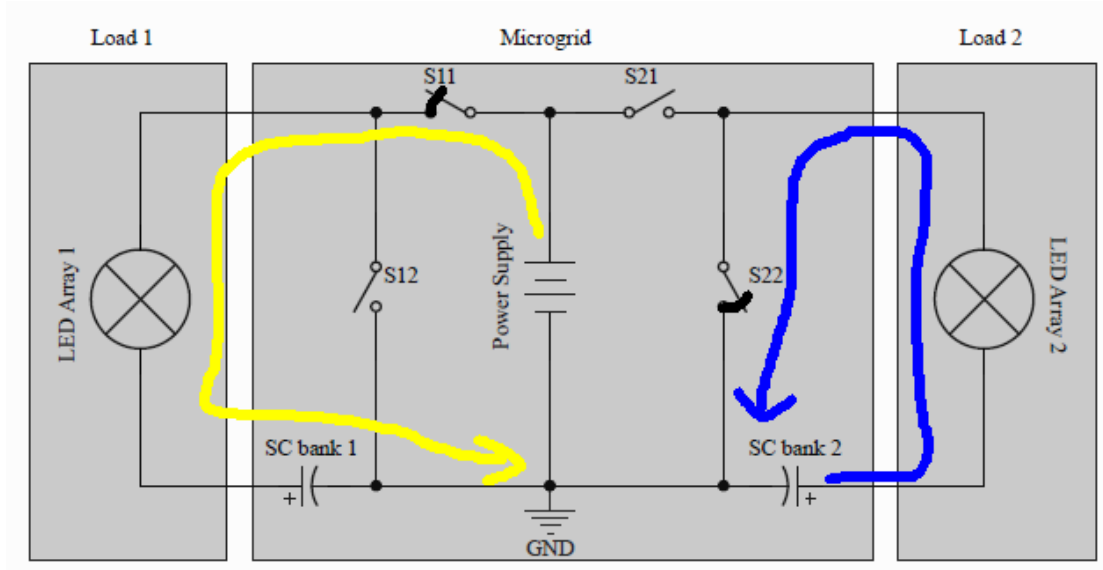


Figure 6.3: Stage 2,  $t_2$ – $t_3$ , when the right-hand SC bank 2 was disconnected from its power source and released its stored energy to power the LED array 2.

During this time  $t_1$ – $t_2$ – $t_3$  period, the efficiency of the system can be calculated by using following formula (Equation 6.1):

$$eff = \frac{\int_{t_1}^{t_2} U_{LED}(t) \cdot I_{LED}(t) dt + \int_{t_2}^{t_3} U_{LED}(t) \cdot I_{LED}(t) dt}{\int_{t_1}^{t_2} U_S(t) \cdot I_S(t) dt} \times 100\% \quad (6.1)$$

The efficiency of each of either half of the DC microgrid system, SC bank 1 or SC bank 2, can be calculated by using the same formula (Equation 6.1). The integration in the denominator and numerator can be replaced by using an accumulation with an interval of 1 s (Equation 6.2 below). This significantly simplifies the calculation:

$$eff = \frac{\sum_{t=t_1}^{t_2} U_{LED}(t) \cdot I_{LED}(t) + \sum_{t=t_2}^{t_3} U_{LED}(t) \cdot I_{LED}(t)}{\sum_{t=t_1}^{t_2} U_S(t) \cdot I_S(t)} \times 100\% \quad (6.2).$$

The value  $t$  can be assigned to a value from  $t = t_1$  to  $t = t_1 + 1, t_1 + 2, \dots, t_2, t_2 + 1, t_2 + 2, t_2 + 3, \dots$  to  $t_3$ .

Figures 6.4–6.6 show system efficiency measured on a sunny day, a cloudy day and a rainy day, respectively. As can be seen, higher irradiance yields higher efficiency. This relationship is illustrated in Figure 6.7.

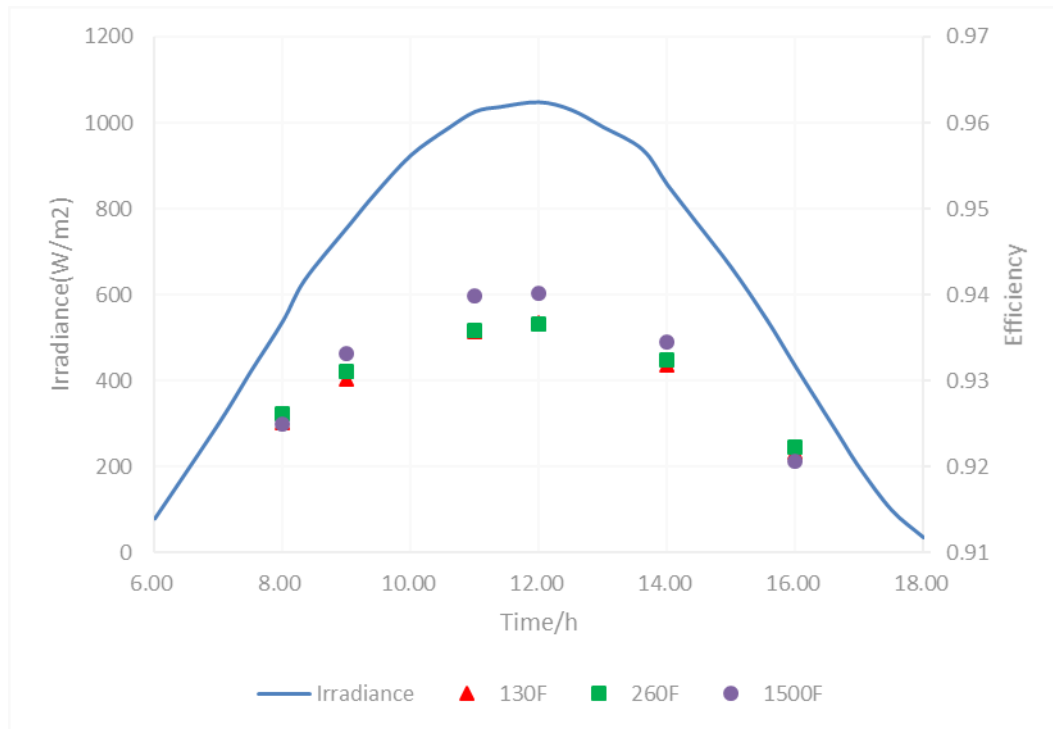


Figure 6.4: Irradiance vs. DC microgrid system efficiency on a sunny day.

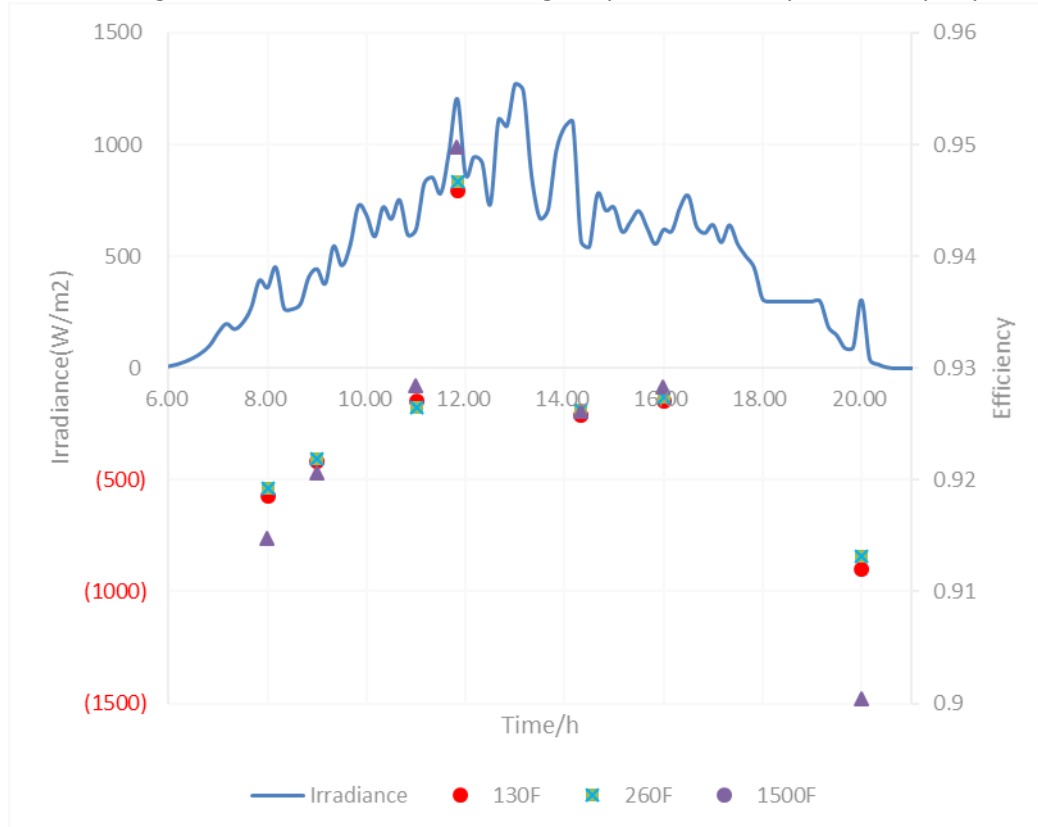


Figure 6.5: Irradiance vs. DC microgrid system efficiency on a cloudy day.

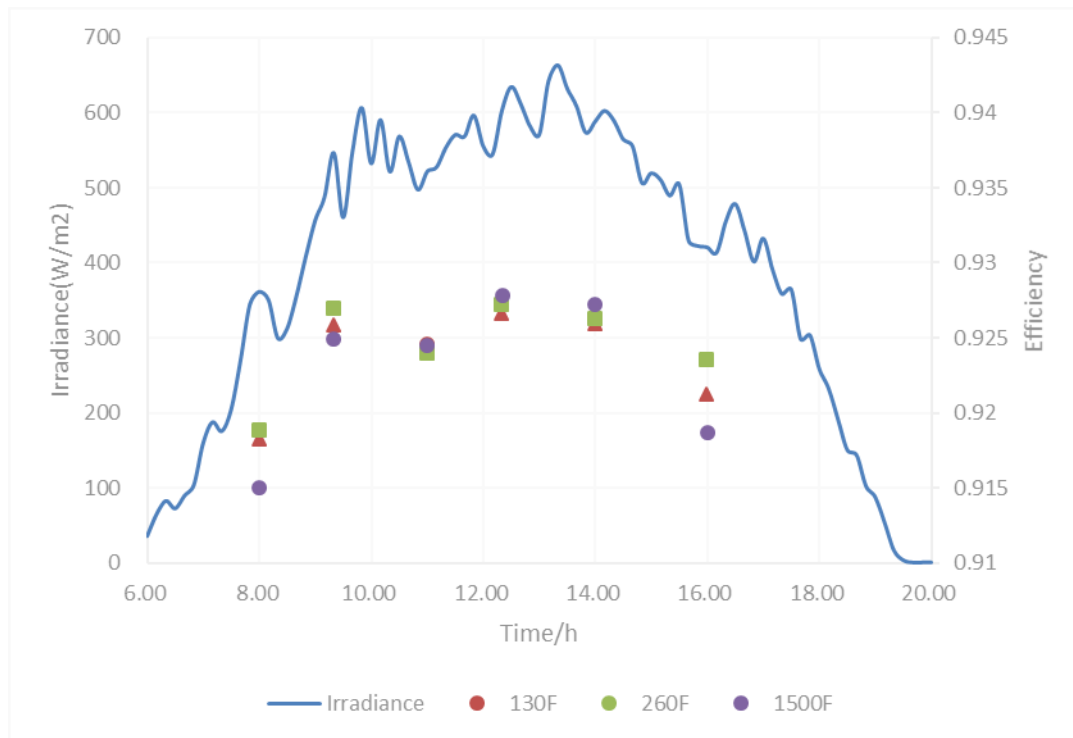


Figure 6.6: Irradiance vs. DC microgrid system efficiency on a rainy day.



Figure 6.7: Efficiency vs. line voltage at various capacitances.



### 6.1.2 Light Emission Times After a Mains Power Outage

The theoretical light emission time ( $T_t$ ) after a mains power outage can be obtained by using Equation 5.18 (described in Chapter 5, Section 5.3, “Selection of SC Bank Size”). Actual data were obtained by suddenly removing the power supply and recording the time from time  $t_6$  (SC terminal voltage [ $V_c$ ], 12 V [ $V_s/2$ ]) to 6 V

Table 6.1: System running time during simulated mains power outage.

SC Capacitance	130 F	260 F	1500 F
$T_t$ (theoretical)	249 s	499 s	2880 s
$T_m$ (measured)	192 s	389 s	2416 s

## 6.2 Discussion and Conclusions

An SC-assisted converter for a DC microgrid system is workable. Under the control of the SC-assisted converter, the total efficiency of the DC microgrid system I designed in the current study was between 90% and 94%. Capacitance differentials have only a minor influence on system efficiency. In fact, efficiency is mainly influenced by irradiance, and a higher irradiance therefore leads to a higher efficiency.

By comparing the theoretical ( $T_t$ ) and actual light emission ( $T_m$ ) times displayed in Table 6.1, it is easy to see that the measured value is less than the theoretical value. This discrepancy can be explained by the following reasons:

The power of the LED lamp array I used was constant (5 W). If the terminal voltage of an LED array ( $U_{LED}$ ) drops, its dynamic resistance drops in proportion to the square of its terminal voltage:

$$R_{LED}(t) = \frac{U_{LED}^2(t)}{P} \quad (6.3)$$

If an LED array is powered by a low-voltage power source, its dynamic resistance is lower. Lower dynamic resistance leads to a higher loop current. In the meantime, a lower dynamic resistance brings about a larger proportion of voltage drop on the loop resistance. Taken together, these interactions cause higher power consumption on the loop resistance. Thus, lower  $V_{LED}$  gives rise to lower efficiency.

When the power supply is removed, LED array is powered by SC bank instead. The terminal voltage of SC bank,  $V_c$ , drops along with its discharging and the efficiency is getting lower and lower. This results in a shorter  $T_m$ . Therefore, in order to run the

DC microgrid system with a relatively high efficiency, the SC's terminal voltage should be maintained within a range with a relatively high lower-limit value.

However, solar cells are influenced by many factors. Air temperature is one of the key factors affecting a solar cell's terminal output. Therefore, conclusions I have reached in the current research are based on conditions in which there is no air temperature fluctuation affecting solar panels.

## 6.3 Recommended Future Developments

Several improvements to my DC microgrid can be implemented in the future. For a start, the temperature factor can be taken into consideration.

The prototype SC assisted converter for DC microgrid for the current project was meant to power a 12 V LED household lighting system (ten LED lamps, 5 W each). Because of inherent LED characteristics, the LED array can be powered in two directions. This system can therefore be simplified and designed to yield a positive +11 V to +13 V or a negative –13 V to –11V output to light up LED lamps. However, this design is not suitable for other DC appliances, such as whiteware with BLDC motors. To improve the design, more switches should be added to retain constant positive output. A LDO regulator is also required, because DC motors are sensitive to voltage fluctuations, even when the fluctuation range is small, as it is in my novel DC microgrid configuration.



# References

- [1]. N. Kularatna, “Energy Storage Devices for Electronic System – Rechargeable Batteries and Supercapacitors”, Burlington : Elsevier Science, 2014.
- [2]. Naoki AyAi\*, Toshiya HisAdA, Toshikazu sHibATA, Hidekazu MiyosHi, Takashi iwAsAki and ken-ichi kiTAyAMA “DC Micro Grid System”, Electric Wire & Cable, Energy
- [3]. Aalborg University website, “DC MICROGRID LABORATORY”.  
<http://www.et.aau.dk/departament/laboratory-facilities/dc-microgrid-lab/>
- [4]. R.Dervisoglu, “Scheme of a proton-conducting fuel cell”.
- [5]. Houston Advanced Research Centre, “Acumentrics Fuel Cell System and Remote Terminal Setup Report”, HARC is a nonprofit research hub, March 2006
- [6]. T. Al-Shemmeri, “Wind Turbines”, Ventus Publishing ApS, 2010
- [7]. New Zealand Wind Energy Association, “New Zealand’s Wind Farms”.  
<http://www.windenergy.org.nz/wind-energy/nz-windfarms>
- [8]. SFGATE, “Introduction to Solar Panels”.  
<http://homeguides.sfgate.com/introduction-solar-panels-79606.html>
- [9]. Richard Hantula, “Science in the Real World: How Do Solar Panels Work?”, Infobase Publishing, 2010
- [10]. Available at  
<https://www.ametek.com/pressreleases/news/2015/august/programmable-power-photovoltaic-simulator-provides-higher-output-and-power>

- [11]. Arrillaga, Jos; High Voltage Direct Current Transmission, second edition, Institution of Electrical Engineers, 1998.
  
- [12]. Garbesi, Karina, Vagelis Vossos, Alan H. Sanstad, and Gabriel Burch, "Optimizing Energy Savings from Direct-DC in U.S. Residential Buildings", Lawrence Berkeley National Laboratory, October, 2011
  
- [13]. ON Semiconductor™, "Linear & Switching Voltage Regulator Handbook". ON Semiconductor™, Feb. 2002
  
- [14]. US Defense Logistics Agency. Available at <https://utw10356.utweb.utexas.edu/sites/default/files/Energy%20Storage%20Comparison.pdf>
  
- [15]. Dan Durbin, Energizer Applications support, Medical Device & Manufacturing (MD&M) West, Anaheim, CA, 15 February 2012
  
- [16]. SuperPower Inc., "Superconducting Magnetic Energy Storage (SMES)", 2014. <http://www.superpower-inc.com/content/superconducting-magnetic-energy-storage-smes>
  
- [17]. T.Q Khan P Bodrogi; Q.T Vinh; H Winkler, "LED Lighting Technology and Perception", Hoboken: Wiley. 2014
  
- [18]. Devdas Shetty Richard Kolk, "Mechatronics system design", Boston: PWS Pub. 1997
  
- [19]. R Krishnan (Ramu) ProQuest (Firm), "Permanent magnet synchronous and brushless DC motor drives", Boca Raton: CRC Press/Taylor & Francis Group. 2009
  
- [20]. Website NIWA: <https://solarview.niwa.co.nz/>

- [21]. P.R. Chappell, "The Climate and Weather of Waikato", 2<sup>nd</sup> edition, 2012
- [22]. Website Wikipedia: [https://en.wikipedia.org/wiki/Solar\\_irradiance](https://en.wikipedia.org/wiki/Solar_irradiance)
- [23]. Revision H. "ELGAR TerraSAS Software Installation and User Manual", Feb 17, 2014
- [24]. Microchip Technology Inc., "PIC16F684 Data Sheet", Microchip Technology Inc., 2007
- [25]. Thomas L. Floyd, "Electronic Devices: Electron Flow Version", 9<sup>th</sup> edition, Prentice Hall, 2012
- [26]. Vrej Barkhordarian, International Rectifier, El Segundo, Ca., "Power MOSFET Basics", International Rectifier
- [27]. Infineon, "SiPMOS<sup>®</sup> Power-Transistor datasheet (SPP80P06P H)", 2011
- [28]. NXP Semiconductors, "datasheet (PSMN8R5-100PS)", 2013



111



## Appendix B: Prototype PCB (SC Assisted Power Converter)

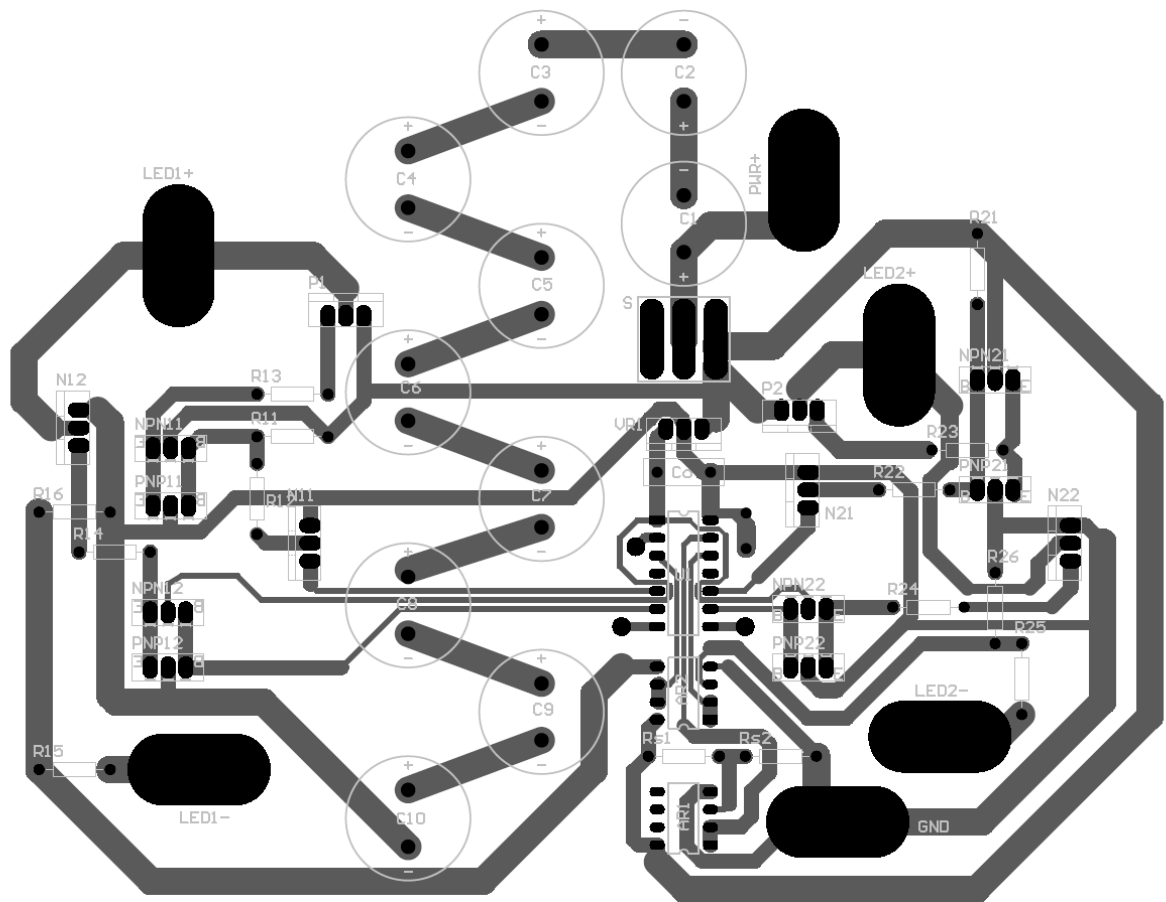


Figure 7.2: Prototype PCB of the SC Assisted Power Converter

## Appendix C: Prototype Circuit (LED loads)

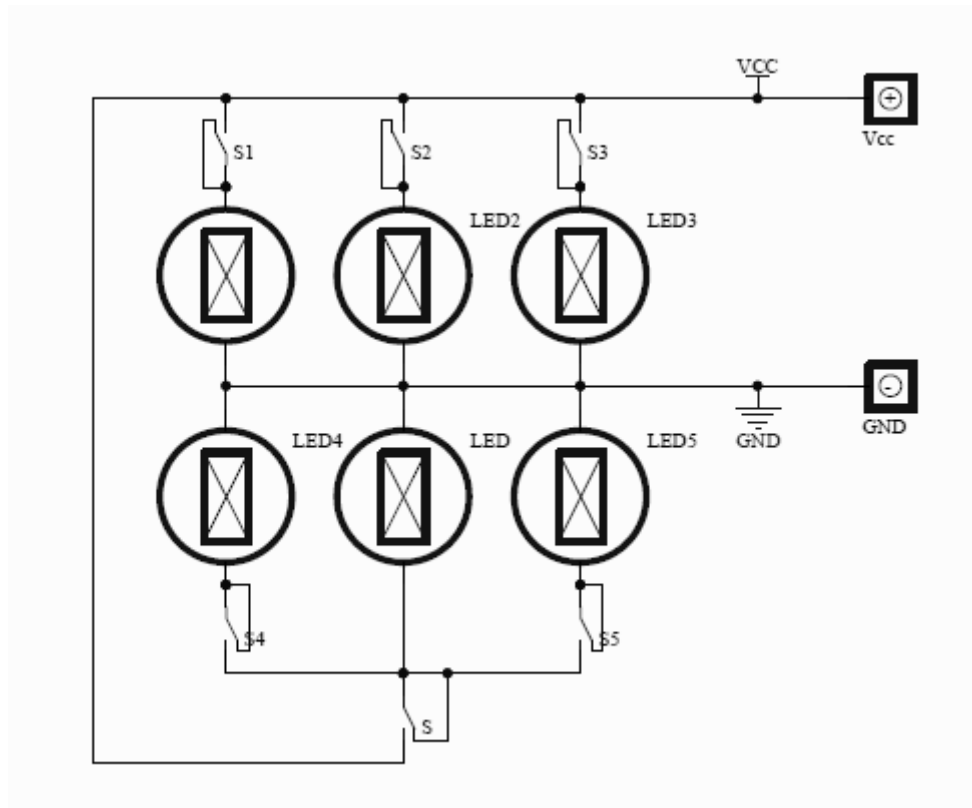


Figure 7.3: Prototype Circuit of the LED loads

## Appendix D: Prototype PCB (LED loads)

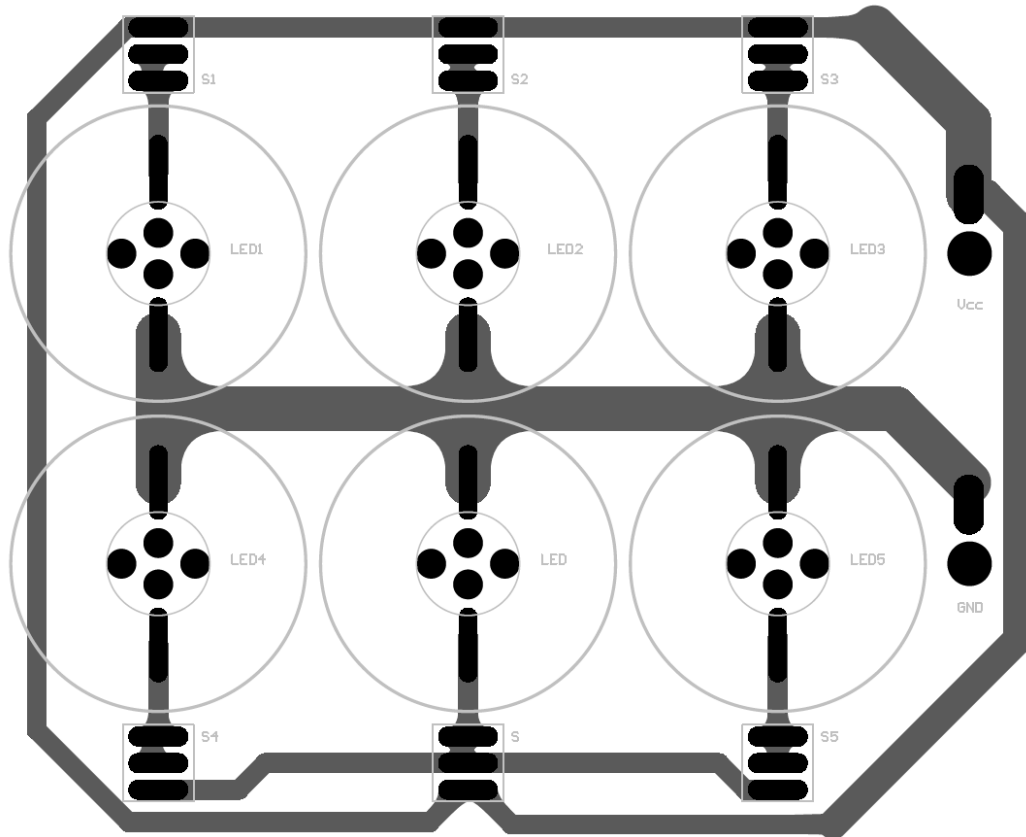


Figure 7.4: Prototype PCB of the LED loads

# Appendix E: Microcontroller Code for Switch Circuit

```
#include<pic.h>

//#define VS RA0

__CONFIG(0x3184);

unsigned char X, Y, Z=0, old, now, state = 1, T, S = 0;
float VS, VC1, VC2, A, B, M, AVE;

void interrupt ISR(void)
{
    TMR1L = 0b00110000;
    TMR1H = 0b00001100;//TMR1=3120, T=0.5s
    TMR1IF = 0;

    if(T == 0b00010010 && X == 0b00000011)
    {
        S = 0;
    }

    Z++;
    if(Z==8)
    {
        Z=0;

        switch (X)
        {
```

```

case 0b00000000://discharge in parallel
    T = 0b00010010;
    break;
case 0b00000001://discharge sc1 and charge sc2
    T = 0b00010001;
    state = 0;
    break;
case 0b00000010://charge sc1 and discharge sc2
    T = 0b00100010;
    state = 0;
    break;
case 0b00000011://charge in parallel
    if(S==1)
    {
        T = 0b00100001;
    }
    else
    {
        T = T | 0b00100000;
        T = T & 0b00101111;
        S = 1;
    }
    break;
default:
    break;
}

PORTC = T;

```

```

    }
}

```

```

void main()

```

```

{
    OPTION_REG = 0b00000000;//P12
    INTCON = 0b11000000;//P13
    PIE1 = 0b00000001;//P14 enable the timer1 overflow interrupt
    PIR1 = 0b00000000;//P15
    OSCCON = 0b01110111;//P20 Oscillator Control
    TRISA = 0b00010111;//P31 RAs configured as input
    PORTA = 0b00000000;//P31
    TRISC = 0b00000000;//P40
    PORTC = 0b00000000;//P40
    T1CON = 0b00110001;//P50 <0>turn on the timer 1
    T2CON = 0b00000000;//P54
    ANSEL = 0b00001111;//P32 RA0-RA2, RA4 configured as analog input
    ADCON1 = 0b00000000;//P70
    ADCON0 = 0b10000001;

    Y=1;RC2=Y;
    _delay(3000000);
    Y=0;RC2=Y;

    while (1)

```

{

ADCON0 = 0b10000001;//P70 <7>right justified; <6>Vdd as reference voltage; <4:2>initially select RA1 as analog channel

asm("NOP;");

asm("NOP;");

asm("NOP;");

GO\_DONE = 1;//start ADC

while (GO\_DONE);

VS = ADRESH \* 256 + ADRESL;//get wanted voltage value from RA0

VS = VS / 27.5;

M = VS / 2;

A = M - 1.5;

B = M + 1.5;

ADCON0 = 0b10001101;//P70

asm("NOP;");

asm("NOP;");

asm("NOP;");

GO\_DONE = 1;//start ADC

while (GO\_DONE);

VC1 = ADRESH \* 256 + ADRESL;

VC1 = VC1 / 44;

ADCON0 = 0b10000101;//P70

asm("NOP;");

asm("NOP;");

```

asm("NOP;");

GO_DONE = 1;//start ADC

while (GO_DONE);

VC2 = ADRESH * 256 + ADRESL;

VC2 = VC2 / 44;


AVE = (VC1 + VC2) / 2;


old = now;


if (AVE < M) { now = 0; }

else { now = 1; }


if (old != now)
{
    state = 1;
}


if(VS<=18)//discharge in parallel
{
    PORTC = 0b00010010;
    T = 0b00010010;
    X = 0b00000000;
}

else if (VC1 <= A && VC2 <= A)
{
    X = 0b00000011;//charge in parallel
}

else if (AVE <= B)

```



```

    {

        if ((T == 0b00010010 || T == 0b00100001) && state == 1)
        {
            if (VC1 <= VC2) { X = 0b00000010; } //charge sc1 and
discharge sc2

            else { X = 0b00000001; } //discharge sc1 and charge sc2

        }

        else if (VC2 - VC1 >= 3 && VC2 >= M) { X =
0b00000010; } //charge sc1 and discharge sc2

        else if (VC1 - VC2 >= 3 && VC1 >= M) { X =
0b00000001; } //discharge sc1 and charge sc2

        }

    else

    {

        X = 0b00000000; //discharge in parallel

    }

}

}

```

//MOSFET driver testing program

/\*

void interrupt ISR(void)

{

TMR1L = 0b00110000;

```

TMR1H = 0b00001100;
TMR1IF = 0;//TMR1=3120, T=0.5s

Z++;
if(Z==8)
{
    Z=0;

switch (X)
{
case 0b00100000://discharge
    T = 0b00100000;
    break;
case 0b00000001://charge
    Y=1;RA5=Y;
    for(long int i=0;i<32760;i++){;}
    for(long int i=0;i<32760;i++){;}
    Y=0;RA5=Y;
    T = 0b00000001;
    break;
case 0b00000000://discharge
    T = 0b00000000;
    break;
default:
    break;
}

//    PORTC = T;
Y=!Y;RC4=Y;

```

```

    }
}
*/

//ADC calibration program
/*
void main()
{
    OPTION_REG = 0b00000000;//P12
    INTCON = 0b11000000;//P13
    PIE1 = 0b00000001;//P14 enable the timer1 overflow interrupt
    PIR1 = 0b00000000;//P15
    OSCCON = 0b01110111;//P20 Oscillator Control
    TRISA = 0b00010111;//P31 RAs configured as input
    PORTA = 0b00000000;//P31
    TRISC = 0b00000000;//P40
    PORTC = 0b00000000;//P40
    T1CON = 0b00110001;//P50 <0>turn on the timer 1
    T2CON = 0b00000000;//P54
    ANSEL = 0b00001111;//P32 RA0-RA2, RA4 configured as analog input
    ADCON1 = 0b00000000;//P70
    ADCON0 = 0b10000001;

    Y=1;RC2=Y;
    _delay(3000000);
    Y=0;RC2=Y;

```

```

while (1)
{

    ADCON0 = 0b10000001;//P70 <7>right justified; <6>Vdd as reference
    voltage; <4:2>initially select RA1 as analog channel

    asm("NOP;");
    asm("NOP;");
    asm("NOP;");
    GO_DONE = 1;//start ADC
    while (GO_DONE);
    VS = ADRESH * 256 + ADRESL;//get wanted voltage value from RA0
    VS = VS / 27.5;

    M = VS / 2;
    A = VS / 2 - 1;
    B = VS / 2 + 1;

    ADCON0 = 0b10001101;//P70
    asm("NOP;");
    asm("NOP;");
    asm("NOP;");
    GO_DONE = 1;//start ADC
    while (GO_DONE);
    VC2 = ADRESH * 256 + ADRESL;//get current Vout from RA4
    VC2 = VC2 / 44;

    if(VS<=18)//discharge in parallel

```

```

        {
            if(VC2<6){X=0b00000000;}
            else{X = 0b00100000;}
        }
        else if (VC2 < A)
        {
            X = 0b00000001;//charge in parallel
        }
        else if (VC2 > B)
        {

            X = 0b00100000;

        }

//if(VC2>16){PORTC=0b00000100;}
//else{PORTC=0b00000000;}

    }

}

*/

```

## Appendix F: PV Simulator Codes for Creating Irradiance Profiles of a Cloudy Day and a Rainy Day

Table 7.1: a table used to create Hamilton Cloudy Day Irradiance Profile.

Line Number	Ramp Time	Ramp to Irradiance	Ramp to Temperature	Dwell Time	Dwell Irradiance	Dwell Temperature	Go to Line	Repeat Cycles
1	0	0	25	5000	0	25	1	3
2	0	0	25	4800	0	25	0	0
3	590	1	25	10	1	25	0	0
4	590	3	25	10	3	25	0	0
5	590	9	25	10	9	25	0	0
6	590	17	25	10	17	25	0	0
7	590	30	25	10	30	25	0	0
8	590	47	25	10	47	25	0	0
9	590	70	25	10	70	25	0	0
10	590	103	25	10	103	25	0	0
11	590	159	25	10	159	25	0	0
12	590	199	25	10	199	25	0	0
13	590	175	25	10	175	25	0	0
14	590	204	25	10	204	25	0	0
15	590	269	25	10	269	25	0	0
16	590	392	25	10	392	25	0	0
17	590	361	25	10	361	25	0	0
18	590	452	25	10	452	25	0	0
19	590	269	25	10	269	25	0	0
20	590	265	25	10	265	25	0	0
21	590	288	25	10	288	25	0	0
22	590	408	25	10	408	25	0	0
23	590	444	25	10	444	25	0	0
24	590	379	25	10	379	25	0	0
25	590	546	25	10	546	25	0	0
26	590	460	25	10	460	25	0	0
27	590	548	25	10	548	25	0	0
28	590	725	25	10	725	25	0	0
29	590	684	25	10	684	25	0	0
30	590	590	25	10	590	25	0	0
31	590	721	25	10	721	25	0	0
32	590	668	25	10	668	25	0	0

<b>33</b>	590	753	25	10	753	25	0	0
<b>34</b>	590	597	25	10	597	25	0	0
<b>35</b>	590	621	25	10	621	25	0	0
<b>36</b>	590	827	25	10	827	25	0	0
<b>37</b>	590	853	25	10	853	25	0	0
<b>38</b>	590	783	25	10	783	25	0	0
<b>39</b>	590	968	25	10	968	25	0	0
<b>40</b>	590	1205	25	10	1205	25	0	0
<b>41</b>	590	865	25	10	865	25	0	0
<b>42</b>	590	944	25	10	944	25	0	0
<b>43</b>	590	921	25	10	921	25	0	0
<b>44</b>	590	734	25	10	734	25	0	0
<b>45</b>	590	1112	25	10	1112	25	0	0
<b>46</b>	590	1082	25	10	1082	25	0	0
<b>47</b>	590	1270	25	10	1270	25	0	0
<b>48</b>	590	1241	25	10	1241	25	0	0
<b>49</b>	590	863	25	10	863	25	0	0
<b>50</b>	590	672	25	10	672	25	0	0
<b>51</b>	590	708	25	10	708	25	0	0
<b>52</b>	590	973	25	10	973	25	0	0
<b>53</b>	590	1078	25	10	1078	25	0	0
<b>54</b>	590	1102	25	10	1102	25	0	0
<b>55</b>	590	569	25	10	569	25	0	0
<b>56</b>	590	543	25	10	543	25	0	0
<b>57</b>	590	779	25	10	779	25	0	0
<b>58</b>	590	706	25	10	706	25	0	0
<b>59</b>	590	719	25	10	719	25	0	0
<b>60</b>	590	610	25	10	610	25	0	0
<b>61</b>	590	655	25	10	655	25	0	0
<b>62</b>	590	704	25	10	704	25	0	0
<b>63</b>	590	629	25	10	629	25	0	0
<b>64</b>	590	556	25	10	556	25	0	0
<b>65</b>	590	620	25	10	620	25	0	0
<b>66</b>	590	613	25	10	613	25	0	0
<b>67</b>	590	719	25	10	719	25	0	0
<b>68</b>	590	772	25	10	772	25	0	0
<b>69</b>	590	635	25	10	635	25	0	0
<b>70</b>	590	605	25	10	605	25	0	0
<b>71</b>	590	642	25	10	642	25	0	0
<b>72</b>	590	564	25	10	564	25	0	0
<b>73</b>	590	640	25	10	640	25	0	0
<b>74</b>	590	555	25	10	555	25	0	0

<b>75</b>	590	550	25	10	550	25	0	0
<b>76</b>	590	449	25	10	449	25	0	0
<b>77</b>	590	311	25	10	311	25	0	0
<b>78</b>	590	299	25	10	299	25	0	0
<b>79</b>	590	185	25	10	185	25	0	0
<b>80</b>	590	148	25	10	148	25	0	0
<b>81</b>	590	91	25	10	91	25	0	0
<b>82</b>	590	95	25	10	95	25	0	0
<b>83</b>	590	305	25	10	305	25	0	0
<b>84</b>	590	40	25	10	40	25	0	0
<b>85</b>	590	18	25	10	18	25	0	0
<b>86</b>	590	5	25	10	5	25	0	0
<b>87</b>	0	0	25	5000	0	25	87	3
<b>88</b>	0	0	25	1200	0	25	0	0

Table 7.2: a table used to create Hamilton Rainy Day Irradiance Profile.

<b>Line Number</b>	<b>Ramp Time</b>	<b>Ramp to Irradiance</b>	<b>Ramp to Temperature</b>	<b>Dwell Time</b>	<b>Dwell Irradiance</b>	<b>Dwell Temperature</b>	<b>Go to Line</b>	<b>Repeat Cycles</b>
<b>1</b>	0	0	25	5000	0	25	1	3
<b>2</b>	0	0	25	4800	0	25	0	0
<b>3</b>	590	9	25	10	9	25	0	0
<b>4</b>	590	18	25	10	18	25	0	0
<b>5</b>	590	35	25	10	35	25	0	0
<b>6</b>	590	64	25	10	64	25	0	0
<b>7</b>	590	82	25	10	82	25	0	0
<b>8</b>	590	72	25	10	72	25	0	0
<b>9</b>	590	89	25	10	89	25	0	0
<b>10</b>	590	103	25	10	103	25	0	0
<b>11</b>	590	159	25	10	159	25	0	0
<b>12</b>	590	187	25	10	187	25	0	0
<b>13</b>	590	175	25	10	175	25	0	0
<b>14</b>	590	204	25	10	204	25	0	0
<b>15</b>	590	269	25	10	269	25	0	0
<b>16</b>	590	344	25	10	344	25	0	0
<b>17</b>	590	361	25	10	361	25	0	0
<b>18</b>	590	350	25	10	350	25	0	0
<b>19</b>	590	299	25	10	299	25	0	0



20	590	312	25	10	312	25	0	0
21	590	356	25	10	356	25	0	0
22	590	408	25	10	408	25	0	0
23	590	456	25	10	456	25	0	0
24	590	487	25	10	487	25	0	0
25	590	546	25	10	546	25	0	0
26	590	460	25	10	460	25	0	0
27	590	548	25	10	548	25	0	0
28	590	606	25	10	606	25	0	0
29	590	532	25	10	532	25	0	0
30	590	590	25	10	590	25	0	0
31	590	521	25	10	521	25	0	0
32	590	568	25	10	568	25	0	0
33	590	534	25	10	534	25	0	0
34	590	497	25	10	497	25	0	0
35	590	521	25	10	521	25	0	0
36	590	527	25	10	527	25	0	0
37	590	553	25	10	553	25	0	0
38	590	570	25	10	570	25	0	0
39	590	568	25	10	568	25	0	0
40	590	596	25	10	596	25	0	0
41	590	555	25	10	555	25	0	0
42	590	544	25	10	544	25	0	0
43	590	602	25	10	602	25	0	0
44	590	634	25	10	634	25	0	0
45	590	612	25	10	612	25	0	0
46	590	582	25	10	582	25	0	0
47	590	570	25	10	570	25	0	0
48	590	642	25	10	642	25	0	0
49	590	663	25	10	663	25	0	0
50	590	632	25	10	632	25	0	0
51	590	608	25	10	608	25	0	0
52	590	573	25	10	573	25	0	0
53	590	588	25	10	588	25	0	0
54	590	602	25	10	602	25	0	0
55	590	589	25	10	589	25	0	0
56	590	564	25	10	564	25	0	0
57	590	555	25	10	555	25	0	0
58	590	506	25	10	506	25	0	0
59	590	519	25	10	519	25	0	0
60	590	510	25	10	510	25	0	0
61	590	489	25	10	489	25	0	0

<b>62</b>	590	504	25	10	504	25	0	0
<b>63</b>	590	429	25	10	429	25	0	0
<b>64</b>	590	422	25	10	422	25	0	0
<b>65</b>	590	420	25	10	420	25	0	0
<b>66</b>	590	413	25	10	413	25	0	0
<b>67</b>	590	455	25	10	455	25	0	0
<b>68</b>	590	478	25	10	478	25	0	0
<b>69</b>	590	442	25	10	442	25	0	0
<b>70</b>	590	401	25	10	401	25	0	0
<b>71</b>	590	432	25	10	432	25	0	0
<b>72</b>	590	390	25	10	390	25	0	0
<b>73</b>	590	358	25	10	358	25	0	0
<b>74</b>	590	364	25	10	364	25	0	0
<b>75</b>	590	298	25	10	298	25	0	0
<b>76</b>	590	303	25	10	303	25	0	0
<b>77</b>	590	258	25	10	258	25	0	0
<b>78</b>	590	232	25	10	232	25	0	0
<b>79</b>	590	191	25	10	191	25	0	0
<b>80</b>	590	150	25	10	150	25	0	0
<b>81</b>	590	143	25	10	143	25	0	0
<b>82</b>	590	102	25	10	102	25	0	0
<b>83</b>	590	87	25	10	87	25	0	0
<b>84</b>	590	53	25	10	53	25	0	0
85	590	16	25	10	16	25	0	0
86	590	3	25	10	3	25	0	0
87	0	0	25	5000	0	25	87	3
88	0	0	25	1200	0	25	0	0